ABSTRACT

A STUDY OF ^{206}Pb BY INELASTIC SCATTERING OF 35 MeV PROTONS

By

Joseph Eugene Finck

Using high resolution techniques the inelastic scattering of 35 MeV protons by ^{206}Pb have been measured. A resolution of 6 to 9 keV allowed identification of approximately 180 levels of ^{206}Pb with excitation energies up to 6.8 MeV. Angular distributions of most of these states are measured. L-transfers and deformation parameters are determined by comparison of the measured angular distributions to collective model calculations. Strongly excited collective states are compared to analogous states in ^{207}Pb and ^{208}Pb and the overall distribution of inelastic strength in ^{206}Pb is compared to ^{208}Pb. Microscopic calculations of natural parity states are presented and allow a test of theoretical RPA and TDA wave functions. Unnatural parity states with well determined wave functions are also studied microscopically and permit an examination of the central and noncentral forces in the effective interaction.

A STUDY OF ^{206}Pb BY INELASTIC SCATTERING OF 35 MeV PROTONS

By

Joseph Eugene Finck

A DISSERTATION

Submitted to
Michigan State University
in parital fulfillment of the requirements
for the degree of

DOCTOR OF PHILOSOPHY

Department of Physics

1982

ACKNOWLEDGEMENTS

I would like to thank Professor G. M. Crawley for his constant guidance and assistance during the time that this work was performed. Professor J. S. Kovacs is also thanked for his support and understanding during my graduate career. Dr. J. A. Nolen, Jr. is thanked for his aid with this project and many helpful comments.

I would also like to recognize the staffs of the Michigan State Cyclotron Laboratory, Princeton Cyclotron Laboratory, and Northern Michigan University Physics Department. I am especially grateful for the aid and hospitality of Dr. R. Kouzes at Princeton and Dr. D. Fowler at Northern Michigan. Without these people this work would not have been possible.

Working with Bill Wagner, Rick Steele, and Paul Smith as a novice graduate student at the lab was an invaluable educational experience. In particular, my escapades with Paul will never be forgotten.

Bruce Hasselquist and Jim Duffy provided much companionship and support as officemates, especially during prelims together.

All my friends are thanked. In particular the members -- old and new -- of the Nuclear Beer Group. I am indebted to Reg Ronningen and Wayne Bentley for their

kindkness and comradery. Special thanks must be given to Jim Carr and Carol Dors for their close friendship. These individuals made my days as a graduate student most enjoyable and special.

I am grateful to the communities of Michigan State University and East Lansing for providing a nonpareil academic and pleasant social atmosphere for me to study and live in.

I owe a large debt to my parents for their support and prayers. To my wife, Deborah, I am grateful for her encouragement, understanding, and patience. Mostly, I am thankful for her love. My daughter, Elizabeth -- born during the preparation of Chapter IV of this thesis -- is recognized for her inspiration.

This thesis is dedicated to my entire family.

TABLE OF CONTENTS

LIST OF TABLES

LIST OF FIGURES

FIGURE PAGE

FIGURE PAGE

CHAPTER I

INTRODUCTION

The lead region has always been an attractive area to test nuclear models. Nuclei in this mass region have been studied both experimentally and theoretically. The bulk of this work has involved the structure of the doubly-magic nucleus ^{208}Pb. Many of these studies have also extended to the single-hole structure of ^{207}Pb and the single-particle structure of ^{209}Bi which are now well-established. An examination of ^{206}Pb is a further step toward the more complex structure that exist away from closed shells.

Experiments previously performed on ^{206}Pb include inelastic scattering [Refs. I.1, I.2, and I.3] which has given information about the strongly excited states. Information about the microscopic structure of many of the low-lying states has been provided by decay studies [Refs. I.4, I.5, and I.6], transfer reactions [Refs. I.7, I.8, I.9, and I.10], and isobaric analog resonance experiments [Refs. I.11 and I.12]. The spins and parities of many higher-lying levels have also been determined by these experiments. Using the shell model which describes ^{206}Pb as two neutron holes in the ^{208}Pb core, energies and wave

functions of the low-lying levels of ^{206}Pb have been calculated [Refs. I.13 and I.14]. With this background a detailed study of inelastic proton scattering from ^{206}Pb, including collective and microscopic calculations, has been undertaken.

A direct reaction, such as inelastic proton scattering, can be used as a means to obtain spectroscopic information. In direct reaction experiments a beam of particles with a certain energy is focused on a target. The number of outgoing particles of a certain energy as a function of the angle between the incoming beam and the outgoing particles (the angular distribution) is measured. From these data the energy of the levels of the investigated nucleus can be directly determined; information about the spin and parity of the excited levels, and the spectroscopic strength for the excitation of these levels can be obtained by comparing the measured angular distributions with calculations assuming a specific configuration for the level considered.

Of all the direct reactions available proton scattering is the most appealing reaction to investigate nuclear structure and interactions. Almost all levels in a nucleus can be excited by means of inelastic scattering of protons with a beam energy for above the Coulomb barrier. However, the cross sections can be low. The structure of the states can be determined from comparison of the

experimental angular distribution for the level with that obtained from macroscopic or microscopic distorted wave calculations. When there are accurate wave functions available from model calculations microscopic calculations are preferred because these provide a better check on the proposed structure of the state. As the shape of angular distributions at forward angles and the magnitude of the overall angular distribution are very sensitive to the different configurations in the wave functions of the state, microscopic calculations are a suitable test for the wave functions.

The possibility of finding states which have not been seen before, together with the possibility of comparing the experimental angular distributions of the states with model calculations provide the motivation for a high resolution (p, p') experiment on ^{206}Pb.

A proton inelastic scattering experiment on ^{206}Pb has been reported [Refs. I.1, I.2, and I.3] at 24.5 MeV bombarding energy with an energy resolution of approximately 25 keV. This experiment identified 30 levels, and spin and parity assignments for the most strongly excited states were made. Using a collective model calculation, the reduced transition rates for some of these states were extracted. In this experiment, the angular distributions were compared only with the collective model predictions. The theoretical tools for a microscopic analysis were not

well developed at the time that this experiment was done. Furthermore, only states below 4.6 MeV of excitation energy were observed and in this region states weakly excited were not extracted. In addition, the resolution limited the number of states that could be analyzed unambiguously. This represents the most extensive study of ^{206}Pb (p, p') to date.

With the availability of particle accelerators with increased intensity and improved resolution, along with advances in magnetic spectrographs and particle detection devices, weakly excited levels and close lying excited levels can be resolved and studied. The microscopic description of nucleon-nucleus scattering has also progressed. Now with a better understanding of exchange effects and the nucleon-nucleon interaction, microscopic inelastic reaction theory can be used to study nuclear properties [Ref. I.15].

This thesis reports a study of ^{206}Pb (p, p') performed at 35 MeV with an energy resolution of 6 to 9 keV. Experimental procedures are described in Chapter II. Approximately 180 levels of ^{206}Pb with excitation energies up to 6.8 MeV are observed. Measured distributions for 144 of these levels are displayed. In Chapter III these results of the experiment are presented.

In the remaining chapters the theoretical models are compared with experimental results. The collective

model is used in fitting many of the measured angular distributions, and L-assignments and deformation parameters are obtained for these states. Systematics of strongly excited collective states in ^{206}Pb, ^{207}Pb, and ^{208}Pb are examined, and inelastic strengths of ^{206}Pb and ^{208}Pb are compared. Microscopic calculations are performed for a number of natural and unnatural parity states. The microscopic examination of natural parity states permits the testing of wave functions since such transactions depend little on the noncentral two-body interaction. Wave functions obtained from the random phase and Tamm-Dancoff approximations are examined. Unnatural parity transitions to levels with well determined wave functions allow the two-body central, tensor, and spin-orbit forces to be studied. In this study two different sets of forces are employed for comparison with experimental results.

In Appendix I, the methods used in the analysis of the data are outlined. This includes a description of the computer programs used to perform data reduction, determine excitation energies, extract angular distributions, and plot the results. Appendix II give examples of input to the distorted wave programs used in this study. Measured angular distributions of ^{206}Pb (p, p') are tabulated in Appendix III. Appendix IV lists abstracts of published papers to which I have contributed while a student at Michigan State University.

REFERENCES FOR CHAPTER I

I.1 J. Saundinos, G. Vallois, and O. Beer, Nucl. Sci. Appl. 3 (1967), 22.

I.2 G. Vallois, J. Saudinos, and O. Beer, Phys. Lett. 24B (1967), 512.

I.3 G. Vallois, Centre d'Etudes Nucleaives de Saclay, Report CEA-R-3500 (1968).

I.4 J. C. Manthuruthil, D. C. Camp, A. V. Ramayya, J. H. Hamilton, J. J. Pinajian, and J. W. Doornebos, Phys. Rev. C 6 (1972), 1870.

I.5 J. E. Draper, R. J. McDonald, and N. S. P. King, Phys. Rev. C 16 (1977), 1594.

I.6 D. F. Coope, L. F. Cannell, and M. K. Brussel, Phys. Rev. C 15 (1977), 1977.

I.7 W. A. Lanford, PHys. Rev. C 16 (1977), 988.

I.8 W. A. Lnaford and G. M. Crawley, Phys. Rev. C 9 (1974), 646.

I.9 R. Tickle and J. Bardwick, Phys. Rev. 166 (1968), 1167.

I.10 E. R. Flynn, R. A. Broglia, R. Liotta, and B. S. Nilsson, Nucl. Phys. A221 (1974), 509.

I.11 J. Solf, C. F. Moore, E. Grosse, and P. von Brentano, Nucl. Phys. A139 (1969), 523.

I.12 P. Richard, N. Stein, C. D. Kavaloski, and J. S. Lilley, Phys. Rev. 171 (1968), 1308.

I.13 W. W. True and C. W. Ma, Phys. Rev. C 3 (1971), 2421.

I.14 J. Vary and J. N. Ginocchio, Nucl. Phys. A166 (1971), 479.

I.15 G. R. Satchler, Comm. Nucl. and Part. Phys. 5 (1972), 39.

CHAPTER II

EXPERIMENTAL PROCEDURE

The experiment was performed using 35 MeV proton beams from the Michigan State University and Princeton University sector-focused cyclotrons. The Michigan State cyclotron delivered a proton beam of between 500- and 1500-nA average current on target. The average current from the Princeton cyclotron was between 50- and 150-nA.

Throughout the experiment ^{206}Pb targets of about 0.1 mg/cm^2 thickness were used. The targets were prepared by vacuum evaporation of the isotope, enriched to 97.22%, on a 20 $\mu g/cm^2$ carbon foil with a support of two layers of formvar. This choice of target thickness was based on a study by Wagner [Ref. II.1] which showed that lead targets of this thickness affect the resolution very little. In addition, targets of this thickness yield tolerable count rates, and skewing of peak shapes due to straggling of the protons in the target was reduced.

The beam on target was monitored by measuring the total charge collected in the Faraday cup and by measuring the number of beam particles elastically scattered into a NaI(TI) detector placed at an angle of 90° relative to the incident beam. This angle was chosen because 90° lies

near a relative maximum of the elastic cross section for ^{206}Pb and also gives a good separation of protons elastically scattered from lead and light mass contaminants in the target. The relative normalization obtained by these two measurements agree to within 5%.

The spectra from the part of the experiment at Michigan State were obtained using nuclear emulsions in the focal plane of the Enge split-pole magnetic spectrograph. This plate data was taken with a 0.6 milisteradian (1° x 2°) solid angle at forward angles and a 1.2 milisteradian (2° x 2°) solid angle at backward angles. A stainless steel absorber of thickness 0.25 mm was placed immediately before 20 inch Kodak NTB 25 μm nuclear emulsions. The absorber stopped all particles other than protons, and decreased the proton energy. This enhanced the proton tracks in the emulsion and did not significantly broaden the line width. On-line determination of the focal plane line width was optimized by adjusting the dispersion of the beam across the target using a "speculator" technique [Ref. II.2]. Once the dispersion was optimized, the resolution remained constant throughout the experiment. The resolution of the plate data ranges from 6-9 keV (FWHM). Each plate run covers a range of excitation energies from the ground state to about 7.0 MeV.

A typical spectrum of plate data is shown in Figure II.1. States of well-determined spin and parity have been

Figure II.1

Typical spectrum of protons scattered by ^{206}Pb obtained with a photographic plate. States of well-determined spin and parity are identified. The resolution is about 6 keV.

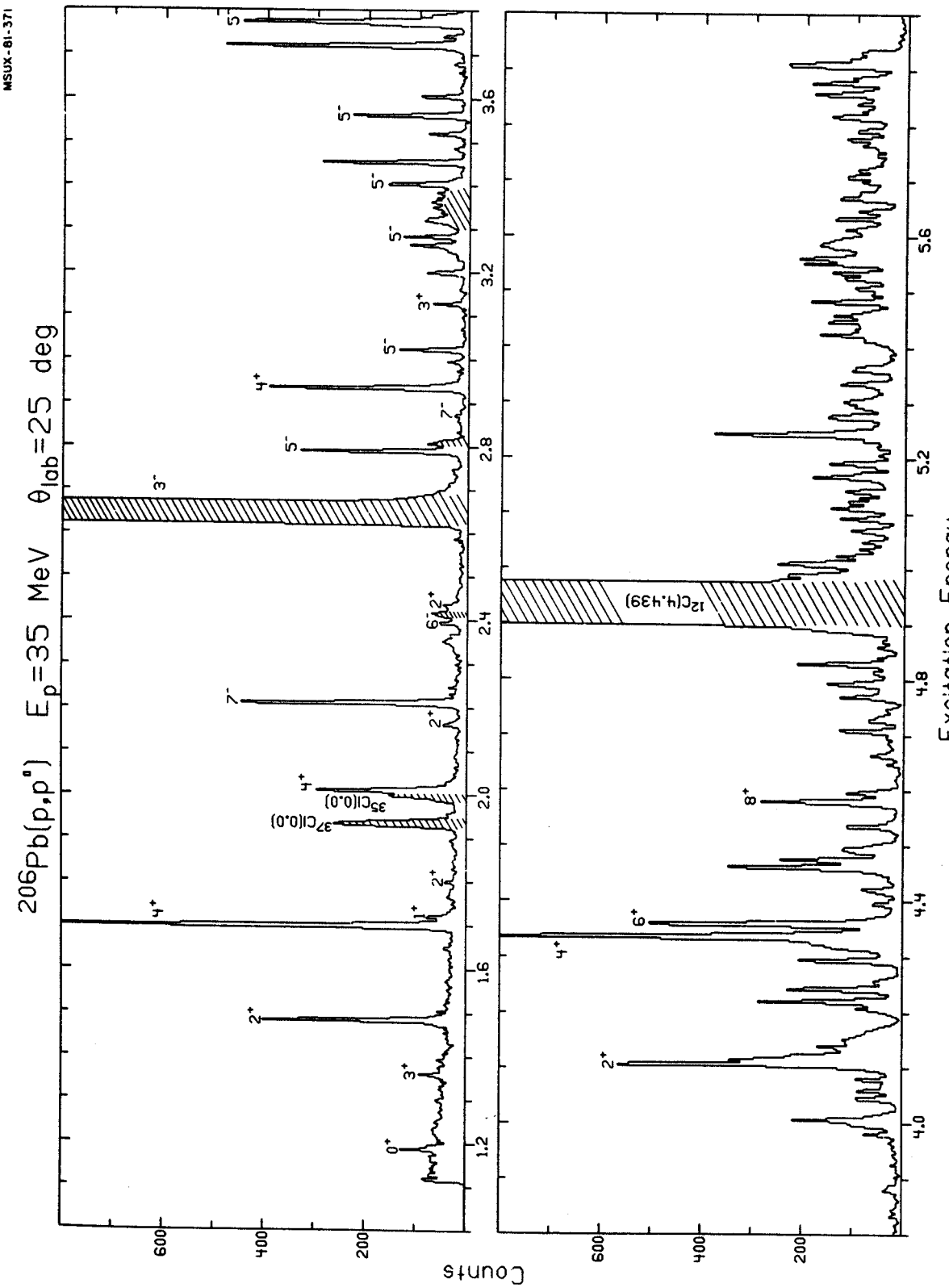
MSUX-81-371
206Pb(p,p') Ep=35 MeV θlab=25 deg
Counts
Excitation Energy
0+
3+
2+
4+
1+
2+
37Cl(0.0)
35Cl(0.0)
4+
2+
7-
6,8 2+
3-
5-
4+
7-
5-
3+
5-
5-
5-
5-
12C(4.439)
4+
6+
8+
2+
200
400
600
1.2
1.6
2.0
2.4
2.8
3.2
3.6
4.0
4.4
4.8
5.2
5.6

Figure II.1

identified. Some strongly excited states, such as the ground state, the first excited state, and the 3^- state at 2.648 MeV of excitation, produce proton tracks too dense to scan. However, their positions can easily and accurately be determined by the plate scanner. This aids in the energy calibration of the spectra.

Most states below 4 MeV of excitation appear to be completely resolved. Of special interest in this study are the unnatural parity states. These states, being weakly excited, present an experimental challenge. In particular the 1^+ state at 1.708 MeV requires very high resolution to be extracted from the shoulder of the strongly excited 4^+ state. In all plate spectra the 1^+ state was clearly separated from the 4^+ state and could be easily extracted.

The density of states above 4 MeV of excitation becomes increasingly large. Many of the states appear to be completely resolved. Peaks whose widths indicate possible multiplet structure were extracted by an interative procedure using the program SCOPEFIT [Ref. II.3]. A description of this program, and other programs used in the data analysis, is given in Appendix I.

At Princeton the quadrupole-dipole-dipole-dipole (QDDD) spectrograph was used. When excited states were examined the solid angle was opened to about 3.6 milisteradian (2° x 6°). The solid angle was closed to 1.2

milisteradian (2° x 2°) when observing the elastic peak. This was done to decrease the number of particles striking the detector, thus reducing dead-time losses. The detector used in the focal plane of the QDDD was a 20 cm long resistive-division position-sensitive gas proportional counter backed by a plastic scintillator in coincidence. The data acquisition and analysis was performed by the program TOY [Ref. II.4] on a Sigma-2 computer. The program gates the position spectrum from the gas proportional counter by a window on a particle identifier consisting of the total proportional counter signal versus the scintillator signal. In addition, the position spectrum was gated by the particle time-of-flight (TOF) spectrum (measured relative to the cyclotron rf signal). The TOF is an aid in particle identification and was used to reduce background in the proton spectra.

Data taken with the proportional counter must be done in three passes because of the large dispersion of the QDDD. Each pass covers an energy range of 2.5 MeV. The three passes overlap encompassing levels from the ground state to states up to 5.5 MeV of excitation. The energy resolution of this data is 15 to 20 keV. Data at 40°, taken in three segments, are displayed in Figure II.2. The only counter data used in the analysis in this study are levels labeled in Figure II.2.

Both methods of acquiring data offer unique

Figure II.2

Typical spectrum of protons scattered by ^{206}Pb obtained with the proportional counter.

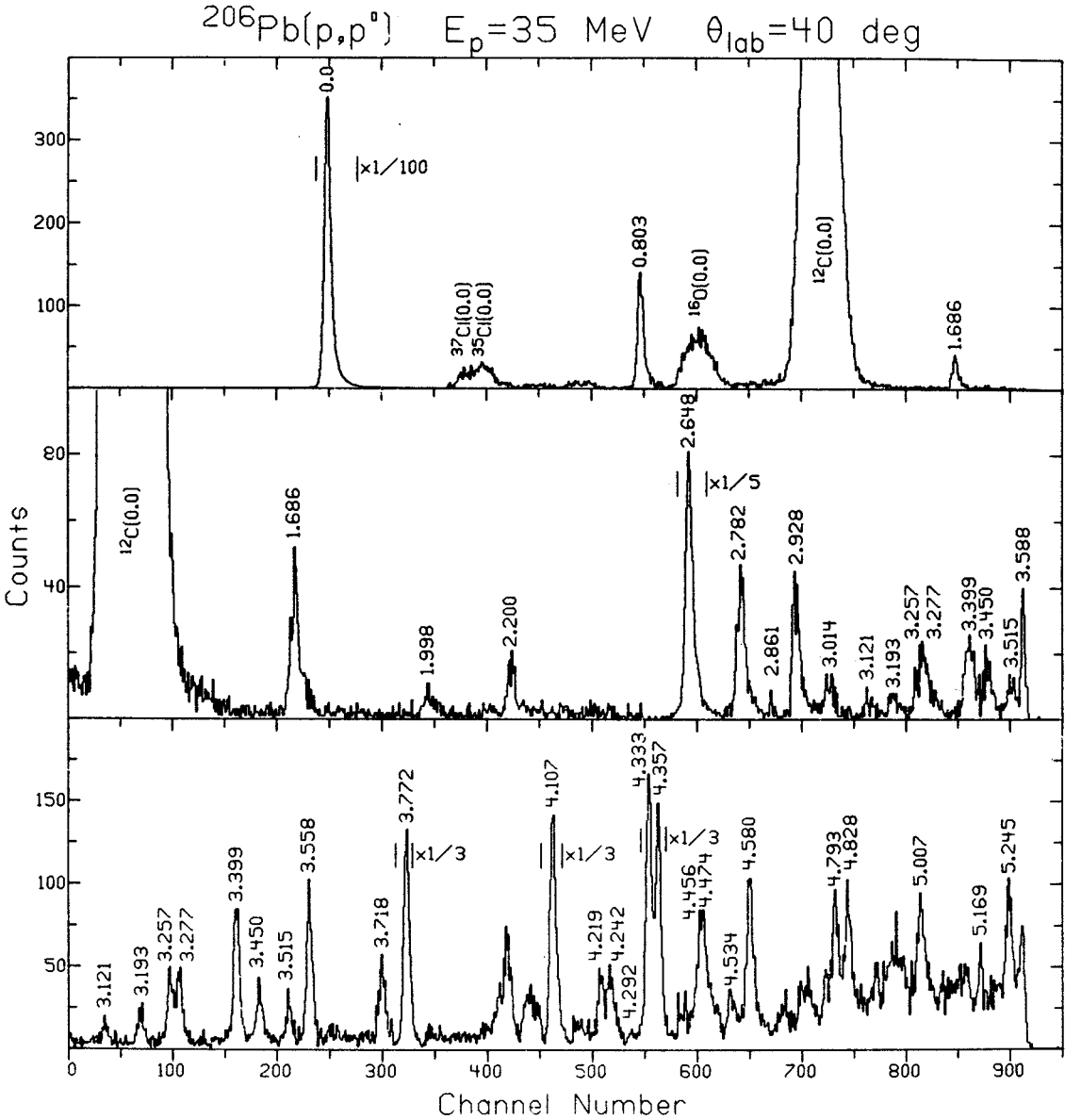
206Pb(p,p°) Ep=35 MeV θlab=40 deg
Counts
Channel Number
0.0
×1/100
37Cl(0.0)
35Cl(0.0)
0.803
16O(0.0)
12C(0.0)
1.686
12C(0.0)
1.686
1.998
2.200
2.648
×1/5
2.782
2.928
2.861
3.014
3.121
3.193
3.257
3.277
3.399
3.450
3.515
3.588
3.121
3.193
3.257
3.277
3.399
3.450
3.515
3.558
3.718
3.772
×1/3
4.107
×1/3
4.219
4.242
4.292
4.333
4.357
×1/3
4.456
4.474
4.534
4.580
4.793
4.828
5.007
5.169
5.245

Figure II.2

advantages. Data taken with the nuclear emulsions have far better resolution allowing weakly excited and close lying states to be analyzed. The linearity of the plates yield accurate excitation energies. The proportional counter gives more accurate cross section data for strongly excited states because it is not limited by the number of counts in a peak. Because energy resolution is not as curcial in this part of the experiment, a comparatively large solid angle could be used and data was accumulated at a rapid rate. The counter data also has the advantage of livetime data taking, while the data taken with the photographic plates is passive. Due to the time required to scan a plate, the results from this part of the experiment were typically not known for months.

REFERENCES FOR CHAPTER II

II.1 W. T. Wagner, Ph.D. thesis, Michigan State University, Unpublished (1974).

II.2 H. G. Blosser, G. M. Crawley, R. deForest, E. Kashy, and B. H. Wildenthal, Nucl. Instr. and Meth. 91 (1971), 61.

II.3 H. David and R. Fox, Unpublished.

II.4 R. Kouzes, Ph.D. thesis, Princeton University, Unpublished (1974).

CHAPTER III

EXPERIMENTAL RESULTS

Listed in Tables III.1 and III.2 are the excitation energies of the approximately 180 levels of ^{206}Pb observed in this experiment. In Table III.1 the levels with excitation energy below 4.6 MeV are compared with the results of a recent compilation [Ref. III.1] and an inelastic proton scattering experiment [Ref. III.2] with an incident proton energy of 24.5 MeV. Above 4.6 MeV of excitation, the correspondence of levels seen in different reactions is uncertain due to the high level density and uncertainty of excitation energy. As a result the data in this region, displayed in Table III.2, is not compared with previous results.

To determine the energies of identified ^{206}Pb states only the data taken with the nuclear emulsions are used. This data not only has the advantage of high resolution, but also is very linear along the entire length of the plate. All levels listed in these tables were clearly observed in the photographic plate data at a minimum of three angles. The energy calibration of each plate exposure was determined using both ^{206}Pb states and well-known levels of nuclei which were present as impurities in the

TABLE III.1 Energy Levels, L-transfers, and Deformation Parameters for ^{206}Pb. A comparison is Made With Previous Results.

Present Work			24 MeV (p,p') Ref. 1			Compilation Ref. 2	
$E_x \pm \Delta E_x$ [a]	L	β_L	E_x [a]	L	β_L	E_x [a]	J^π
0.00[b]						0.00	0^+
0.8031[b]	2	.066	0.803	2	.068	0.8031	2^+
1.170±.003						1.1651	0^+
1.344±.002	$J^\pi=3^+$[c]		1.328			1.3406	3^+
1.469±.002	2	.015	1.459			1.467	2^+
1.686±.001	4	.030	1.684	4	.042	1.6841	4^+
1.708±.003	$J^\pi=1^+$[c]					1.703	1^+
1.787±.002			1.789			1.784	2^+
1.9977[b]	4	.017	1.996	4	.023	1.9977	4^+
2.151±.003	(2)	.009				2.149	(2^+)
2.20023[b]	7	.022	2.199	7	.031	2.20023	7^-
						2.315	0^+
						2.379	
2.385±.002	$J^\pi=6^-$[c]		2.381			2.3843	6^-
						2.3914	

TABLE III.1 Continued.

Present Work			24 MeV (p,p') Ref. 1			Compilation Ref. 2	
$E_x \pm \Delta E_x$ [a]	L	β_L	E_x [a]	L	β_L	E_x [a]	J^π
2.422±.033	(2)	.066				2.424	2^+
2.6479 [b]	3	.108	2.648	3	.115	2.6479	3^-
						2.6585	9^-
2.78226 [b]	5	.026	2.787			2.78226	5^-
2.831±.005						2.8264	$(4^-,5^-)$
2.861±.005						2.8646	7^-
2.928 [b]	4	.030	2.981			2.928	4^+
						2.9396	6^-
2.960±.002							
2.988±.003						2.979	
3.014±.003	5	.016	3.020	5	.021	3.01649	5^-
3.033±.033							
3.121±.003	$(J^\pi=3^{+c})$		3.124			3.122	(3^+)
3.139±.006							
3.193±.003	(5)	.011				3.194	

TABLE III.1 Continued.

Present Work			24 MeV (p,p') Ref. 1			Compilation Ref. 2	
$E_x \pm \Delta E_x$ [a]	L	β_L	E_x [a]	L	β_L	E_x [a]	J^π
3.224±.005						3.2255	$(6^-,7^-)$
						3.2442	(4^-)
3.257±.001	6	.018	3.267				
3.277±.001	5	.015				3.2793	5^-
3.328±.005							
3.377±.002						3.383	(7^-)
3.399±.001	5	.020	3.403	5	.023	3.4028	5^-
3.450±.001	4	.020	3.453	3	.019	3.453	
3.478±.004						3.484	
3.515±.003	(5)	.012				3.519	$(3^+,4^+)$
3.558±.002	5	.022	3.560	5	.024	3.5629	5^-
						3.595	
3.603±.004						3.605	
3.655±.005							
3.675±.006						3.676	

TABLE III.1 Continued.

Present Work			24 MeV (p,p') Ref. 1			Compilation Ref. 2	
$E_x \pm \Delta E_x$ [a]	L	β_L	E_x [a]	L	β_L	E_x [a]	J^π
3.718±.002	3	.023	3.721			3.722	
3.737±.004	($J^\pi=1^+$ [c])					3.744	(1^+)
3.772±.002	5	.043	3.776	5	.077	3.768	(5^-)
3.795±.006						3.791	
3.827±.005						3.833	
3.883±.005							
3.898±.005						3.902	
						3.950	
						3.9576	10^+
3.963±.005	(8)	.012				3.963	(4^+)
3.980±.005							
3.997±.005						3.990	
4.006±.003	(4)	.022	4.006			4.008	(4^+)
						4.0272	(12^+)
4.044±.003	(6,7)	.014,.016				4.040	

TABLE III.1 Continued.

Present Work			24 MeV (p,p') Ref. 1			Compilation Ref. 2	
$E_x \pm \Delta E_x$ [a]	L	β_L	E_x [a]	L	β_L	E_x [a]	J^π
						4.055	
4.059±.005	(5)	.014	4.075			4.067	(5^-)
4.073±.007							
						4.094	
4.107±.002	2	0.047	4.128	2	.064	4.116	(2^+)
4.123±.003	6	.022					
4.145±.005						4.150	
4.168±.004	(3)	.009	4.191			4.162	
4.183±.005							
4.219±.003	(4)	.017	4.259			4.218	
4.242±.003	(2)	.016				4.238	(5^-)
4.292±.005	(3)	.014				4.292	
						4.326	(1)
						4/345	(6^+)
4.333±.002	4	.055	4.368	4	.067	4.353	(4^+)

TABLE III.1 Continued.

Present Work			24 MeV (p,p') Ref. 1			Compilation Ref. 2	
$E_x \pm \Delta E_x$ [a]	L	β_L	E_x [a]	L	β_L	E_x [a]	J^π
4.357±.003	6	.054	4.386	6	.061	4.390	(6^+)
4.391±.005	(5)	.012					
4.420±.005							
						4.430	
4.456±.005	(5)	.020					
4.474±.003	5	.016				4.478	
4.496±.005	(5,6)	.001,.012				4.492	
4.534±.004	5	.016				4.534	
						4.555	
4.580±.003	8	.033	4.600	8	.045	4.602	(8^+)

a. All energies are in MeV.
b. Level used in energy calibration.
c. Spin and parity adopted from Ref.

TABLE III.2 Energy Levels, L-transfers, and Deformation Parameters for ^{206}Pb.

Present Work			Present Work			Present Work		
E_x[a] $\pm\Delta E_x$	L	β_L	E_x[a] $\pm\Delta E_x$	L	β_L	E_x[a] $\pm\Delta E_x$	L	β_L
4.595±.005			4.916±.004	(3)	.015	5.245±.008	(3)	.022
4.614±.007	(3)	.004	4.939±.004	(6)	.020	5.279±.005		
4.647±.005			4.960±.007	(3)	.018	5.296±.006		
4.664±.004	5	.011	4.986±.003	(3)	.018	5.309±.004		
4.69±.007			5.007±.004	(4)	.024	5.332±.007	(3)	.011
4.710±.004	(4,5)	.015,.016	5.025±.005			5.365±.006		
4.729±.006			5.045±.006			5.403±.006		
4.742±.005			5.069±.006			5.422±.066	(4)	.019
4.770±.004			5.092±.004	(3,4)	.013,.012	5.435±.007		
4.793±.005	5	.022	5.111±.005	(4)	.015	5.452±.008	(4)	.016
4.809±.006	(5,6)	.013,.014	5.126±.006	(5)	.014	5.463±.006	(3)	.014
4.828±.004	(7)	.023	5.138±.007			5.485±.004	(4)	.017
4.860±.006	(6)	.010	5.169±.004			5.507±.006		
4.873±.004			5.190±.005			5.533±.066	(4)	.018
4.889±.005	(3)	.015	5.209±.005			5.544±.007		
4.901±.004			5.227±.008			5.561±.008	(4)	.022

TABLE III.2 Continued.

Present Work			Present Work			Present Work		
E_x[a] ± ΔE_x	L	β_L	E_x[a] ± ΔE_x	L	β_L	E_x[a] ± ΔE_x	L	β_L
5.588±.008	(5)	.020	5.843±.008			6.146±.007		
5.599±.008			5.860±.007			6.154±.005		
5.619±.008			5.885±.004			6.167±.006		
5.640±.008	(3)	.012	5.911±.007	(4)	.023	6.181±.007		
5.653±.008			5.949±.007			6.198±.007	(6)	.011
5.676±.006			5.959±.005			6.229±.008		
5.687±.004			5.974±.005			6.264±.006	(5)	.012
5.703±.008	(5)	.015	5.990±.008			6.284±.008		
5.715±.007			6.001±.005			6.302±.007		
5.722±.007			6.023±.007			6.314±.006		
5.747±.008			6.040±.005			6.332±.006		
5.763±.008			6.065±.008			6.346±.006		
5.779±.008	(5)	.014	6.071±.004			6.382±.008		
5.796±.007	(4,5)	.014,.013	6.083±.007			6.408±.008		
5.823±.008			6.117±.007			6.433±.007		

TABLE III.2 Continued.

Present Work		
E_x[a] $\pm \Delta E_x$	L	β_L
6.444±.007		
6.459±.007		
6.480±.007		
6.496±.009		
6.524±.009		
6.545±.010		
6.574±.008		
6.593±.007		
6.617±.008		
6.634±.010		
6.655±.008		
6.689±.011		
6.692±.007		
6.761±.005		
6.806±.006		

target. The ^{206}Pb states used had focal plane positions clearly determined in this experiment, and had excitation energies established in other high resolution experiments [Refs. III.3, III.4, III.5, and III.6]. These calibration states are indicated in Table III.1. The levels of ^{12}C and ^{16}O strongly excited by inelastic proton scattering, as well as the ground states of ^{35}Cl and ^{37}Cl were used whenever possible. The presence of impurity states in the ^{206}Pb spectra also allows the scattering angle to be accurately determined by kinematics.

The excitation energies given in Tables III.2 and III.2 include statistical uncertainties plus an additional error of 1 keV per 500 keV of excitation energy for states beyond 3.5 MeV of excitation energy. This systematic error is an estimate of both the interpolation error and the uncertainties in the focal plan positions caused by the high level density.

Below about 4.6 MeV of excitation energy most states are well-resolved and the agreement with previous work is very good. Several new levels have been identified in this region including two relatively strongly excited states at 3.257 and 3.980 MeV of excitation energy. A level previously reported at 2.658 MeV is not seen in this experiment. Even if this level is excited in the present experiment it could not be resolved from the state at 2.648 MeV of excitation energy in the counter data, and

because the 2.648 MeV state is the strongest excited state in this reaction the particle density is too intense to analyze in the plate data. Other levels previously reported in this region, yet not seen in this experiment, are probably very weakly excited, and an upper limit of 10 μb/sr can be put on their maximum cross section.

Angular distributions for inelastic states seen at four or more angles are shown in Figures III.1 through III.3. The cross sections are displayed with their corresponding excitation energies. Error bars indicate statistical errors and are drawn only when greater than the symbol size. The curves drawn through the data are included as guides to the eye and do not represent theoretical fits to the data. These angular distributions are also tabulated in Appendix III.

Figure III.1

Measured inelastic cross sections. The lines drawn through the data points are included to guide the eye and do not represent theoretical fits to the data.

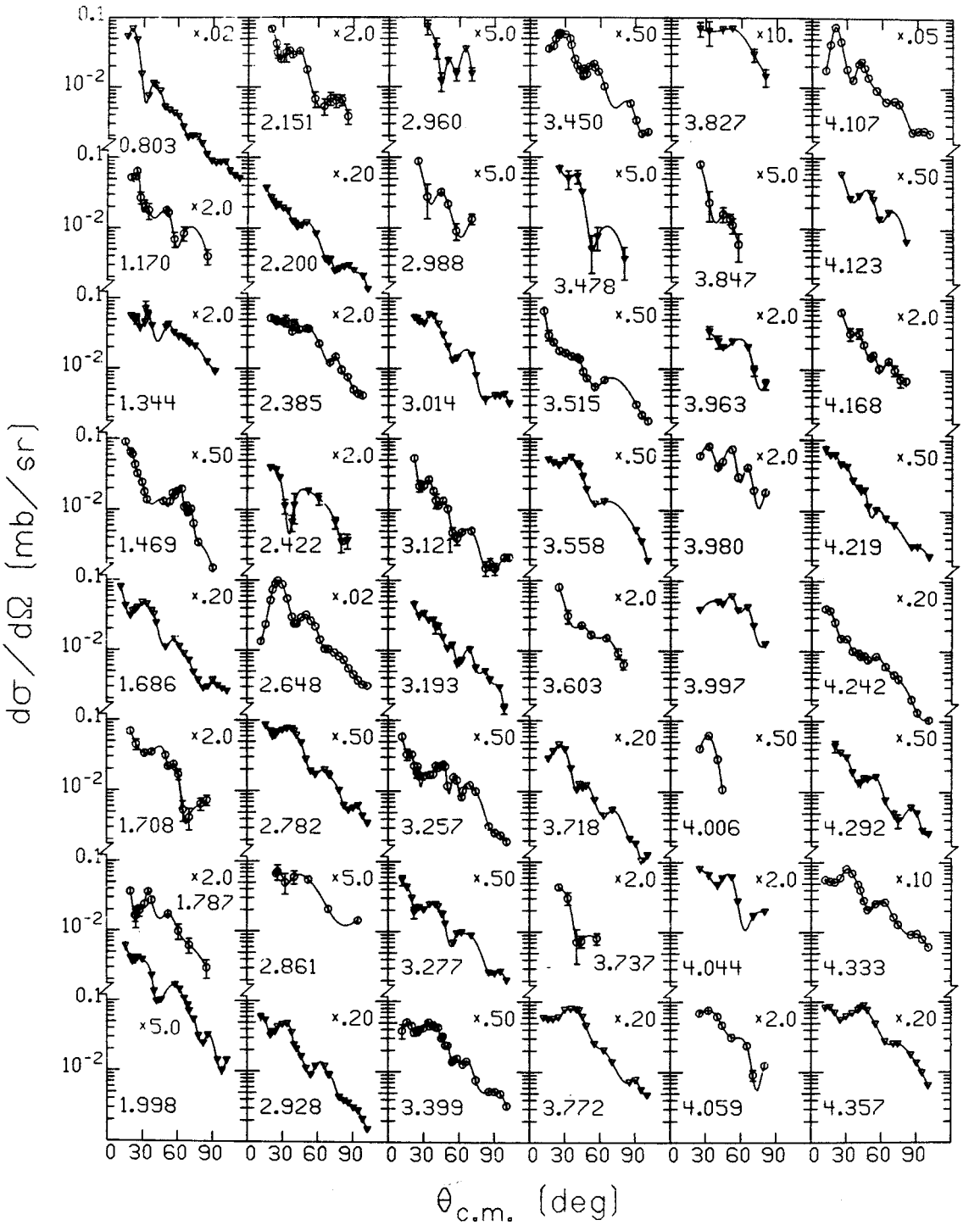
dσ / dΩ (mb / sr)
θc.m. (deg)
0 30 60 90
0.803
1.170
1.344
1.469
1.686
1.708
1.787
1.998
2.151
2.200
2.385
2.422
2.648
2.782
2.861
2.928
2.960
2.988
3.014
3.121
3.193
3.257
3.277
3.399
3.450
3.478
3.515
3.558
3.603
3.718
3.737
3.772
3.827
3.847
3.963
3.980
3.997
4.006
4.044
4.059
4.107
4.123
4.168
4.219
4.242
4.292
4.333
4.357

Figure III.1

Figure III.2

Same as Figure III.1.

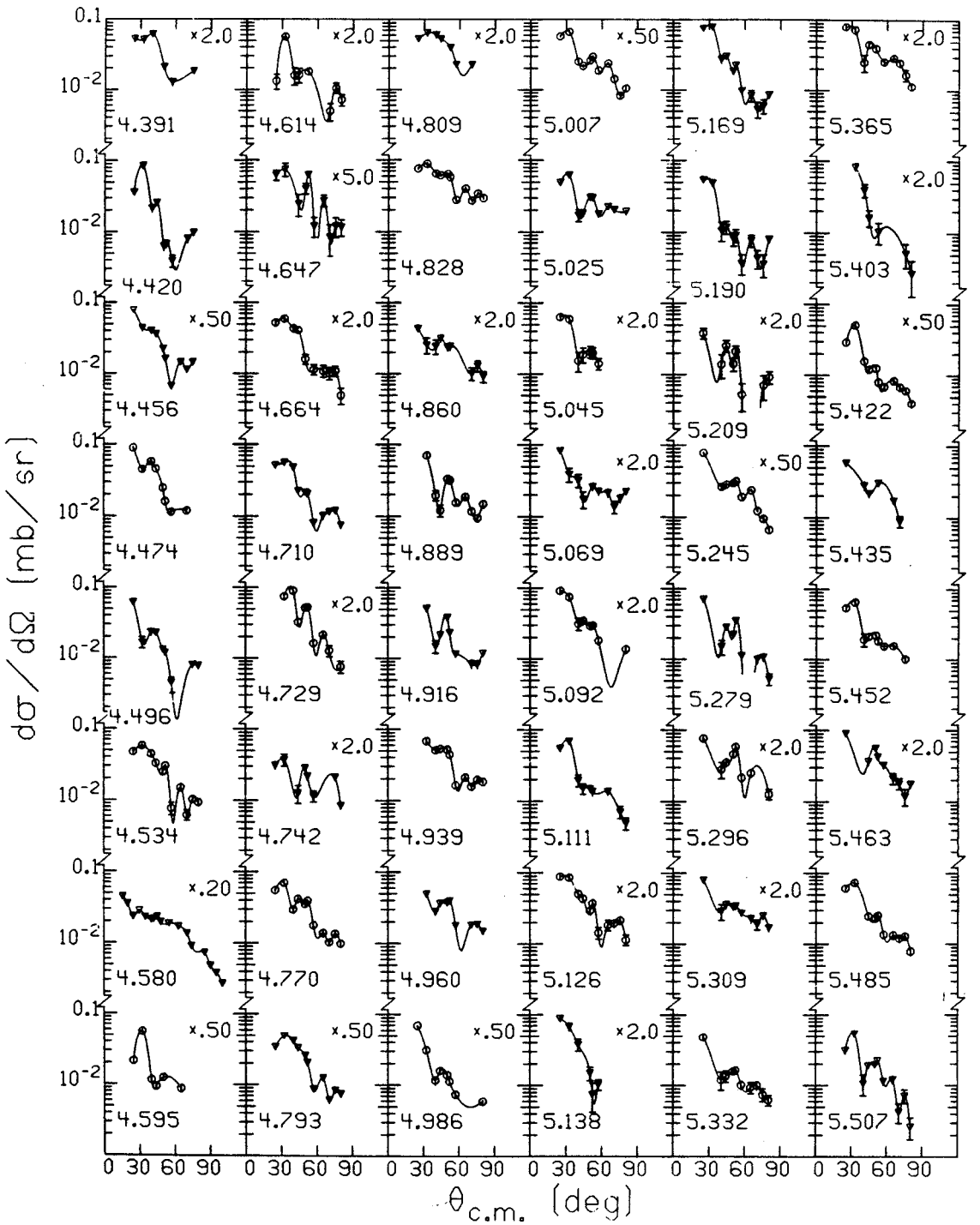
dσ/dΩ (mb/sr)
θc.m. (deg)
0 30 60 90
4.391
4.420
4.456
4.474
4.496
4.534
4.580
4.595
4.614
4.647
4.664
4.710
4.729
4.742
4.770
4.793
4.809
4.828
4.860
4.889
4.916
4.939
4.960
4.986
5.007
5.025
5.045
5.069
5.092
5.111
5.126
5.138
5.169
5.190
5.209
5.245
5.279
5.296
5.309
5.332
5.365
5.403
5.422
5.435
5.452
5.463
5.485
5.507

Figure III.2

Figure III.3

Same as Figure III.1.

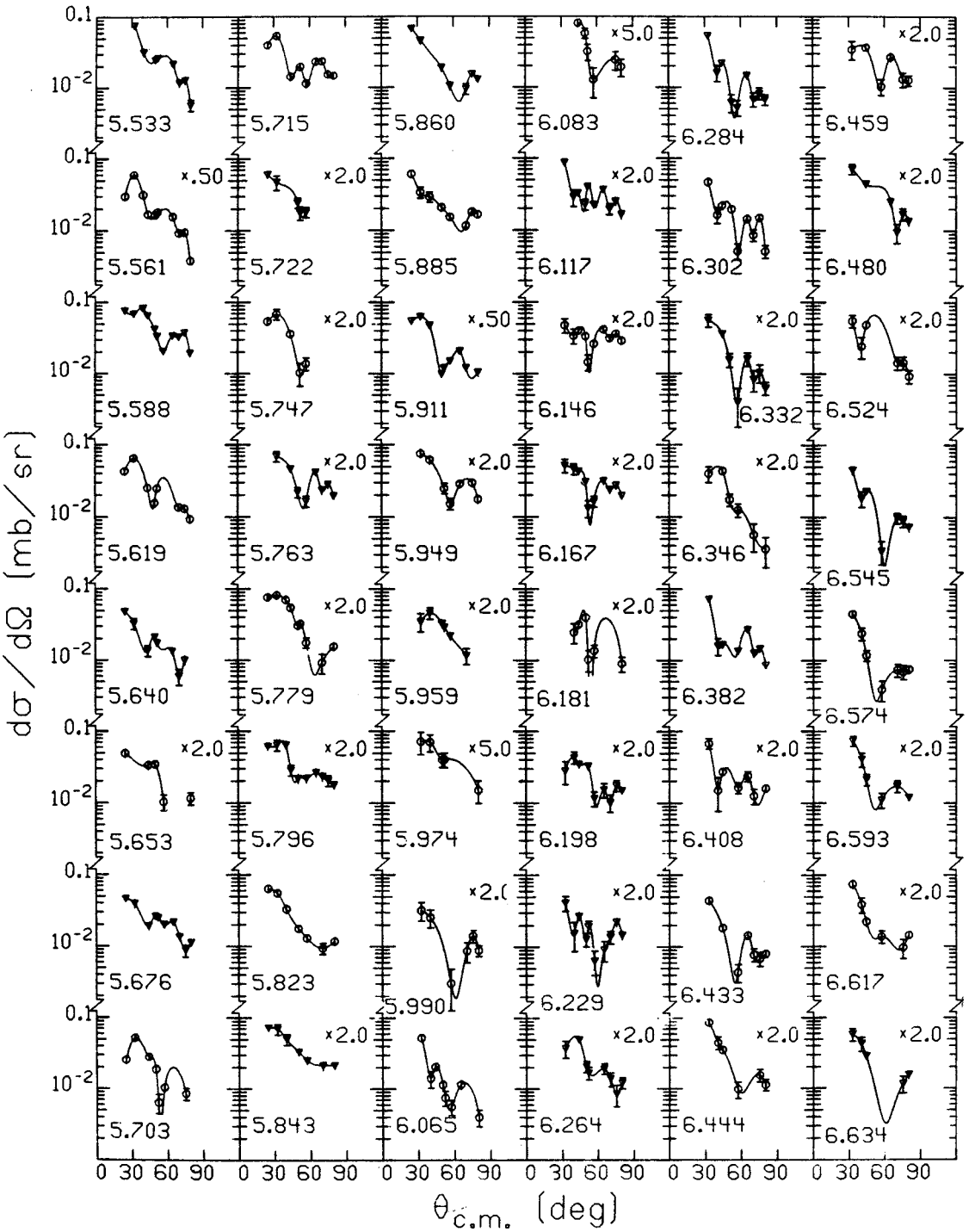
dσ/dΩ (mb/sr)
θc.m. (deg)
0 30 60 90
5.533
5.715
5.860
6.083
6.284
6.459
5.561
5.722
5.885
6.117
6.302
6.480
5.588
5.747
5.911
6.146
6.332
6.524
5.619
5.763
5.949
6.167
6.346
6.545
5.640
5.779
5.959
6.181
6.382
6.574
5.653
5.796
5.974
6.198
6.408
6.593
5.676
5.823
5.990
6.229
6.433
6.617
5.703
5.843
6.065
6.264
6.444
6.634

Figure III.3

REFERENCES FOR CHAPTER III

III.1 M. P. Webb, Nucl. Data 26, No. 1 (1979), 145.

III.2 G. Vallois, J. Saundinos, and O. Beer, Phys. Lett. 24B (1967), 512.

III.3 W. A. Lanford and G. M. Crawley, Phys. Rev. C 9 (1974), 646.

III.4 W. A. Lnaford, Phys. Rev. C 16 (1977), 988.

III.5 M. Kanbe, M. Fujioka, K. Hisatake, Nucl. Phys. A192 (1972), 151.

III.6 J. C. Manthurathil, D. C. Camp, A. V. Ramayya, J. H. Hamilton, J. J. Pinajian, and J. W. Doornebos, Phys. Rev. C 6 (1972), 1870.

CHAPTER IV

COLLECTIVE MODEL ANALYSIS

The usual method of extracting information on the spin and parity of a state and on the transition strength for the excitation of the level in a direct reaction is by making a comparison of the measured cross section with the results of a calculation using the Distorted Wave Born Approximation (DWBA). With this approach the experimental angular distributions are compared to DWBA angular distributions which have a characteristic shape determined by the strengths of each L-transfer involved. The problem is simplified here because ^{206}Pb has a 0^+ ground state. Thus, in a one step direct reaction all natural parity transitions can involve only one L-transfer. For a spherical nucleus such as ^{206}Pb, the collective vibrational model can be used to obtain the characteristic L-transfer shape.

The DWBA method is described here only briefly. A detailed description of the DWBA method is given in References IV.1, IV.2, IV.3.

A. Description of the DWBA Method

In DWBA the differential cross section $d\sigma/d\Omega$ for the direct reaction A(a,b)B is proportional to the square of

the transition amplitude.

$$T^{DW} = J\int d\vec{r}_\alpha \int d\vec{r}_\beta \chi_\beta^{(-)}(\vec{k}_\beta,\vec{r}_\beta)\langle B,b|V|A,a\rangle \chi_\alpha^{(+)}(\vec{k}_\alpha,\vec{r}_\alpha). \quad \text{(IV.1)}$$

Here $\vec{r}_\alpha$ is the displacement of the projectile a relative to the target nucleus A, $\vec{r}_\beta$ is the displacement of the outgoing particle b relative to the residual nucleus B, and J is the Jacobian of the transformation to these coordinates. The distorted initial and final waves are represented by $\chi_\alpha^{(-)}$ and $\chi_\beta^{(-)}$ respectively. The remaining factor in the transition amplitude is the matrix element of the interaction causing the transition, taken between the internal states of the colliding pairs:

$$\langle B,b|V|A,a\rangle = \int \psi_B \psi_b V \psi_A \psi_a d\xi. \quad \text{(IV.2)}$$

Here ξ represents all coordinates independent of $\vec{r}_\alpha$ and $\vec{r}_\beta$. The potential V is equal to $V_\beta - U_\beta$, where V_β is the interaction between B and b and U_β is the potential that generates the distorted wave χ_β. Usually one takes for U_β the potential that describes the elastic scattering.

For inelastic scattering two different approaches are possible: the macroscopic and the microscopic DWBA. The macroscopic DWBA will be examined here; in Chapter V the microscopic DWBA will be considered.

In the macroscopic DWBA the collective model is used to describe the wave functions ψ_A and ψ_B, and the potential U_β is assumed to be the optical potential, deformed similar

to the nucleus. In this case the equipotential surfaces can be characterised by

$$R(\theta,\phi) = R_o(1+\sum_{Lm} \alpha_{Lm} Y_L^m(\theta,\phi)), \qquad \text{(IV.3)}$$

where α_{Lm} are the deformation parameters and and are the polar coordinates in the lab coordinate system. The potential U' felt by the projectile can be expanded into a Taylor series according to

$$U'(R) = U(R_o) = U(R/(1+\sum_{Lm} \alpha_{Lm} Y_L^m(\theta,\phi)))$$

$$= U(R) - \sum_{Lm} \alpha_{Lm} Y_L^m (dU/dR) + \text{higher order terms.} \qquad \text{(IV.4)}$$

The first term of the right hand side of equation IV.4 is the potential which gives rise to the elastic scattering. The term linear in α_{Lm} induces inelastic scattering to collective states of multipolarity L. The higher order terms are neglected in DWBA calculations. With this formula the DWBA cross section can be calculated. For excitation of vibrational states one finds [Ref. IV.4]:

$$\frac{d\sigma}{d\Omega}(\theta) \sim \frac{\beta_L^2}{2L+1} \sigma_L(\theta), \qquad \text{(IV.5)}$$

$$\sigma_L(\theta) = \sum_m \left| \int dr \chi_\beta^{(-)}(\vec{k}_\beta, r) r \frac{dU}{dr} Y_L^m \chi_\alpha^{(+)}(\vec{k}_\alpha, r) \right|^2, \qquad \text{(IV.6)}$$

and

$$\beta_L^2 = \sum |\alpha_{Lm}|^2 = (2L+1)\frac{\hbar\omega_L}{2C_L}. \qquad \text{(IV.7)}$$

For this excitation ω_L is the frequency of the vibration

and C_L the "spring constant". For rotational excitation a similar expression can be written containing the frequency and moment of inertia of the deformed nucleus.

The collective description for inelastic scattering is rather simple, since only the optical model potential is needed to perform the distorted wave calculations. The only adjustable parameter is β_L^2. The value of β_L^2 for excitation of a level is found by normalization of the DWBA angular distribution to the experimental one:

$$\beta_L^2 = \left(\frac{d\sigma}{d\Omega}\right)_{exp} / \left(\frac{d\sigma}{d\Omega}\right)_{DW}. \qquad \text{(IV.8)}$$

The deformation parameter β_L may be used to determine the reduced transition probability G_L in single particle units (s.p.u.). This relation is given by:

$$G_L = \frac{(3+L)^2}{4\pi(2L+1)} Z^2 \beta_L^2, \qquad \text{(IV.9)}$$

where Z is the atomic number of the target.

Another quantity of interest is the fraction of the energy-weighted sum rule (EWSR) limit for a particular multipole contained in the observed transitions. The sum of the observed energy weighted transition strength is given by:

$$S_L = \sum_f G_{L_f} E_f, \qquad \text{(IV.10)}$$

where the sum is taken over all final states f of energy E_f reached by a particular multipolarity L.

Although equation IV.6 is only valid for the

excitation of collective states, the calculated angular distribution is also used generally to assign L-values. This is often possible because the shape of the angular distribution is mostly determined by the angular part of the matrix element (Equation IV.2). However, the L-values obtained should be treated with caution especially when the fit is not very good.

B. Elastic Scattering and the Optical Model

For comparison with the measured angular distributions, the DWBA collective model calculations were performed using the computer code DWUCK [Ref. IV.5]. A sample of the input to this code may be found in Appendix II. The optical model parameters used in the analysis are the general set of Becchetti-Greenless [Ref. IV.6]. Because the Becchetti-Greenless parameters are functions of the particle energy, the energy dependence of the incoming and outgoing distorted waves is accounted for. The set of optical model parameters used is listed on Table IV.1.

A comparison of the measured elastic scattering angular distribution with a calculation using these parameters is shown in Figure IV.1. Since the target thicknesses were known only approximately, the normalization of elastic scattering to this calculation is used to determine the value for the thickness of the different targets. Using this procedure the absolute cross sections are

believed to be accurate within ten percent.

C. L-transfers and Deformation Parameters

Angular distributions for natural parity states are very characteristic of the angular momentum transfer. Comparisons of collective model fits to identified states are displayed in Figures IV.2 and IV.3 and discussed below. The L-transfers are determined by comparing the data with theoretical angular distributions, and with experimental cross sections of states with unambiguous L-assignments. The experimental cross sections used in this comparison include both ^{206}Pb states observed in this experiment and ^{208}Pb states observed in the 35 MeV proton study by Wagner et al [Ref. IV.7]. The deformation parameters and L-transfer assignments for states with excitation energies below 4.6 MeV are given in Table III.1 for comparison with the measurements of References IV.8 and IV.9. Where possible those states with angular distributions of unidentifiable shape have J^{π} adopted from Reference IV.8. The L-assignments and deformation parameters of levels above 4.6 MeV are given in Table III.2. Since above 4.6 MeV so many new states are observed in the present experiment and the correspondence of levels seen in different experiments is uncertain, the results of this experiment are not compared to previous studies in this region.

TABLE IV.1

OPTICAL MODEL PARAMETERS USED IN DWBA CALCULATIONS

	V_R	r_R	A_R	W_V	W_{SF}	r_I
In:	-53.247	1.170	0.750	-5.000	-5.497	1.320
Out:	-54.099	1.170	0.750	-4.415	-6.126	1.320

	A_I	V_{SO}	W_{SO}	r_{SO}	A_{SO}	r_C
In:	0.653	-6.20	0.00	1.010	0.750	1.189
Out:	0.653	-6.20	0.00	1.010	0.750	1.189

Figure IV.1

Comparison of the measured elastic angular distribution with the DWBA calculation explained in the text.

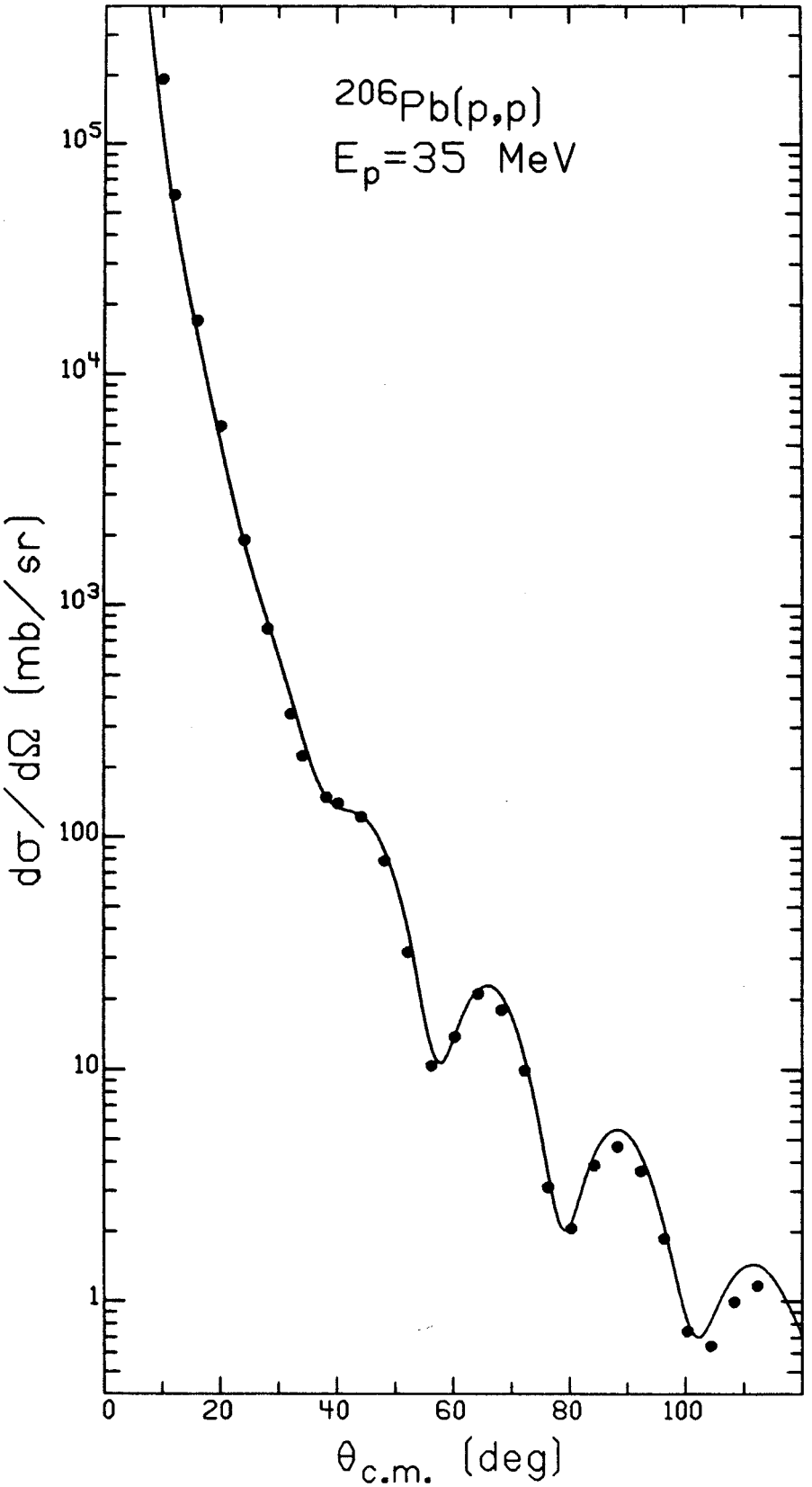
^{206}Pb(p,p)
E_p=35 MeV
10^5
10^4
10^3
100
10
1
dσ/dΩ (mb/sr)
0
20
40
60
80
100
$\theta_{c.m.}$ (deg)

Figure IV.1

Figure IV.2

Collective model fits for identified states. Displayed with the fits are the excitation energy of the state and the deformation parameter, β_L, corresponding to orbital angular momentum transfer L.

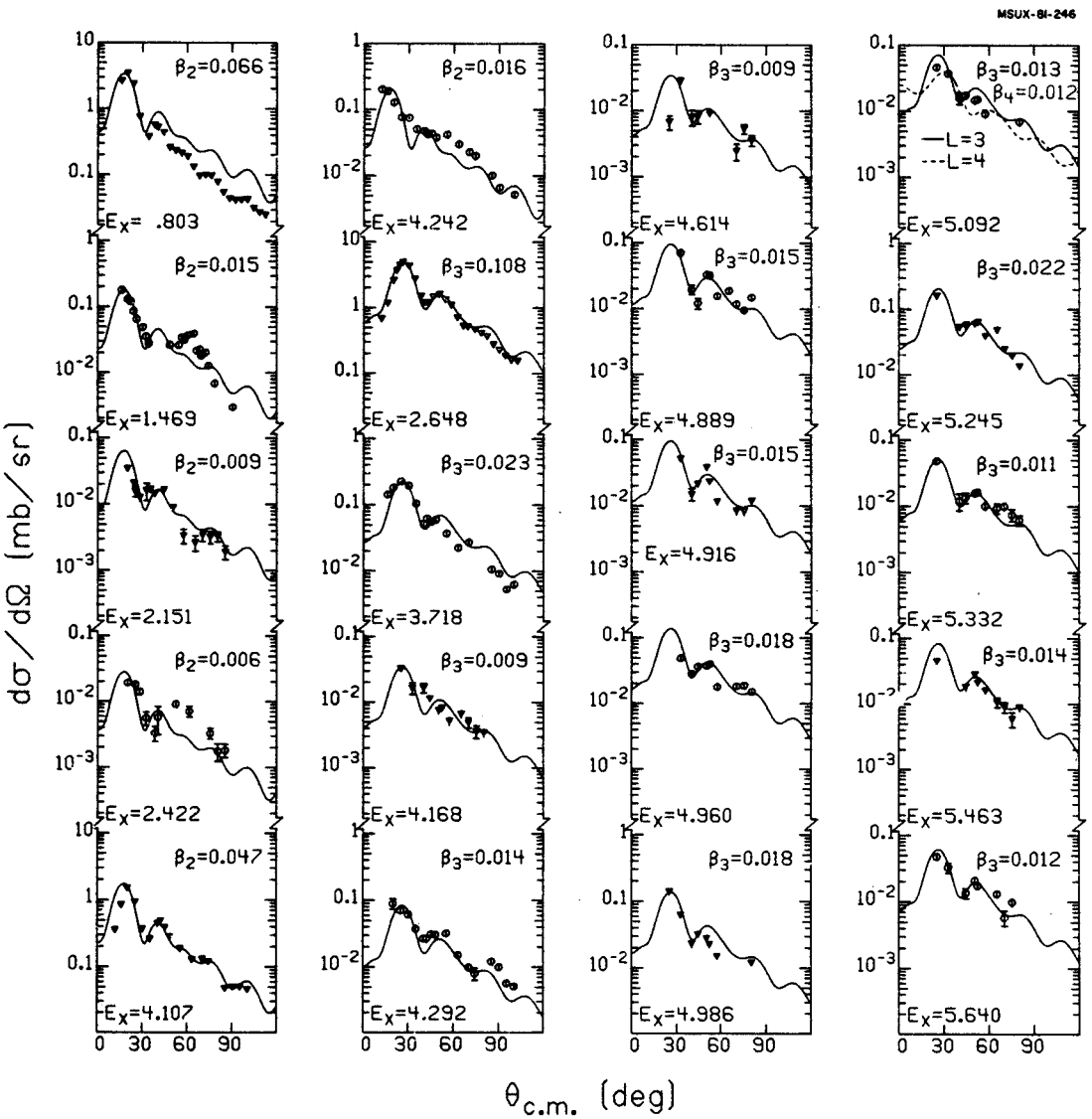
MSUX-81-246
dσ/dΩ (mb/sr)
θc.m. (deg)
β2=0.066
Ex= .803
β2=0.015
Ex=1.469
β2=0.009
Ex=2.151
β2=0.006
Ex=2.422
β2=0.047
Ex=4.107
β2=0.016
Ex=4.242
β3=0.108
Ex=2.648
β3=0.023
Ex=3.718
β3=0.009
Ex=4.168
β3=0.014
Ex=4.292
β3=0.009
Ex=4.614
β3=0.015
Ex=4.889
β3=0.015
Ex=4.916
β3=0.018
Ex=4.960
β3=0.018
Ex=4.986
β3=0.013
β4=0.012
—L=3
---L=4
Ex=5.092
β3=0.022
Ex=5.245
β3=0.011
Ex=5.332
β3=0.014
Ex=5.463
β3=0.012
Ex=5.640

Figure IV.2

Figure IV.3

Same as Figure IV.2

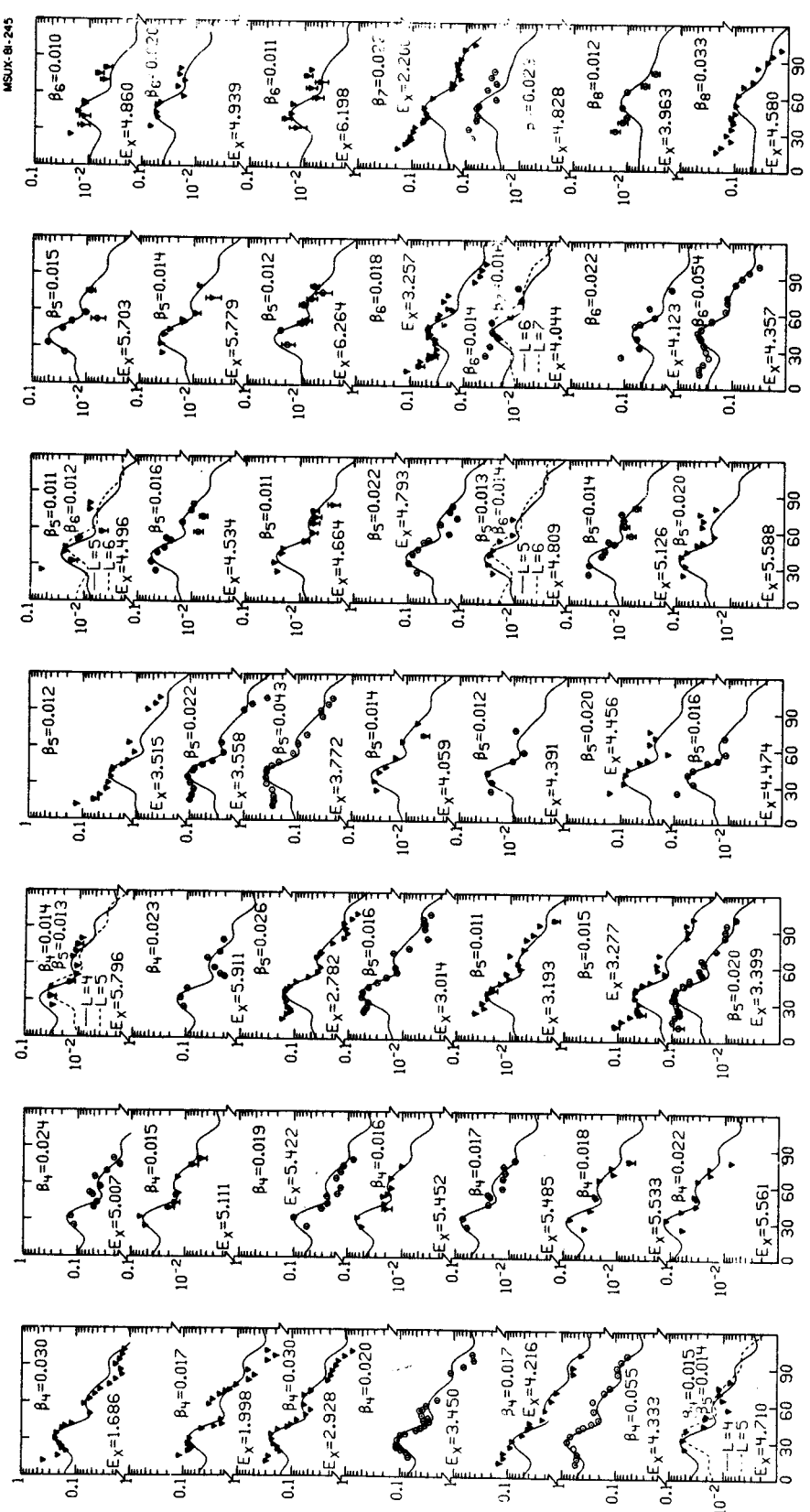

Figure IV.3

C-1. L=2 Transitions

Six probable quadrupole states were observed. These states have 17% of the total expected strength given by an EWSR. Most of the L=2 strength is concentrated in the first excited state at 0.803 MeV and a state at 4.107 MeV. These two states have transition strengths of 11.7 and 5.9 s.p.u. respectively. A well known 2^+ state at 1.469 MeV was observed. The excitation energy of this state is not in agreement with decay studies [Ref. IV.10] but is consistent with the energy measured in transfer reaction experiments [Ref. IV.11]. The states at 2.151 and 2.422 MeV were previously assigned a J^π value of 2^+. These levels are observed weakly excited in the present experiment but their angular distributions do show the characteristic L=2 shape. A state at 4.242 MeV was previously identified as a 5^- state [Ref. IV.12]. This experiment suggests an assignment of L=2.

Inelastic proton scattering from ^{208}Pb [Ref. IV.7] also identified six L=2 states with approximately the same total strength. However, all six states observed in ^{208}Pb had energies above 4 MeV of excitation.

C-2. L=3 Transitions

Previous experiments have only definitely identified one 3^- state at 2.648 MeV of excitation. Two other states at 5.444 and 6.045 MeV of excitation were tentatively assigned a J^π value of 3^- [Ref. IV.12]. The 2.648 MeV

level is the strongest excited state observed in the present experiment with a transition strength of 32.1 s.p.u. exhausting about 18% of an EWSR. The 3^- strength is fractioned and many other states with a characteristic L=3 shape were observed. In particular, the levels at 3.718 and 5.245 MeV are relatively strongly excited. The angular distribution of the 5.092 MeV state is fit equally well with L=3 or L=4 shapes so that the L-transfer is not uniquely determined. The observed 3^- states have 26% of the total expected strength given by the EWSR.

C-3. L=4 Transitions

The dominant 4^+ state observed was the 4.333 MeV level with a transition strength 8.8 s.p.u. The other well known levels at 1.686, 1.998, and 2.928 MeV were observed with transition strengths of 2.6, 0.8, and 2.6 s.p.u. respectively. New 4^+ states were identified which were not previously reported, notably the relatively strongly excited (>1 s.p.u.) states at 3.450, 5.007, 5.422, 5.561, and 5.911 MeV of excitation. There is some ambiguity in assigning the J^π of the levels at 4.710 and 5.796 MeV. Both of these levels could probably be equally well fit by an L=4 or an L=5 shape. The observed 4^+ states have 24% of the expected strength given by the EWSR.

C-4. L=5 Transitions

All known 5^- states were observed, the strongest being the state at 3.772 MeV of excitation with 5.8 s.p.u. of transition strength. Previously unreported levels at 4.456, 4.793 and 5.588 MeV are all relatively strongly excited. The L=5 assignment of the level at 3.515 MeV is in disagreement with the tentative 3^+ or 4^+ assignment of Reference IV.11. Before the first maximum at 37 degrees, this angular distribution is not fit well by a L=5 shape as can be seen in Figure IV.3. On the basis of this fit an assignment of L=5 seems rather weak. However, it has been previously noted [Ref. IV.13] that the predicted collective model cross section for large angular momentum transfer is usually smaller than the measured data at forward angles. This difference between data and theory is amplified as the spin of the state increases. An example of similar behavior can be observed by examining two well known 5^- states in ^{206}Pb at 2.782 and 3.277 MeV. Both states show this phenomena where forward angle data tend to rise relative to the calculation. Indeed the shape of the measured 3.277 MeV state is nearly identical to the state in question. As a result of the similarity of the 3.515 MeV state with established levels it has been tentatively assigned to be an L=5 transition.

C-5. L=6 Transitions

The only previously observed level seen in this

experiment is the strongly excited state at 4.357 MeV with 9.7 s.p.u. of transition strength. New L=6 levels observed include relatively strongly excited states at 3.257, 4.123, and 4.939 MeV.

C-6. L≥7 Transitions

Only two states were unambiguously identified as involving L=7 transitions. The established level at 2.200 MeV was identified with 1.7 s.p.u. of transition strength and a previously unidentified state at 4.828 MeV is tentatively assigned an L=7 shape with transition strength of 1.9 s.p.u. Transfer reaction experiments [Refs. IV.11, and IV.14] have found more L=7 strength in ^{206}Pb, and this experiment identifies states at similar excitation energies. However, these states are weakly excited and their angular distributions do not contain enough information to make reasonable L-assignments.

Two 8^+ states were observed with the strongest being the level at 4.580 MeV. This state has a transition strength of 4.2 s.p.u.

D. Systematics of Collective States in Lead Nuclei

The strongest states excited by direct reactions in the doubly magic nucleus ^{208}Pb are the collective 3^-, 5^-, 2^+, 4^+, 6^+, 8^+ levels between 2.5 and 5.0 MeV of excitation. Many experiments have been performed to examine the corresponding weak coupling states in ^{207}Pb

[c.f. Ref. IV.15 and referenced contained therein]. Several experiments [Refs. IV.9, IV.16, IV.17] have also been performed on ^{206}Pb to observe the analogous collective states in this nucleus. These experiments show a strong correlation in both energy and strength of the collective states in the three nuclei with the exception of the L=5 states. These states are now examined in the present experiment, and an explanation of the anomaly in the 5^- strength is sought.

Angular distributions of the even parity collective states are shown in Figure IV.4. The data are compared to the empirical angular distributions for the analogous states in ^{208}Pb [Ref. IV.7] and to collective model calculations. The agreement between the calculated angular distributions and the experimental results is generally very good. The shapes of the angular distributions of corresponding states in ^{206}Pb and ^{208}Pb are similar, but the states of ^{206}Pb are all weaker by approximately 30%. There is, however, still a one-to-one correspondence of the strong collective positive parity states in ^{206}Pb with those in ^{208}Pb, ie. the fractionation is not significant.

The angular distributions of the 3^- and 5^- collective states in ^{206}Pb are shown in Figure IV.5. Two states at 3.193 and 3.515 MeV excitation energy, which were not previously identified as 5^- states, have angular distributions which are fit best by an L=5 shape. The L=4

Figure IV.4

Angular distributions for positive parity excitations in proton scattering from ^{206}Pb. The solid lines represent collective DWBA calculations. The dashed lines represent interpolation of corresponding levels in ^{208}Pb. The excitation energy, Ex (MeV), indicated for each state is the value determined from the present data with uncertainties given in the text.

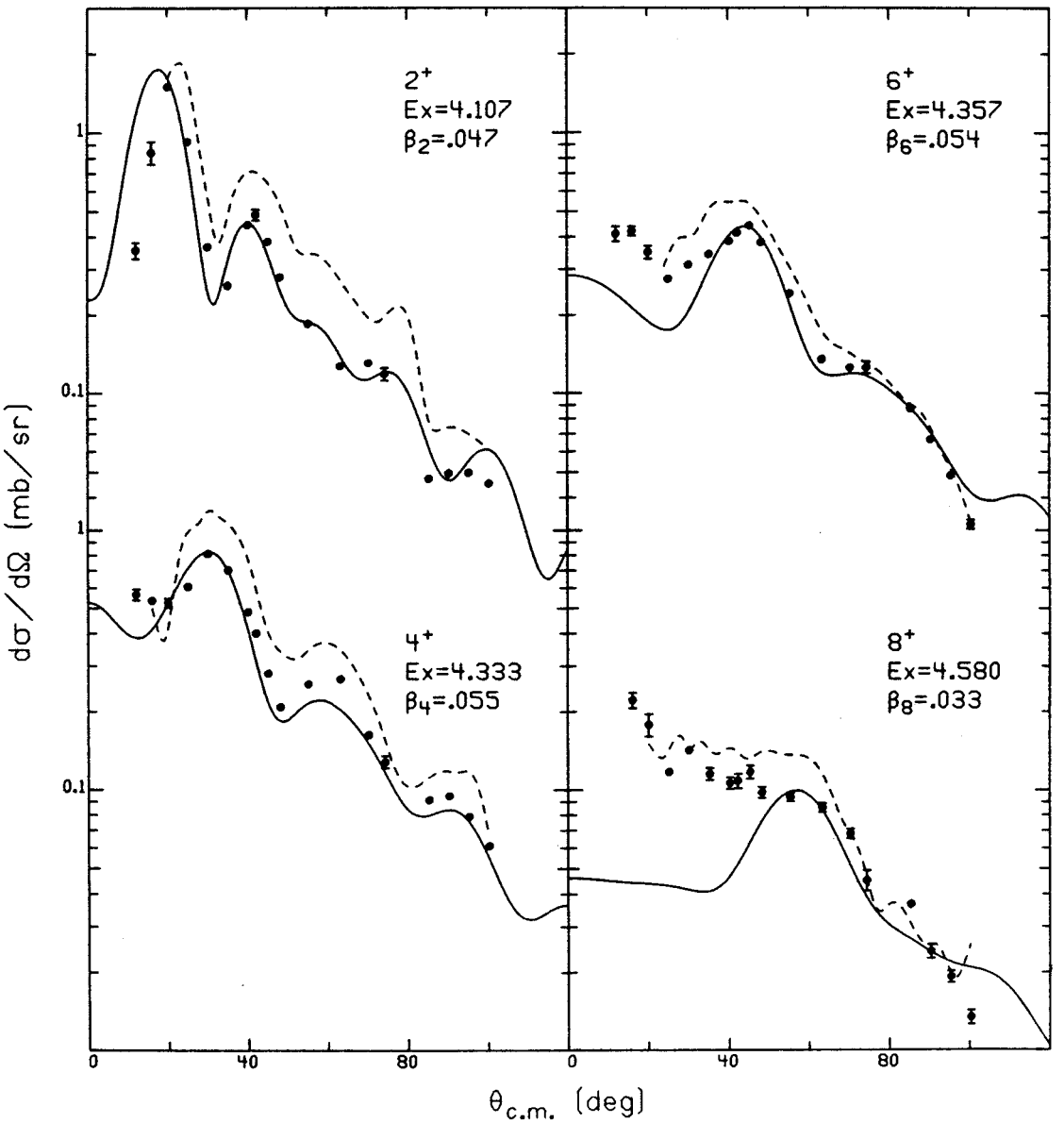
2+
Ex=4.107
β2=.047
6+
Ex=4.357
β6=.054
4+
Ex=4.333
β4=.055
8+
Ex=4.580
β8=.033
dσ/dΩ (mb/sr)
θc.m. (deg)
0
40
80
1
0.1

Figure IV.4

Figure IV.5

Angular distributions for negative parity excitations in proton scattering from ^{206}Pb. The solid lines represent collective DWBA calculations. The dashed lines shown with the 2.648 and 3.772 MeV states are interpolations of corresponding levels in ^{208}Pb [Ref. IV.7]. The excitation energy, Ex (MeV), indicated for each state is the value determined from the present data with uncertainties given in the text.

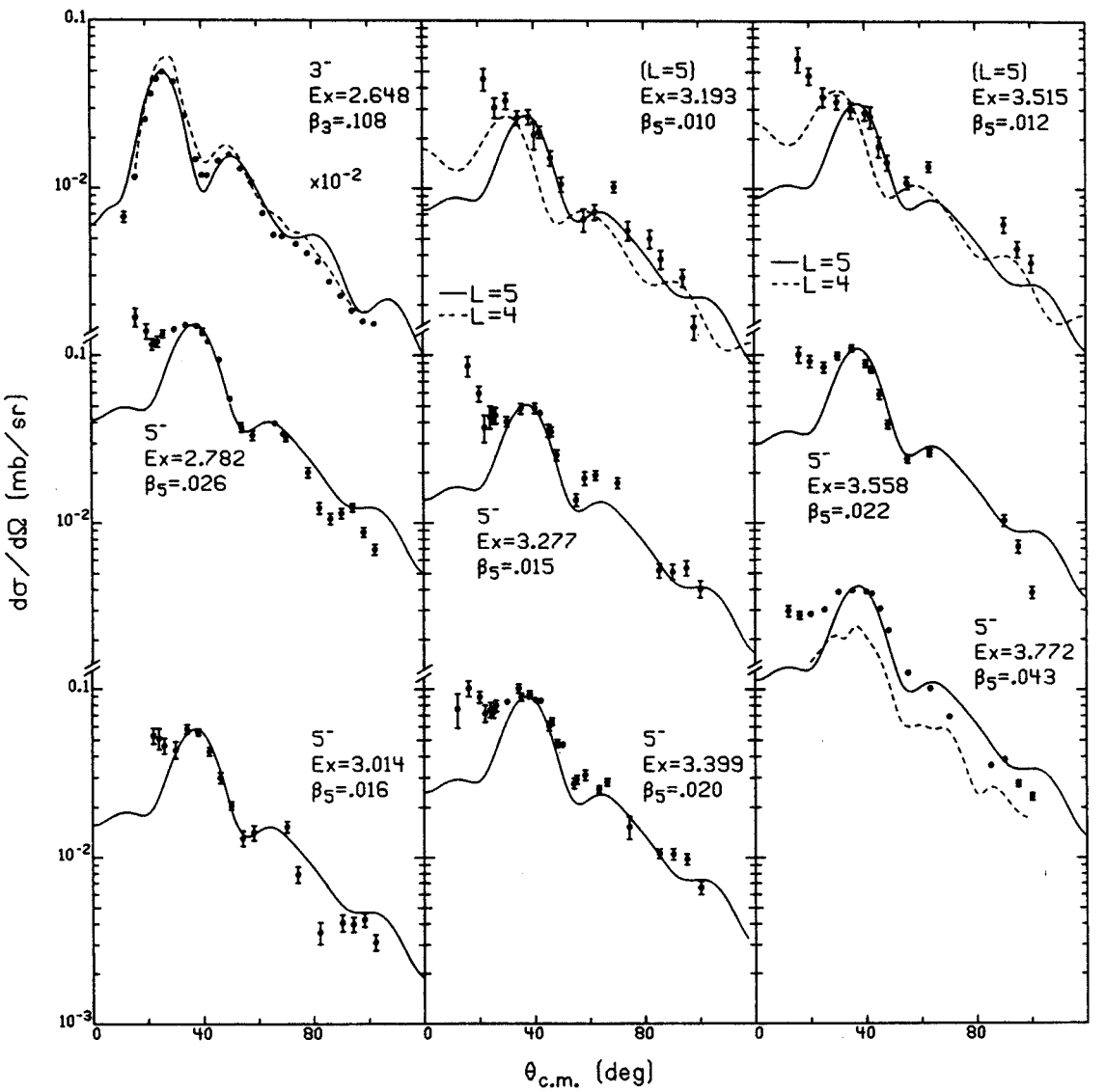
3⁻
Ex=2.648
β3=.108
x10⁻²
(L=5)
Ex=3.193
β5=.010
(L=5)
Ex=3.515
β5=.012
—L=5
---L=4
—L=5
---L=4
5⁻
Ex=2.782
β5=.026
5⁻
Ex=3.277
β5=.015
5⁻
Ex=3.558
β5=.022
5⁻
Ex=3.014
β5=.016
5⁻
Ex=3.399
β5=.020
5⁻
Ex=3.772
β5=.043
dσ/dΩ (mb/sr)
θc.m. (deg)

Figure IV.5

calculation is also shown for comparison. The 3^- state at 2.648 MeV of excitation is the strongest excited state in ^{206}Pb and, like the even parity states, has a similar angular distribution with about 70% of the strength of the 2.615 MeV 3^- state in ^{208}Pb.

However, in contrast with the states discussed above, there are eight 5^- states in ^{206}Pb with significant strength as opposed to two such states in ^{208}Pb. The 5^- state in ^{206}Pb at 3.772 MeV of excitation probably corresponds to the 5^- state in ^{208}Pb at 3.709 MeV of excitation [Ref. IV.17], and is slightly stronger than that state. However, it has also been observed that there is no single analog to the 5^- state in ^{208}Pb at 3.198 MeV of excitation in either ^{206}Pb [Ref. IV.17] or ^{207}Pb [Ref. IV.15]. Wagner, et al [Ref. IV.15] have observed six L=5 states in this region in ^{207}Pb with a total of 85% of the core strength in ^{208}Pb. ^{206}Pb data shows seven possible L=5 states in this region of excitation summing to 80% of the ^{208}Pb core strength. The summed transition strength is given by the relation

$$\text{Summed transition strength} = [\sum_i \beta_L^2(E_i)]^{\frac{1}{2}}. \qquad \text{(IV.11)}$$

In figure IV.6 the levels of interest here of all three nuclei are plotted with their relative strengths shown. A comparison of these collective levels with transition strengths for all individual levels is presented in Table IV.2. These results suggest a spreading of the L=5

Figure IV.6

Levels for which angular distributions were measured together with those measured in Ref. IV.15. The numbers give the transition strength.

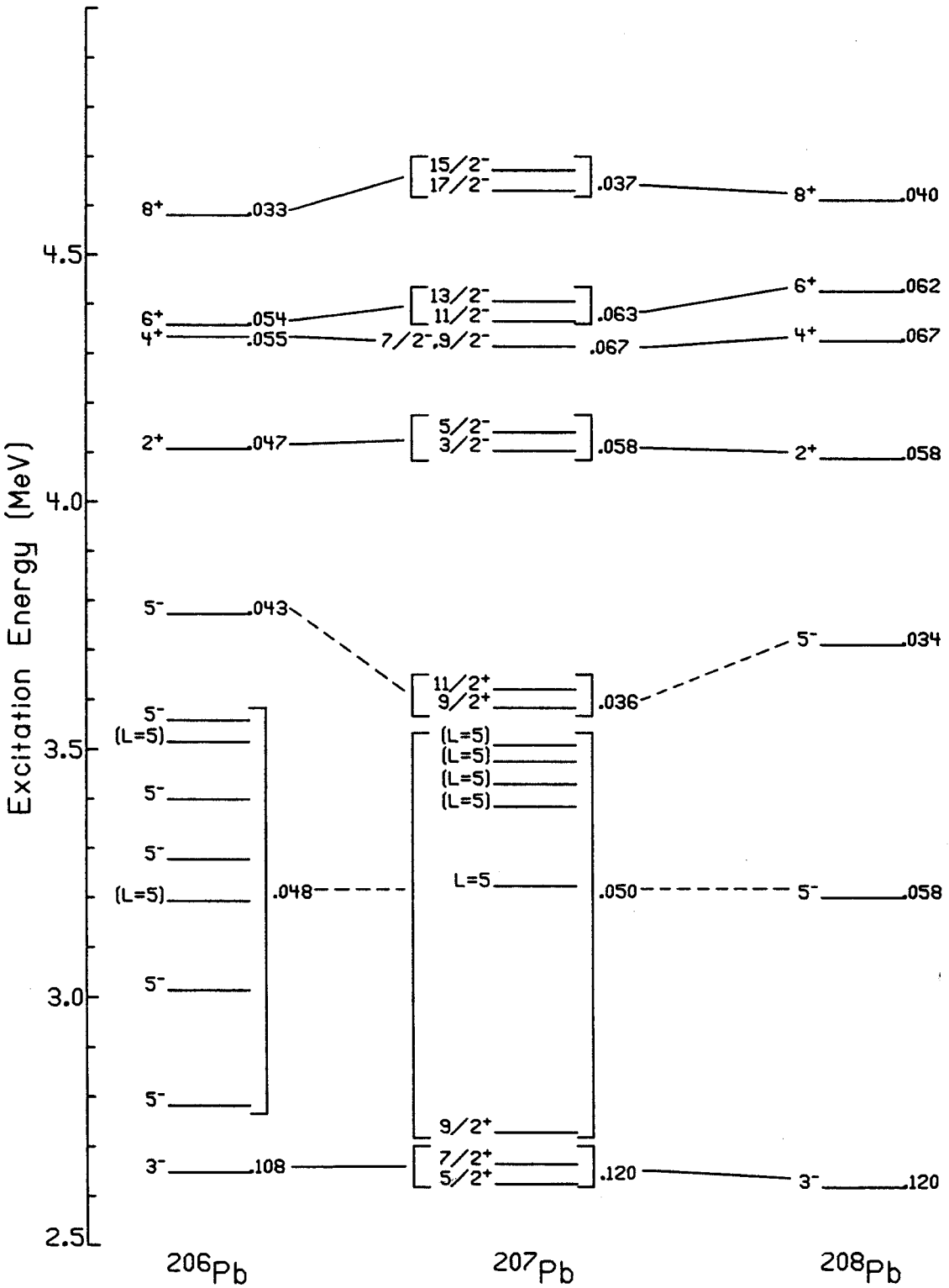
Excitation Energy (MeV)
4.5
4.0
3.5
3.0
2.5
206Pb
207Pb
208Pb
8+ .033
6+ .054
4+ .055
2+ .047
5- .043
5- (L=5)
5-
5-
(L=5) .048
5-
5-
3- .108
15/2- 17/2- .037
13/2- 11/2- .063
7/2-,9/2- .067
5/2- 3/2- .058
11/2+ 9/2+ .036
(L=5) (L=5) (L=5) (L=5)
L=5 .050
9/2+
7/2+ 5/2+ .120
8+ .040
6+ .062
4+ .067
2+ .058
5- .034
5- .058
3- .120

Figure IV.6

strength in both ^{207}Pb and ^{206}Pb with only one or two neutrons removed from the ^{208}Pb core. These phenomena may be explained at least qualitatively by examining the wave functions of these states.

The wave functions of ^{206}Pb have been calculated and examined for the region below 2.6 MeV of excitation, but very little is known about the wave functions of the higher energy levels. Fortunately, much work has been done in this energy region on the nucleus ^{208}Pb [c.f. Refs. IV.18 and IV.19 and references contained therein]. Figure IV.7 is a schematic representation of the location of the single-particle and single-hole neutron and proton shell model orbitals, above and below the N=126, Z=82 magic, shell closing energy gaps. Examining the 5^- state at 3.198 MeV of excitation in ^{208}Pb shows that the wave function has a large aplitude ($\cong$ 0.8) neutron $g_{9/2}, p_{1/2}^{-1}$ component. Hence, if one takes the simplest picture of ^{206}Pb as having an empty $p_{1/2}$ neutron shell then one would expect there to be no 5^- state with significant strength corresponding to the 3.198 MeV state in ^{208}Pb. On the other hand, ^{206}Pb is not so simple and is known to have a $p_{1/2}$ neutron in the ground state with a probability of about 40% [Ref. IV.20] so that some strength will remain. Thus in practice, it appears that the 5^- strength is substantially fractionated over at least seven states in ^{206}Pb and, surprisingly, the total strength is only about 20%

TABLE IV.2

COMPARISON OF THE STRONGLY EXCITED COLLECTIVE LEVELS IN ^{206}Pb, ^{207}Pb, and ^{208}Pb

^{206}Pb			^{207}Pb			^{208}Pb		
E_X	J^π	β_L	E_X	J^π	β_L	E_X	J^π	β_L
2.648	3^-	.108	2.628	$5/2^+$	.076	2.615	3^-	.126
			2.663	$7/2^+$	.087			
2.782	5^-	.026	2.728	$9/2^+$	.024	3.198	5^-	.058
3.014	5^-	.016	3.223	L=5	.013			
3.193	(L=5)	.010	3.384	(L=5)	.027			
3.277	5^-	.015	3.429	(L=5)	.016			
3.399	5^-	.020	3.476	(L=5)	.013			
3.515	(L=5)	.012	3.509	(L=5)	.025			
3.558	5^-	.022						
3.772	5^-	.043	3.583	$9/2^+$	.023	3.708	5^-	.034
			3.620	$11/2^+$	.028			
4.107	2^+	.047	4.103	$3/2^-$	.036	4.086	2^+	.058
			4.140	$5/2^-$	.045			
4.333	4^+	.055	4.313	$7/2^-$, $9/2^-$	.067	4.323	4^+	.067
4.357	6^+	.054	4.364	$11/2^-$	.042	4.424	6^+	.062
			4.404	$13/2^-$	.047			
4.580	8^+	.033	4.630	$17/2^-$	.028	4.610	8^+	.040
			4.671	$15/2^-$	.025			

Figure IV.7

Single-particle and single-hole levels in the lead region. The indicated energies are those at which these levels are fixed experimentally.

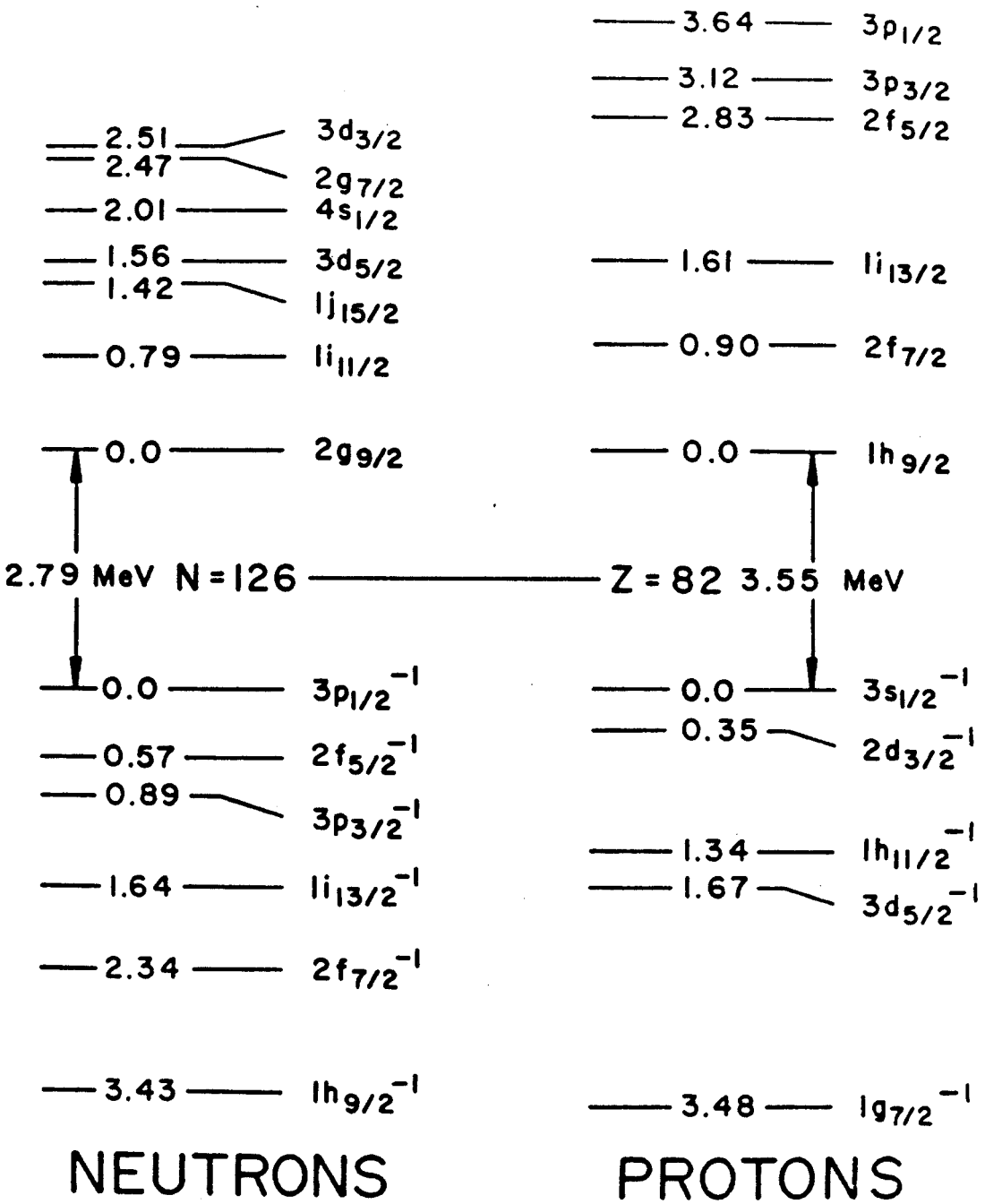
3.64 3p1/2
3.12 3p3/2
2.83 2f5/2
2.51 3d3/2
2.47 2g7/2
2.01 4s1/2
1.56 3d5/2
1.42 1j15/2
0.79 1i11/2
0.0 2g9/2
1.61 1i13/2
0.90 2f7/2
0.0 1h9/2
2.79 MeV N=126
Z=82 3.55 MeV
0.0 3p1/2-1
0.57 2f5/2-1
0.89 3p3/2-1
1.64 1i13/2-1
2.34 2f7/2-1
3.43 1h9/2-1
0.0 3s1/2-1
0.35 2d3/2-1
1.34 1h11/2-1
1.67 3d5/2-1
3.48 1g7/2-1
NEUTRONS
PROTONS

Figure IV.7

less than that observed in ^{208}Pb. This suggests that as well as the $g_{9/2}, p_{1/2}^{-1}$ particle-hole component there might be a more complex collective component present in the 3.198 MeV state of ^{208}Pb, which is difficult to detect in transfer reactions. This behavior is similar to that observed in the ^{40}Ca - ^{48}Ca region [Ref. IV.21], where both the 3^- and 5^- strengths were reduced and fractionated as one moved away from the closed $d_{3/2}$ shell and populated the $f_{7/2}$ shell with neutrons but again the decrease in the 5^- strength was less than expected on the basis of the particle-hole model.

The contrasting character of the 5^- state at 3.772 MeV in ^{206}Pb can also be understood by examining the wavefunction of the corresponding state in ^{208}Pb. The 3.709 MeV level in ^{208}Pb has been shown to be a mixture of many configurations [Refs. IV.18 and IV.19], none of which is dominant, and including only a small amount of $p_{1/2}$ strength. Hence, one would expect this state to behave like the other strongly excited states in ^{206}Pb. However, this state is significantly stronger in ^{206}Pb than in ^{208}Pb, suggesting that this state is possibly gaining collective strength from the fractionated L=5 states at lower excitation energy. The total L=5 strength in all eight 5^- states observed in ^{206}Pb is 96% of the total L=5 strength of the two 5^- states in ^{208}Pb.

E. Comparison of ^{206}Pb and ^{208}Pb Inelastic Strengths

The results of the collective model fits are presented in Figure IV.8 and are compared with the resutls of a similar experiment on ^{208}Pb [Ref. IV.7]. Here the strengths for each L-transfer ranging from 2 to 6, and $L \geq 7$ has been displayed according to excitation energy for each of the two nuclei, ^{206}Pb and ^{208}Pb. The definite correlation in both energy and relative strength of the five strong collective 3^-, 2^+, 4^+, 6^+, and 8^+ states in the two nuclei is again evident from this plot. In addition, this figure also shows that for the first two strong 5^- states in ^{208}Pb there are no similar states in ^{206}Pb.

The distribution of L=3 inelastic strength is quite similar in the two nuclei. This suggests that the octupole strength in this lead region is rather insensitive to the $p_{1/2}$ neutron population. However, the distribution of total inelastic strength in ^{206}Pb and ^{208}Pb is quite different for the other L-transfers.

In ^{208}Pb all the L=2, L=4, L=6, and $L \geq 7$ strength is above 4 MeV of excitation energy. In ^{206}Pb there is a significant excitation of all these L-transfers observed below 4 MeV. The L=5 strength is quite fractionated in ^{206}Pb, especially below 4 MeV of excitation energy. Furthermore, there is relatively little $L \geq 7$ inelastic strength observed in ^{206}Pb.

These results are in contrast to the study of

Figure IV.8

Results of collective model fits of ^{206}Pb compared to ^{208}Pb. The deformation parameter, β_L, is plotted against excitation energy for a number of L-transfers.

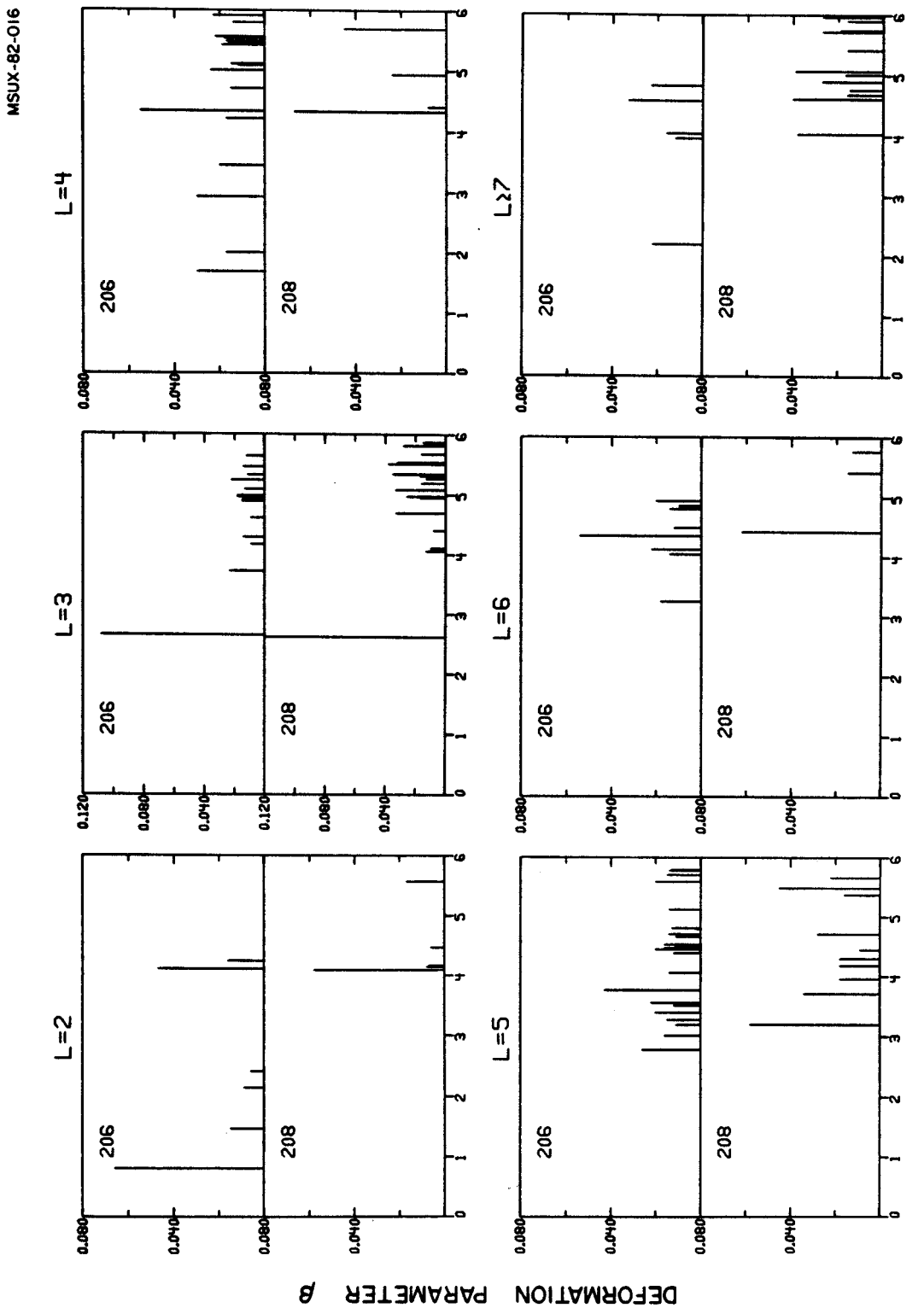
MSUX-82-016
L=2
L=3
L=4
L=5
L=6
L≥7
206
208
DEFORMATION PARAMETER β
EXCITATION ENERGY (MeV)

Figure IV.8

inelastic strength of the three nuclei, ^{207}Pb, ^{208}Pb, and ^{209}Bi, by Wagner et al [Ref. IV.15]. They showed clearly that the distribution of inelastic strength is quite similar in these three nuclei. This suggests a sensitivity in this lead region to the $p_{1/2}$ neutron population of all inelastic strength with the exception of the octupole strength.

F. Summary of the Collective Model Results

Almost one hundred-fifty angular distributions have been measured in the presen ^{206}Pb (p, p') experiment. For half of these transitions L-values have been determined using a macroscopic DWBA analysis. At excitation energies below about 4 MeV, previous studies have identified most of the levels and the results of this experiment agree quite well with these earlier results. A few new levels in this region have been identified in this experiment, and most of the L-assignments for states above 4 MeV of excitation were previously unreported.

The strongly excited even parity and 3^- states in the stable lead nuclei appear to be insensitive to any single particle structure. The 5^- states behave rather differently. When the core state in ^{208}Pb is principally dependent on the $p_{1/2}$ neutron single particle level, and these two neutrons are removed, the L=5 strength is fractionated, implying that the 5^- wave functions are probably more complicated than those suggested by the simple shell

model.

REFERENCES FOR CHAPTER IV

IV.1 G. R. Satchler, Nucl. Phys. 55 (1964), 1.

IV.2 N. Austern, Direct Nuclear Reaction Theories, Wiley, New York (1970).

IV.3 P. E. Hodgson, Nuclear Reactions and Nuclear Structure, Clarendon Press, Oxford (1971).

IV.4 R. H. Bassel, Phys. Rev. 149 (1966), 791.

IV.5 P. D. Kunz, University of Colorado, unpublished.

IV.6 F. D. Becchetti and G. W. Greenlees, Phy. Rev. 182 (1969), 1190.

IV.7 W. T. Wagner, G. M. Crawley, G. R. Hammerstein, and H. McManus, Phys. Rev. C 12 (1975), 757.

IV.8 M. P. Webb, Nucl. Data 26, No. 1 (1979), 145.

IV.9 G. Vallois, J. Saudinos, and O. Beer, Phys. Lett. 24B (1967), 512.

IV.10 J. C. Manthuruthil, D. C. Camp, A. V. Ramayya, J. H. Hamilton, J. J. Pinajian, and J. W. Doornebos, Phys. Rev. C 6 (1972), 1870.

IV.11 W. A. Lanford and G. M. Crawley, Phys. Rev. C 9 (1974), 646.

IV.12 E. R. Flynn, R. A. Broglia, R. Liotta, and B. S. Nilsson, Nucl. Phys. A221 (1974), 509.

IV.13 M. Lewis, F. Bertrand, and C. B. FUlmer, Phys. Rev. C 7 (1973), 1966.

IV.14 W. A. Lanford, Phys. Rev. C 16 (1977), 988.

IV.15 W. T. Wagner, G. M. Crawley, and G. Hammerstein, Phys. Rev. C 11 (1974), 486.

IV.16 J. Saudinos, G. Vallois, and O. Beer Nucl. Sci. Appl. 3 (1967), 22.

IV.17 J. Alster, Phys. Lett. 25B (1967), 459.

IV.18 W. W. True and C. W. Ma, Phys. Rev. C 3 (1971), 2421.

IV.19 H. Heusler and P. von Brentano, Ann. of Phys. 75 (1973), 381.

IV.20 W. A. Lanford, Phys. Rev. C 11 (1975), 815.

IV.21 A. M. Bernstein and E. P. Lippincott, Phys. Rev. Lett. 17 (1966), 321.

CHAPTER

MICROSCOPIC MODEL ANALYSIS

Shell model calculations have been performed on ^{206}Pb [Refs. V.1 and V.2]. These calculations predict both the energy and wave function of low lying natural and unnatural parity states. Since natural parity states are excited primarily by the well understood central force, a comparison of the measured angular distributions to those predicted by microscopic calculations allow a suitable test of the wave functions. Unnatural parity states are excited by central and noncentral forces. Performing microscopic calculations on unnatural parity states with well determined wave functions permit an investigation of the reaction mechanisms for exciting these states.

In this chapter a description of the microscopic DWBA is given first. Then the interactions and wave functions used in the calculations are discussed. Finally predicted cross sections of natural and unnatural parity states are presented and analyzed.

A. Description of the Microscopic DWBA Method for Inelastic Scattering

In the microscopic DWBA one tries to understand inelastic scattering starting from the nucleon-nucleon

interaction and the motion of the individual nucleons. The interaction potential V is assumed to be the sum over two body interactions between the projectile p and the target nucleons i, so $V=\sum_i v_{ip}$.

The interaction v_{ip} has a central part, a tensor part, and a two-nucleon spin-orbit ($L \cdot S$) part [Refs. V.3 and V.4]. The central part of v_{ip} can be written as

$$v_{ip}^{(c)} = V_o g_o(r) + V_\sigma \vec{\sigma}_i \vec{\sigma}_p g_\sigma(r) + V_\tau \vec{\tau}_i \cdot \vec{\tau}_p g_\tau(r) + V_{\sigma\tau} (\vec{\sigma}_i \cdot \vec{\tau}_p)(\vec{\tau}_i \cdot \vec{\tau}_p) g_{\sigma\tau}(r), \qquad (V.1)$$

where spin and isospin operators are represented by σ and τ, or as

$$v_{ip} = V^{SE} + V^{SO} + V^{TE} + V^{TP}, \qquad (V.2)$$

where SE stands for singlet-even, etc.

The interaction v_{ip} can be given a certain shape (for instance a Yukawa shape) and then the strengths V_o, V_σ, V_τ, and $V_{\sigma\tau}$ can be adjusted in order to fit experimental data (phenomenological point of view). A more fundamental approach is to take an effective nucleon-nucleon interaction, such as the long-range part of the Hamada-Johnston potential [Ref. V.5] or a Reid soft-core potential [Ref. V.6], and afterwards make a test with selected experimental data.

For the tensor part of v_{ip} the following form is used

[Ref. V.3]:

$$v_{ip}^{(t)} = \sum_{T=0,1} V_T^{(t)} g^{(t)}(r_{ip}) S_{ip}, \qquad (V.3)$$

with

$$S_{ip} = (\vec{\sigma}_i \cdot \vec{r}_{ip})(\vec{\sigma}_p \vec{r}_{ip})/r_{ip}^2 - (\vec{\sigma}_i \cdot \vec{\sigma}_p)/3. \qquad (V.4)$$

An analogous form is used for the spin-orbit part of v_{ip} with S_{ip} in Equation V.3 replaced by $\vec{L} \cdot \vec{S}$: the two-nucleon spin-orbit operator [Refs. V.7 and V.8].

The effect of exchange has to be taken into account [Refs. V.9]. This leads to the formula [Ref. V.3] for the antisymmetrised form of the transition amplitude (Equation IV.1) which can be written as

$$T = A\langle \chi_f^{(-)}(0) \Phi_{J_f M_f}(1,\cdots,A) - \chi_f^{(-)}(1) \Phi_{J_f M_f}(0,2,3,\cdots,A) \\ |V_{01}| \Phi_{J_i M_i}(1,\cdots,A) \chi_i^{(+)}(0) \rangle, \qquad (V.5)$$

with A being the number of nucleons in the target. Particle 0 is the incoming particle and can be exchanged with one of the target nucleons. The exchange is explicitly included here by the term with $\chi_f^{(-)}$. The Φ_{J_i} and Φ_{J_f} are now fully antisymmetrised wave functions.

Since the interaction V_{01} is a two body interaction, the contributions to the matrix element occur from those parts of the initial and final wave function Φ_i and Φ_f which can only be connected by a single-particle transition, therefore, Equation V.5 can be written as

$$T_{if} = \sum_{j_1,j_2} \langle \Phi_{J_f} | a_{j_2}^{\dagger} a_{j_1} | \Phi_{J_i} \rangle \langle \chi_f^{(-)}(0)\phi_{j_2}(1) - \chi_f^{(-)}(1)\phi_{j_2}(0) \, | V_{01} | \chi_i^{(+)}(0)\phi_{j_1}(1) \rangle . \qquad (V.6)$$

The first term on the right hand side of Equation V.6 is the spectroscopic amplitude S ($a^{\dagger}$ is a creation operator and a is an annihilation operator). In this way the transition amplitude T can be written as a weighted sum of all inelastic scattering amplitudes in which a single bound nucleon in the j_1 shell is promoted to the j_2 shell. The value of the spectroscopic amplitude must be obtained from shell model calculations.

B. Forces Used in the Microscopic Calculations

In this study two different forces are employed for comparison to experimental results. The first set of interactions (Force A) uses the Serber exchange mixture for the central part of the interaction. This effective force has been found [Refs. V.10, V.11, and V.12] to be a good representation of the phenomenological force determined by fitting definitive reaction data. The Serber mixture had strengths of V_0= -30: V_σ=10: V_τ=10: $V_{\sigma\tau}$=10 MeV, and the radial form was taken to be a 1 fermi range Yukawa. The tensor force was taken from the works by Crawley et al [Ref. V.13] and by Fox and Austin [Ref. V.14], and resulted from fitting the crucial (1^+, T=0) to (0^+, T=1) transition in ^{14}N(p,p') ^{14}N(2.31 MeV) with a tensor force of the one pion exchange potential (OPEP)

with a r^2-Yukawa shape. The range was obtained by matching the OPEP and the strength adjusted to fit the nitrogen data. This study assumed that the tensor isoscalar portion was zero. The $\vec{L} \cdot \vec{S}$ force was taken from studies by Fox and Austin [Ref. V.14], in which the spin-orbit potential was obtained by matching the cutoff Hamda-Johnston potential. The radial shape was given by two Yukawas with respective proton and neutron strengths (ranges) of 29.1 and 20.1 MeV (0.577 fm) and -1496 and -752 MeV (0.301 fm). This set of interactions was used in a previous study of ^{208}Pb (p,p') by Wagner et al [Ref. V.15].

The second set of interactions (Force B) is from a study by Bertsch et al [Ref. V.16]. The force is derived by fitting to the harmonic oscillator matrix elements of the Reid [Ref. V.6] or Hamada and Johnston [Ref. V.17] nucleon-nucleon potentials. Several choices for the individual terms in the interaction are given in Reference V.16. The present calculations have utilized the sum of the interactions labeled 1, 4, 11, 14, 16, and 18 in Table 1 of that paper. This set is obtained mostly from the Reid interaction, and is the set preferred by the authors of Reference V.16. Similar sets of interactions were previously utilized in a study of 40 MeV protons inelastically scattered from ^{24}Mg [Ref. V.18], and in a study of unnatural parity states of ^{88}Sr excited by 17.2 MeV protons [Ref. V.19]. The latter study is of particular

interest here because ^{88}Sr, being two protons removed from the doubly magic nucleus ^{90}Zr, is similar in structure to ^{206}Pb, which is two neutrons removed from the doubly-magic nucleus ^{208}Pb.

C. Wave Functions Used in the Microscopic Calculations

The wave functions of the low-lying levels of ^{206}Pb are described by two neutron holes in the ^{208}Pb core. Shell model calculations based on these two interacting neutron holes have been performed for ^{206}Pb with both the Tamm-Dancoff approximation (TDA) and the random phase approximation (RPA). In the present microscopic calculations wave functions derived from both methods are utilized. The TDA wave functions have been obtained from the work of True and Ma [Ref. V.20], who employe a phenomenological nucleon-nucleon interaction of a Gaussian central force plus a weak-coupling force, with a conventional shell-model calculation. RPA wave functions come from the work of Vary and Ginocchio [Ref. V.21] who use a central interaction. In general the energies predicted by the TDA are in slightly better agreement with experimental results than the RPA predictions. However, electromagnetic transition rates are given more accurately with the RPA.

D. Results of Microscopic Calculations

Microscopic calculations were performed for identified unnatural parity states and a number of low-lying

natural parity states with the code DWBA-70 of Schaeffer and Raynal [Ref. V.22]. The code utilizes the helicity formalism [Ref. V.23] and allows the treatment of real interactions with central, tensor, and spin-orbit components, and an exact treatment of "knock-on" exchange. A sample of the input to DWBA-70 may be found in Appendix II.

D-1. Natural Parity States

Microscopic calculations of the angular distributions of natural parity states predicted by both sets of interactions and by both sets of wave functions are shown in Figures V.1 through V.4. Both direct and direct-plus-exchange calculations are presented. An asterisk indicates the direct calculation. For these microscopic calculations, the results with Force A are given by the solid curves while the dashed curves indicate results using Force B.

Considered first are states of normal parity lying below the dominant 3^- level at 2.648 MeV. Displayed in Figure V.1 are cross sections predicted by the RPA wave functions of the first excited 0^+ state, the first five 2^+ states, the first two 4^+ states and the first 7^- state. The strongest state in this region of excitation is the first excited state of ^{206}Pb, the 2^+ state of 0.803 MeV. The shape of this angular distribution is reproduced well by the calculation. However, its magnitude is underestimated by about a factor of three. Levels of moderate

Figure V.1

Microscopic model fits for low-lying natural parity states using RPA wave functions. The solid lines correspond to calculations done with Force A; the dashed curves show results using Force B. The asterisks indicate only direct calculations. The curves without asterisks indicate calculations including exchange effects.

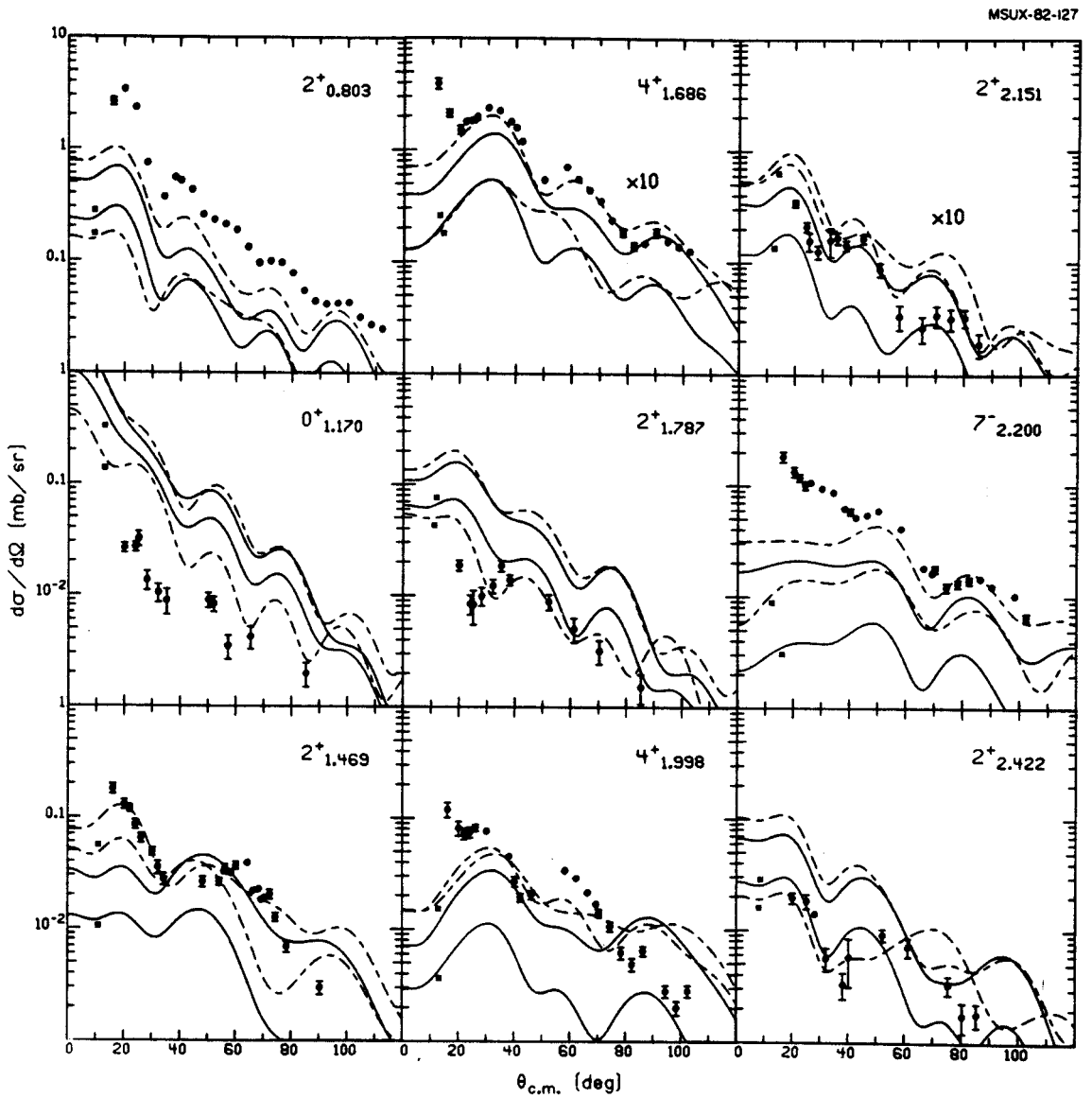
MSUX-82-127
2+ 0.803
4+ 1.686
×10
2+ 2.151
×10
0+ 1.170
2+ 1.787
7- 2.200
2+ 1.469
4+ 1.998
2+ 2.422
dσ/dΩ (mb/sr)
θc.m. (deg)

Figure V.1

strength in this region of excitation energy include the 2^+ state at 2.469 MeV, both 4^+ states, and the 7^- state. The shape and strength of these angular distributions are very well reproduced, especially by the calculations using Force B. Force B does better than Force A in matching the magnitude of the angular distributions and in reproducing the shape of these states of moderate strength. The success of Force B is especially clear at forward angles. The weakly excited 2^+ state at 2.151 MeV of excitation is best fit by Force A. The remaining weak 0^+ state and 2^+ states are overestimated by these calculations, however, the shapes are well reproduced in general.

Figure V.2 shows measured angular distributions of these same low-lying natural parity states compared with microscopic calculations using TDA wave functions. The 2^+ state at 0.803 MeV is underestimated by about an order of magnitude. The data for the collective 1.686 MeV 4^+ level is also stronger than predicted. In general the angular distributions of these states calculated using the TDA wave functions reproduce the weakly excited states as well as the RPA calculations, but give poorer agreement than the RPA calculations for the strongly and moderately excited states.

Examining the wave functions in detail reveals some differences between the RPA and TDA predictions. For all the 2^+ states, the 0^+ state and the 7^- state examined

Figure V.2

Same as Figure V.2 with TDA wave functions used in the calculations.

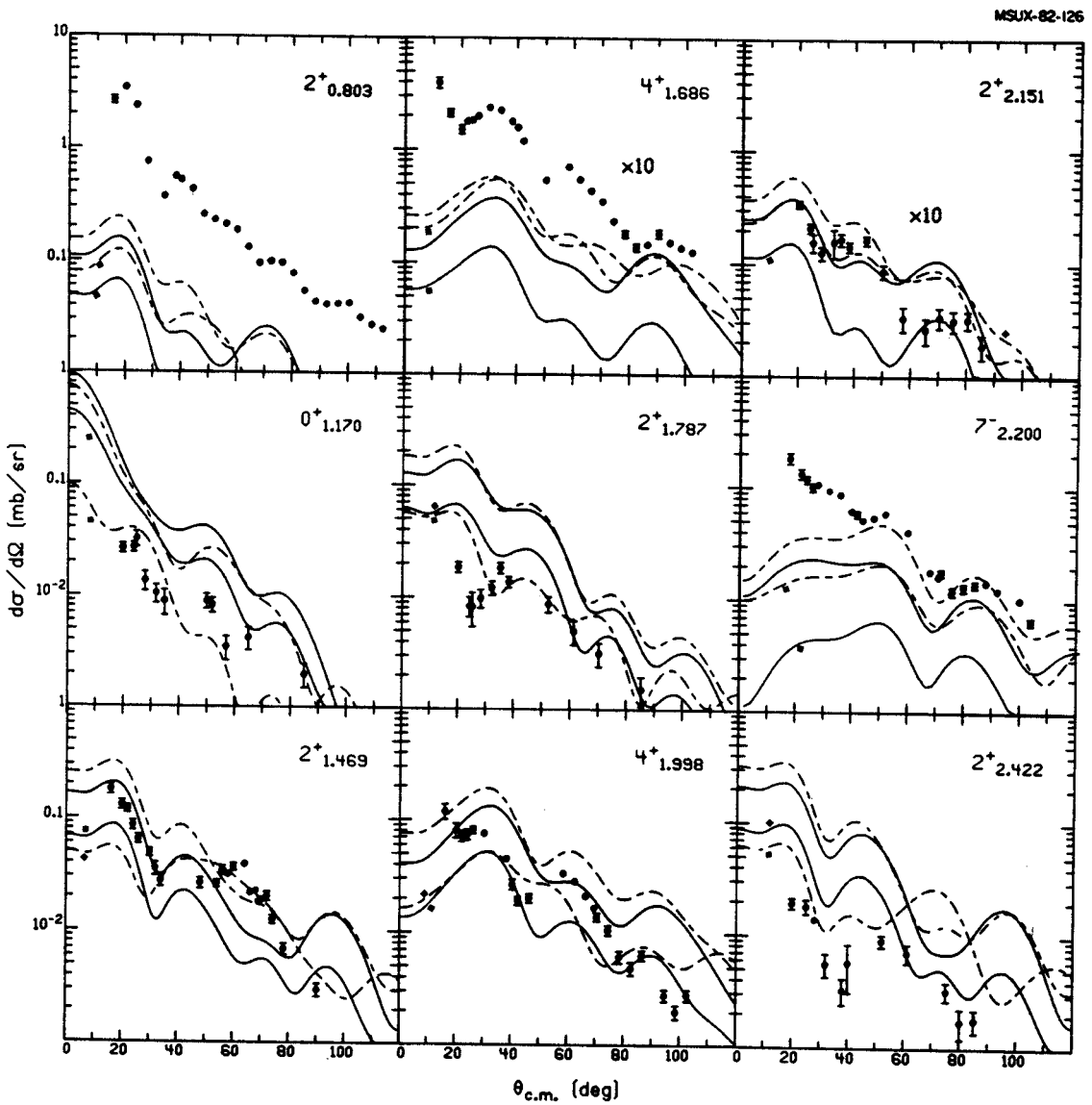
MSUX-82-126
2+0.803
4+1.686
×10
2+2.151
×10
0+1.170
2+1.787
7-2.200
2+1.469
4+1.998
2+2.422
dσ/dΩ (mb/sr)
θc.m. (deg)

Figure V.2

here, the main particle-hole component is consistently larger in the RPA wave functions. As an example, consider the 2^+ state at 0.803 MeV of excitation energy. The two predictions give:

$$\psi_{RPA} = .79|p_{1/2},f_{5/2}^{-1}>+.51|p_{1/2},p_{3/2}^{-1}>+.20|f_{5/2},f_{5/2}^{-1}>+$$
$$.18|p_{3/2},p_{3/2}^{-1}>+.17|p_{3/2},f_{7/2}^{-1}>+.12|f_{5/2},p_{3/2}^{-1}>,$$

$$\psi_{TDA} = .71|p_{1/2},f_{5/2}^{-1}>+.54|p_{1/2},p_{3/2}^{-1}>+.27|f_{5/2},f_{5/2}^{-1}>+$$
$$.21|p_{3/2},p_{3/2}^{-1}>+.20|p_{3/2},f_{7/2}^{-1}>+.17|f_{5/2},p_{3/2}^{-1}>.$$

The result is an improved fit with the RPA wave functions for all these levels except the 0^+ state. This suggests that these states have primarily a single particle-hole configuration, and that the 0^+ state is probably a mixture of several particle-hole components.

There is a major discrepancy between the predicted wave functions for the two 4^+ states. Both the TDA and the RPA predict these 4^+ states to have a configuration which is a combination of the $|f_{5/2},f_{5/2}^{-1}>$ and $|f_{5/2},p_{3/2}^{-1}>$ neutron particle-hole components. One of these components is always paramount while the second is of moderate strength. Other particle-hole components contribute only modestly to these wave functions. The RPA predicts the configuration of the 4^+ state at 1.686 MeV to be dominated by the $|f_{5/2},f_{5/2}^{-1}>$ component, and the 4^+ state at 1.998 MeV is dominated by the $|f_{5/2},p_{5/2}^{-1}>$ configuration. The

TDA wave functions for these two states have the same configurations of these particle-hole components, only reversed. The angular distributions of these 4^+ states are clearly predicted better using the RPA wave functions.

Examined next are several highly collective natural parity states with excitation energies around 3 MeV. In Figure V.3 measured angular distributions of the 4^+ state at 2.928 MeV, the 5^- states at 2.782 and 3.014 MeV, and the 6^+ state at 3.257 MeV are compared with calculations using RPA wave functions. The shape of these angular distributions are all reasonably well reproduced. The first 5^- state and the 4^+ state are underestimated by the calculations. The magnitude of the second 5^- state and the 6^+ state are accurately predicted by the calculations, especially by Force A. Shown in Figure V.4 are calculated angular distributions of these states using TDA wave functions. These wave functions yield very different results. With the exception of the second 5^- state, the predicted magnitudes fall far short of the data, by as much as a factor of 30 in the case of the 6^+ state. As was the case with some of the low-lying states the systematic difference between the two sets of wave functions is that the RPA wave functions have a larger concentration of strength in the principal particle-hole component. The RPA predicts the wave functions of both 5^- states to have an almost pure single particle-hole configuration, and the 4^+

Figure V.3

Microscopic Model fits for higher-lying natural parity states using RPA wave functions. The meanings of the curves and asterisks are the same as in Figure V.1.

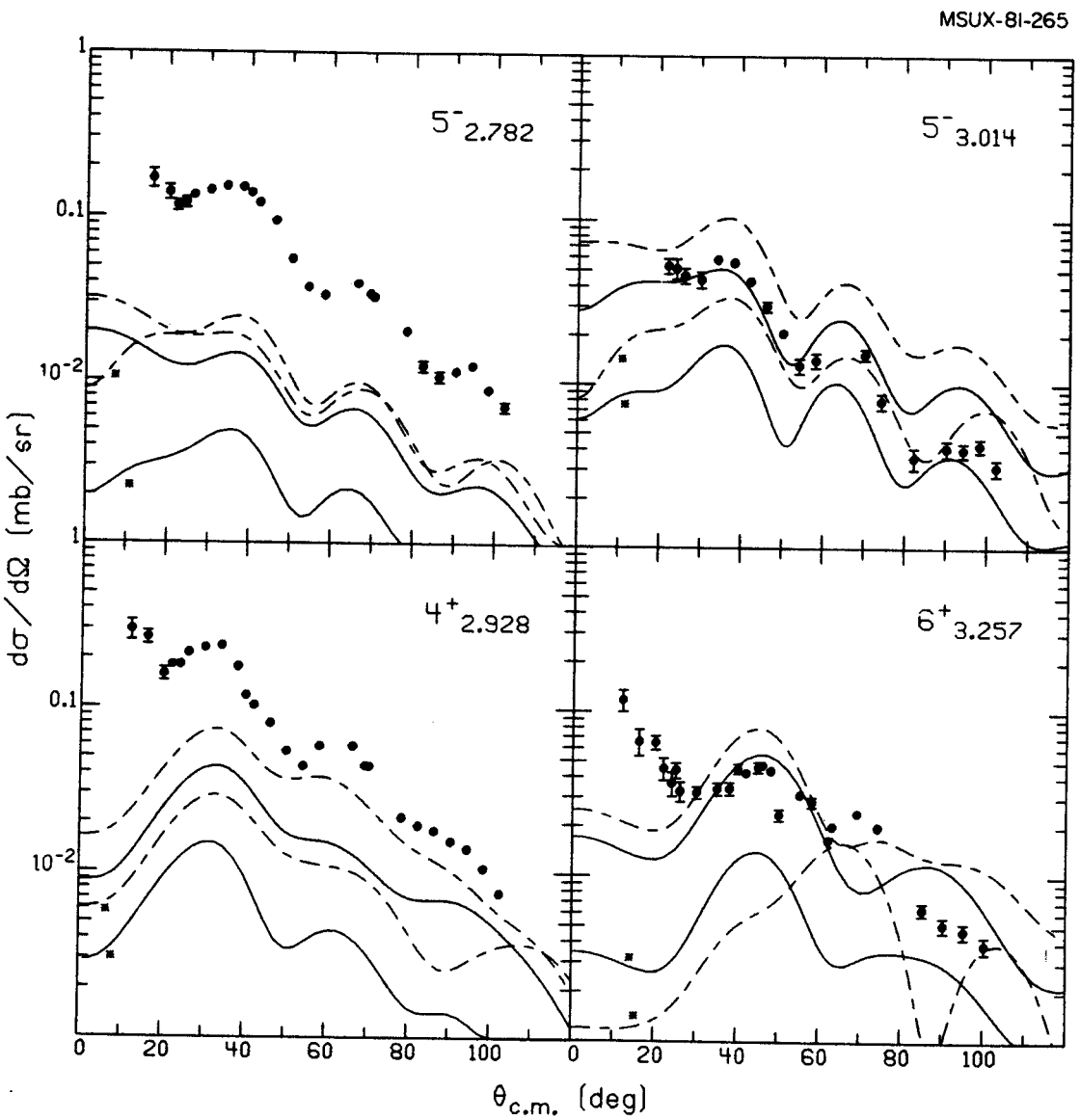
MSUX-81-265
5⁻ 2.782
5⁻ 3.014
4⁺ 2.928
6⁺ 3.257
dσ/dΩ (mb/sr)
θc.m. (deg)
1
0.1
10⁻²
0
20
40
60
80
100

Figure V.3

Figure V.4

Same as Figure V.3 with the TDA wave functions used in the calculations.

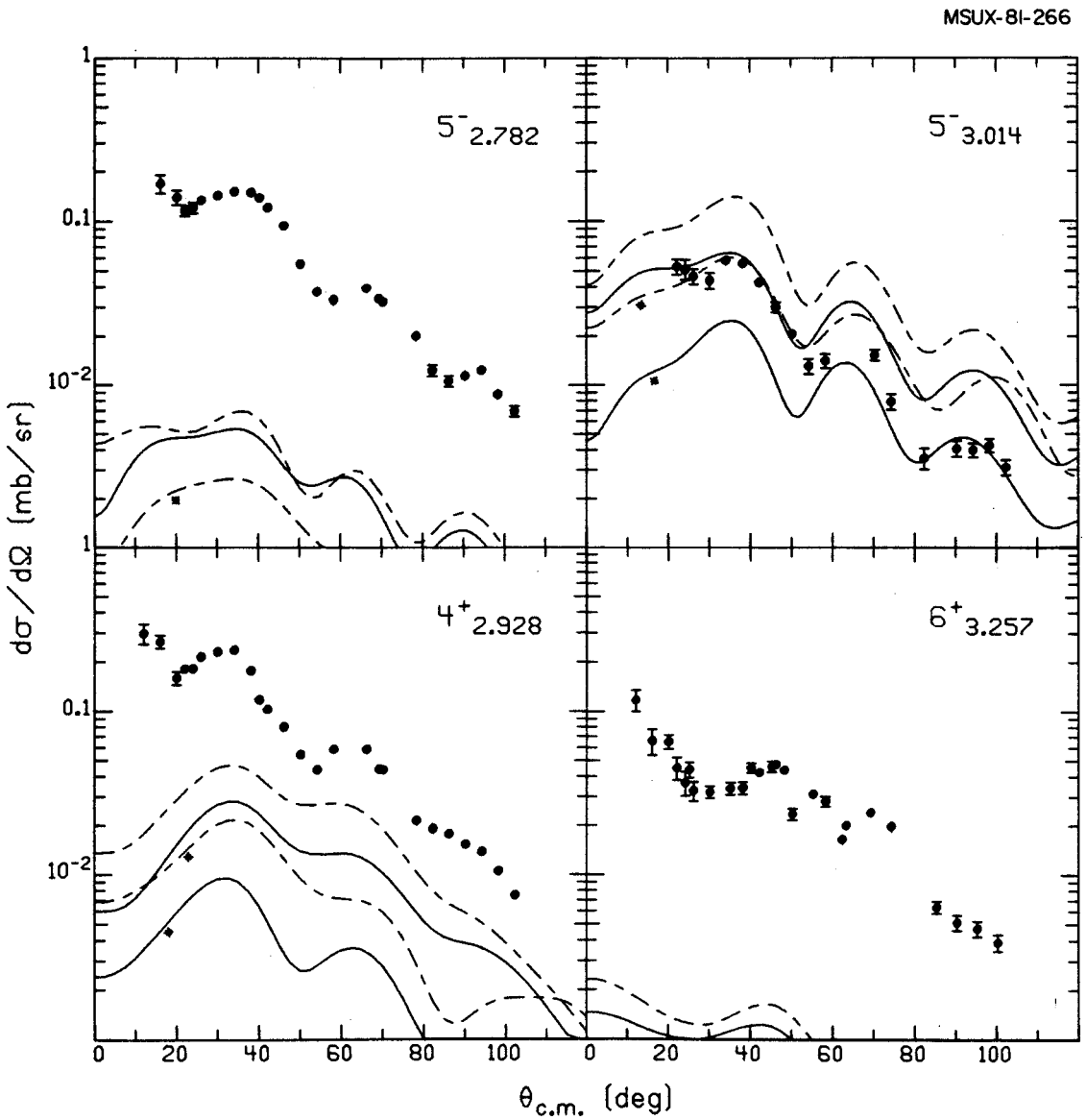
MSUX-81-266
5⁻ 2.782
5⁻ 3.014
4⁺ 2.928
6⁺ 3.257
dσ/dΩ (mb/sr)
θc.m. (deg)
1
0.1
10⁻²
0
20
40
60
80
100

Figure V.4

state to be about 93% pure. The TDA predicts these states to have a configuration of several particle-hole components with the largest component having about 75% of the strength. Here also is another major difference between the two sets of wave functions. The TDA predicts the largest neutron particle-hole component for the 6^+ state to be $|f_{5/2}, f_{7/2}^{-1}>$. The corresponding RPA wave function predicts this state to be an essentially pure $|g_{9/2}, g_{9/2}^{-1}>$ particle-hole state.

In figure V.5 the measured angular distributions of the 2^+ state at 1.469 MeV and the 4^+ state at 1.686 MeV are compared with angular distributions using Force A and Force B. Calculations using both the total forces are presented, and the force is broken down to show the contributions of the central and noncentral component parts independently. The calculations show clearly that the angular distributions of these natural parity states predicted by the total forces are dominated by the central part. For both states the central force is predicted to be larger using Force B. This increased central contribution results in a calculation with the complete Force B which is about fifty percent stronger than the calculation using Force A. Although the noncentral forces contribute weakly, it is instructive to note that the shapes of the tensor and spin-orbit calculations using Force A and Force B are very similar, and the predicted magnitudes are

Figure V.5

Comparison of measured angular distributions with the central and noncentral parts of Force A and Force B.

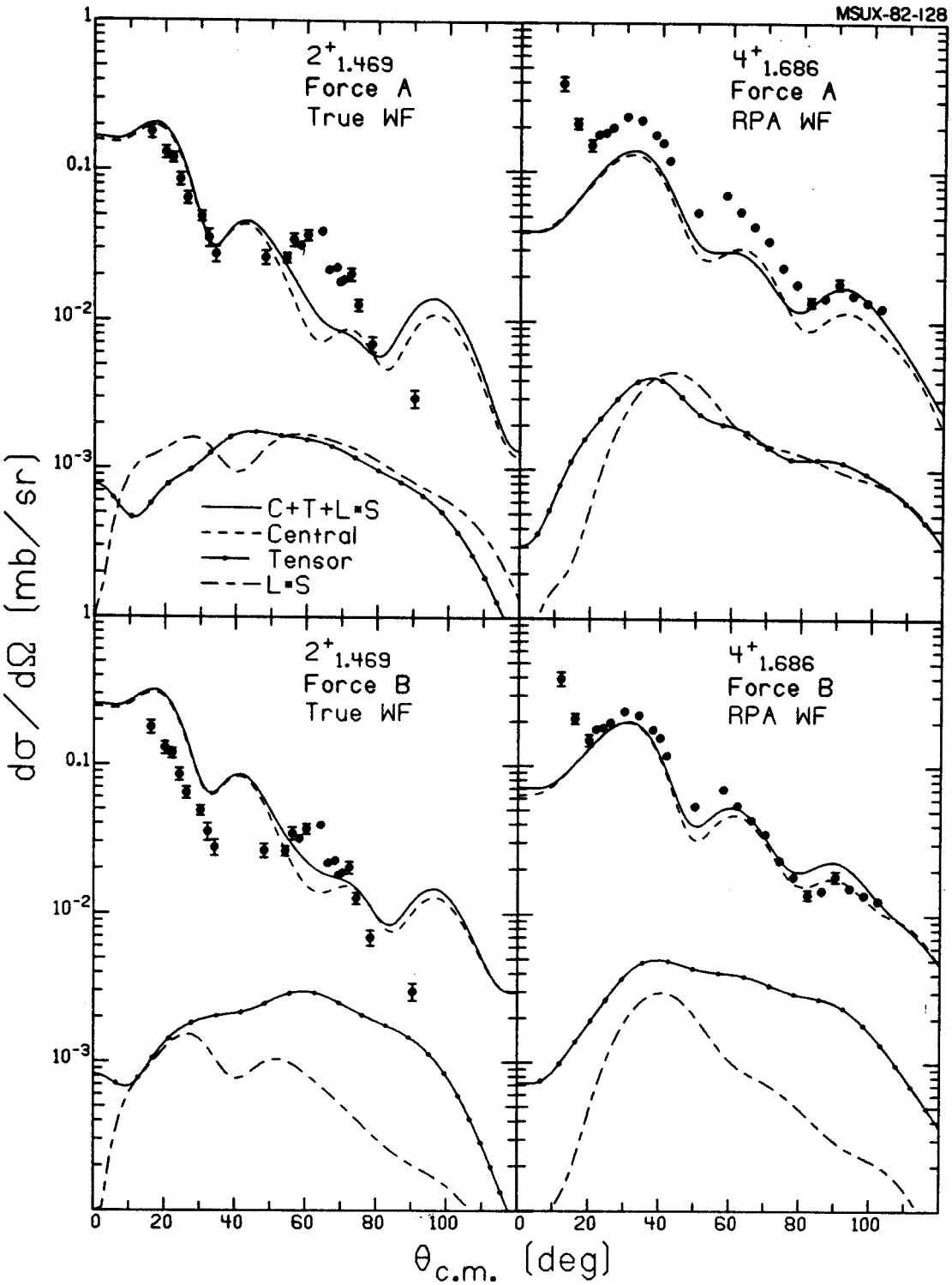
MSUX-82-128
$2^+_{1.469}$
Force A
True WF
$4^+_{1.686}$
Force A
RPA WF
$2^+_{1.469}$
Force B
True WF
$4^+_{1.686}$
Force B
RPA WF
C+T+L•S
Central
Tensor
L•S
dσ / dΩ (mb/sr)
$\theta_{c.m.}$ (deg)
1
0.1
10^{-2}
10^{-3}
0
20
40
60
80
100

Figure V.5

nearly the same.

D-2. Unnatural Parity States

When examining the natural parity states it is difficult to infer more than general information about the interactions. This is due to both the uncertainty in the wave functions of these states, and possibly excitation of these states by collective modes. However, unnatural parity states pose no such problem. Three low-lying unnatural parity states have been firmly identified [Ref. V.24] and both the RPA and TDA predict these to be pure neutron particle-hole states. These three states are the 3^+ state at 1.344 MeV, the 1^+ state at 1.708 MeV, and the 6^- state at 2.385 MeV. The neutron particle-hole configuration of these states is respectively $|p_{1/2},f^{-1}_{5/2}>$, $|p_{1/2},p^{-1}_{3/2}>$, and $|p_{1/2},i^{-1}_{13/2}>$. Calculated angular distributions using both Force A and Force B, and broken down into their central and noncentral constituent parts, are compared to the data in Figure V.6.

The calculations using Force A reproduce the general shape of the data but the magnitude of the 3^+ and 1^+ levels is underestimated by about a factor of three. The data of the 6^- state falls of more rapidly than the calculations predict. For all three states the tensor part of Force A is the dominant interaction. The central force is the weakest interaction and its contribution to the total predicted angular distribution is observed to be

Figure V.6

Same as Figure V.5.

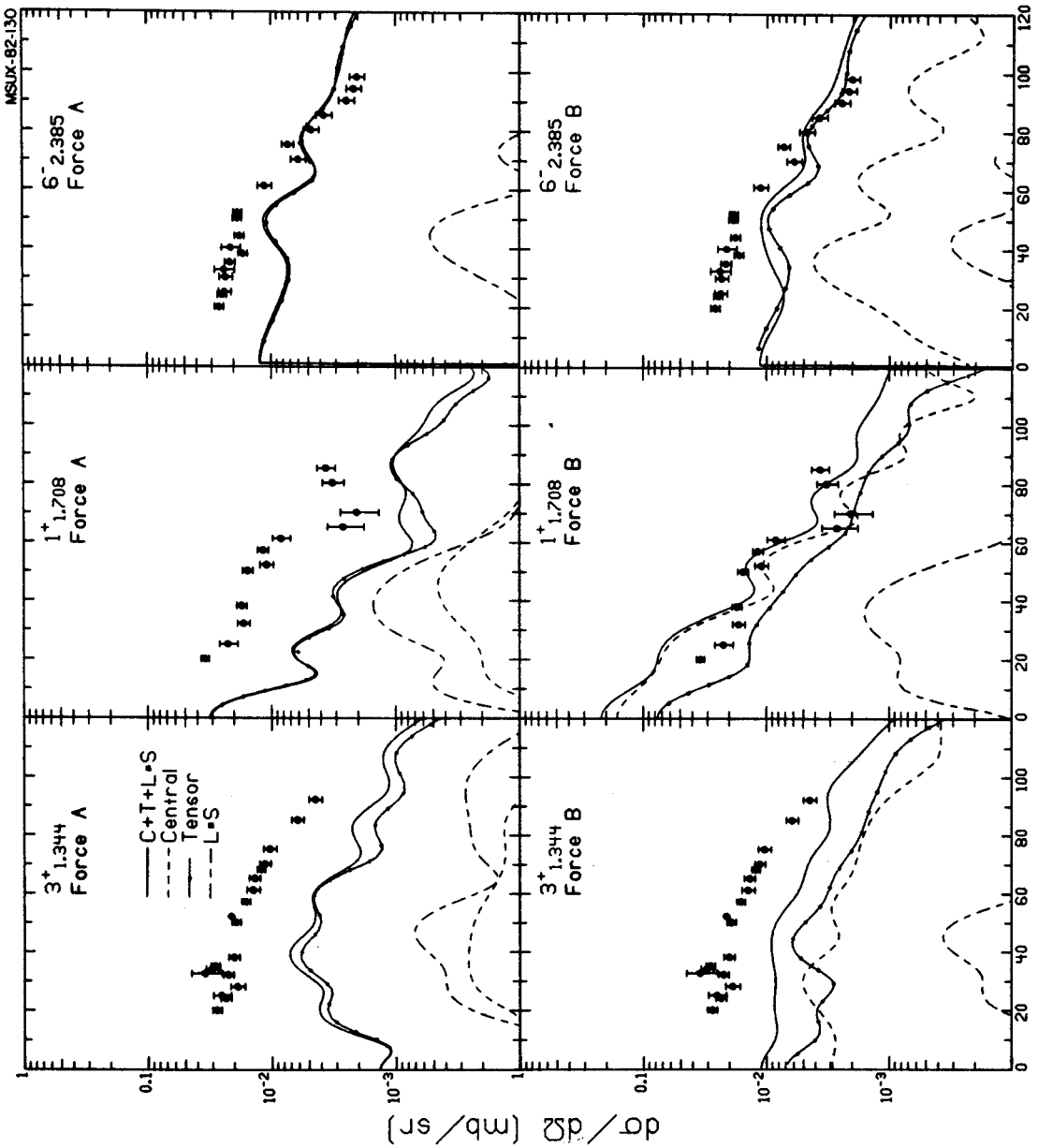
MSUX-82-130
3+ 1.344 Force A
C+T+L•S
Central
Tensor
L•S
1+ 1.708 Force A
6- 2.385 Force A
3+ 1.344 Force B
1+ 1.708 Force B
6- 2.385 Force B
dσ/dΩ (mb/sr)
θc.m. (deg)

Figure V.6

less significant as the total angular momentum of the states examined increases. The only significant contribution by the spin-oribt force is over a limited angular range for the 1^+ state.

When Force B is employed the predicted cross sections are all improved. The shape of the 3^+ state is matched well and the theory underestimates the data by only about a factor of two. The enhancement of the magnitude is caused principally by the increased strength of the central part of the interaction. The central part is observed to be nearly equal in strength to the tensor part. Since these two components are out of phase, the angular distribution predicted by the complete Force B has less structure than is predicted by Force A. Thus, the prediction of Force B compares better with the data. Force B also gives an improved estimate of the magnitude of the 1^+ state. For this state the central force dominates the tensor force at forward angles, and, in fact, the total calculation is larger than the data in this region. However, past thirty degrees, where the central and tensor parts give contributions of similar strength, the shape and magnitude are predicted quite well. The fit to the 6^- state using Force B approaches the slope of the data more closely than the fit obtained using Force A. Once again it is the increased strength of the central part which is responsible for the improvement. The contribution of the

central part of Force B is also observed to decrease significantly as the angular momentum of the state increases. A similar phenomenon is observed with Force A but to a lesser degree. The predicted shape and magnitude of the spin-orbit interaction with both forces is similar for all states.

In addition to the three established unnatural parity states there is evidence for two more unnatural parity states which should be seen in this experiment. A 3^+ state with a pure $|p_{1/2}, f_{7/2}^{-1}>$ neutron particle-hole configuration is predicted at 3.193 MeV of excitation energy by the TDA, and at 3.156 MeV of excitation by the RPA. The level observed at 3.121 MeV has been suggested by a (p, d) experiment [Ref. V.25] to be this 3^+ state. The RPA also predicts a 1^+ state with a $|f_{5/2}, p_{3/2}^{-1}>$ configuration at 3.963 MeV of excitation. Two 1^+ states are predicted by the TDA at 2.317 and 3.759 MeV of excitation energy with pure $|f_{5/2}, p_{3/2}^{-1}>$ and $|f_{5/2}, f_{7/2}^{-1}>$ configurations respectively. The state observed in this experiment at 3.737 MeV has been shown [Ref. V.24] to be a possible candidate for a 1^+ state.

Angular distributions for these two possible unnatural parity states have been calculated with both forces. The results are displayed in Figure V.7 together with the experimental data for the 3.121 and 3.737 MeV states. The magnitude of the cross section for the 3.121 MeV state is

Figure V.7

Same as Figure V.5.

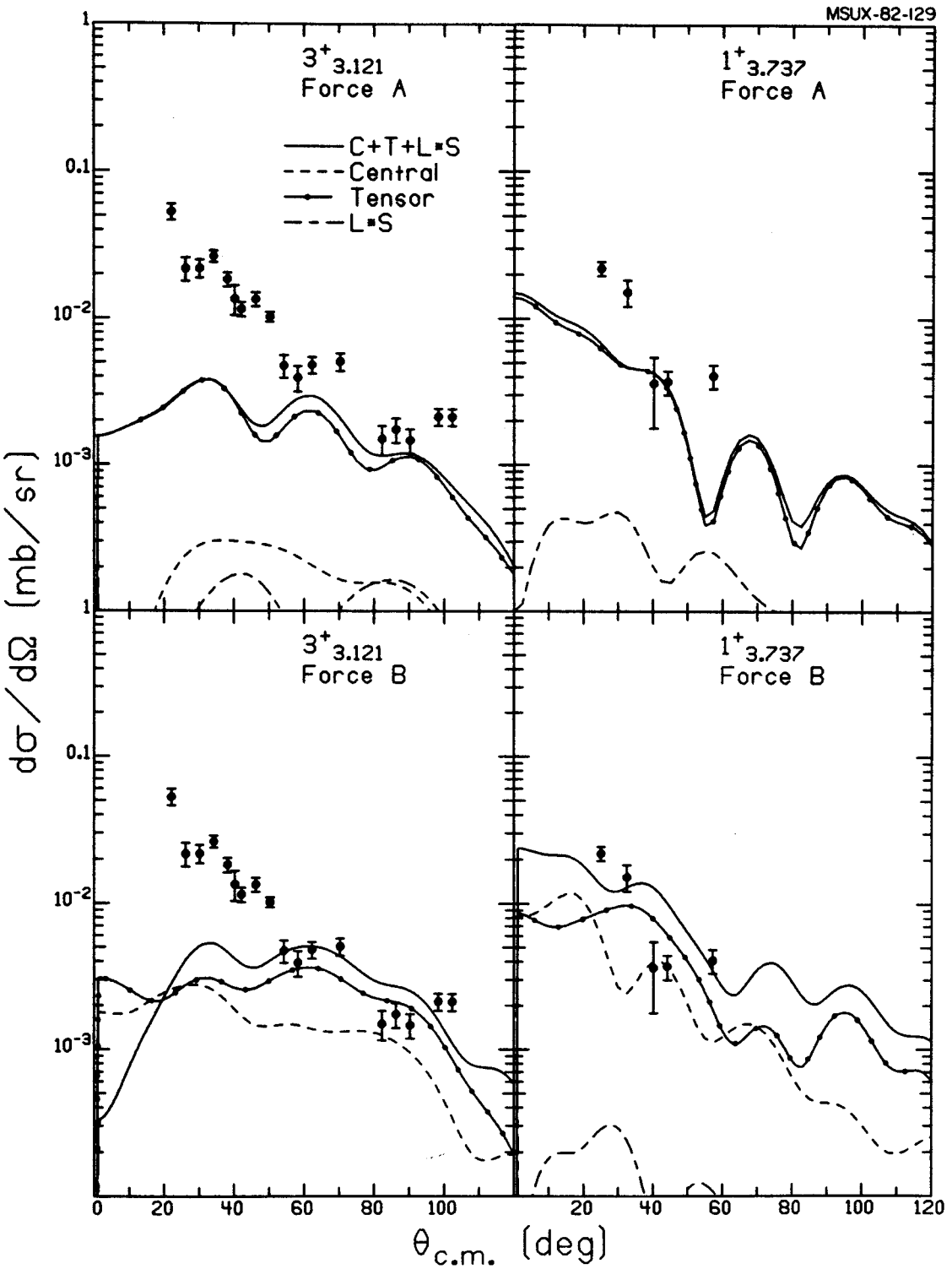
MSUX-82-129
3+ 3.121
Force A
C+T+L*S
Central
Tensor
L*S
1+ 3.737
Force A
3+ 3.121
Force B
1+ 3.737
Force B
dσ/dΩ (mb/sr)
θc.m. (deg)

Figure V.7

underestimated especially at forward angles by Force A which excites this state principally by the tensor part of the force. The calculation done with Force B is somewhat better in reproducing the magnitude. However, the fit at forward angles is still poor. The improved fit is caused by both a slightly larger contribution by the tensor part and a contribution by the central part that is nearly an order of magnitude larger than the central force contribution of Force A.

The calculations performed for the 1^+ state have used the configuration proposed by the RPA. This state lies on the shoulder of a relatively strongly excited L=3 state and is extracted at only a few angles. As a result it is difficult to compare predicted shapes of the angular distributions to the data, but there is enough information to suggest that the magnitude of this state is best reproduced with Force B.

E. Summary of the Microscopic Model Results

Microscopic calculations were performed on most low-lying natural parity states and all unnatural parity states identified in this experiment. These calculations were executed with the program DWBA-70 using realistic interactions and shell model wave functions. "Knock on" exchange contributions to the cross sections were included. The calculations allowed a test of wave functions predicted by the Tamm-Dancoff approximation and the random

phase approximation. Two realistic interactions were employed and compared. Force A used the Serber exchange mixture for the central force, and empirically determined noncentral forces. Force B was derived by fitting to the harmonic oscillator matrix elements of the Reid potential.

Natural parity states with peak cross sections $\gtrsim 0.1$ mb/sr were best fit with Force B. These states were shown to be excited principally by the central part of the interaction, and the central contribution of Force B is as much as fifty percent larger than the central contribution of Force A. The tensor and spin-orbit forces gave little enhancement to the cross sections of natural parity states. The predicted shapes using either force or wave function were found to be very similar to the measured angular distributions. These natural parity states were in general reproduced best with the RPA wave functions. In all cases where the predicted wave functions were significantly different the RPA clearly gave a better fit to the data. Furthermore, it was observed that the RPA wave functions for most of these states had a larger concentration of strength in the primary particle-hole component. With the exception of the 0^+ state this tended to improve all predicted angular distributions. This suggests that these states may be described by a rather simple single particle-hole configuration.

Unnatural parity states are not excited collectively

and the wave functions of these states are predicted by both the RPA and TDA to have a simple single particle-hole configuration. Thus, calculations of these states permit a unique examination of the forces. With Force A calculations of all observed unnatural parity states underestimate the magnitude of the data, while generally reproducing the shape. The calculations have shown that only the tensor part of Force A gave a substantital contribution to the predicted cross section. The results obtained with Force B were all much better. This improvement is caused to some degree to a small increase in the tensor strength for all states, but mainly because of a contribution by the central part which is similar in magnitude to the tensor force. This central force was seen to be most influential for the lower spin states. The resulting calculations using central and noncentral interactions in general match the magnitude of the data reasonably well. This central force also added to the tensor force in such a way as to smooth out the structure in the calculated angular distribution and thus give better agreement with the data.

REFERENCES FOR CHAPTER V

V.1 C. W. Ma and W. W. True, Phys. Rev. C 8 (1973), 2313.

V.2 J. Vary, R. J. Ascuitto, and J. N. Ginocchio, Nucl. Phys. A185 (1972), 349.

V.3 H. V. Geramb and K. A. Amos, Nucl. Phys. A163 (1971), 337.

V.4 G. Bertsch, J. Borysowicz, and H. McManus, Nucl. Phys. A284 (1977), 399.

V.5 W. G. Love, L. W. Owen, R. M. Drisko, G. R. Satchler, R. Stafford, R. J. Philpott, and W. T. Pinkston, Phys. Lett. 29B (1969), 478.

V.6 R. Reid, Ann. of Phys. 55 (1968), 411.

V.7 R. de Swiniarski, Dinh-Lien Pham, and G. Bagieu, Can. J. Phys. 55 (1977), 43.

V.8 H. Hori and K. Sasaki, Prog. Theor. Phys. 25 (1961), 471.

V.9 N. Austern, Direct Nuclear Reaction Structure, Clarendon Press, Oxford (1971).

V.10 W. T. Wagner, G. R. Hammerstein, G. M. Crawley, J. R. Borysowicz, and F. Petrovich, Phys. Rev. C 8 (1973), 2504.

V.11 G. Love, L. Parish, and A. Richter, Phys. Lett. 31B (1970), 167.

V.12 S. M. Austin in The Two-Body Force in Nuclei, eds. S. M. Austin and G. M. Crawley, Plenum Press, New York (1972).

V.13 G. M. Crawley, S. M. Austin, W. Benenson, V. A. Madsen, F. A. Schmittroth, and J. J. Stomp, Phys. Lett. 32B (1970), 92.

V.14 S. H. Fox and S. M. Austin, Phys. Rev. C 21 (1980), 1133.

V.15 W. T. Wagner, G. M. Crawley, G. R. Hammerstein, and H. McManus, Phys. Rev. C 12 (1975), 757.

V.16 G. Bertsch, J. Borysowicz, H. McManus, and W. G. Love, Nucl. Phys. A284 (1977), 399.

V.17 T. Hamada and I. D. Johnston, Nucl. Phys. 34 (1962), 382.

V.18 B. Zwieglinski, G. M. Crawley, W. Chung, H. Nann, and J. A. Nolen, Jr., Phys. Rev. C 18 (1978).

V.19 F. E. Cecil, R. P. Chestnut, and R. L. McGrath, Phys. Rev. C 10 (1974), 2425.

V.20 C. W. Ma and W. W. True, Phys. Rev. C 8 (1973), 2313.

V.21 J. Vary and J. N. Ginocchio, Nucl. Phys. A166 (1971), 479.

V.22 R. Schaeffer and J. Raynal, unpublished.

V.23 J. Raynal, Nucl. Phys. A97 (1967), 572.

V.24 M. P. Webb, Nucl. Data 26, No. 1 (1979), 145.

V.25 W. A. Lanford and G. M. Crawley, Phys. Rev. C 9 (1974), 646.

CHAPTER VI

SUMMARY

Using 35 MeV proton beams from the Michigan State University and Princeton University cyclotrons the nucleus ^{206}Pb was studied by measuring the scattered protons. High resolution techniques were utilized to identify approximately 180 levels in ^{206}Pb. Below 4.6 MeV of excitation energy the agreement with previous studies is very good although several new states were also observed in this region. Many new levels above 4.6 MeV were also measured. Angular distributions are presented for 144 of these states.

Angular distributions predicted by the collective and microscopic models are compared to the data. The collective model calculations allowed the extractions of L-values and deformation parameters. For states where results from other studies were available the agreement is quite good. The L-assignments for most states of high excitation energy were previously unreported. The collective model results for ^{206}Pb were also commpared to the core nucleus ^{208}Pb. This comparison showed a similarity between the two nuclei for some strongly excited states and the L=3 strength. However, the overall distribution of inelastic strength was quite different for multipolarities other

than 3. The strongly excited collective states are compared with analogous collective states in ^{207}Pb and ^{208}Pb. A strong correlation in both energy and strength of these collective states in the three nuclei was observed with the exception of the L=5 states. A possible explanation of the anomaly in the 5^- strengths is given in terms of the core wave functions.

Microscopic calculations performed on natural parity states indicated that these states were excited primarily by the central two-body interaction. RPA and TDA wave functions were tested in calculations. The RPA wave functions, which gave the best fit to the data, suggested that many of the states examined have primarily a single particle-hole configuration. Microscopic calculations for unnatural parity states with well determined wave functions permitted the examination of the two interactions. The magnitude and shape of the angular distributions of these states was best represented using an interaction derived by fitting shell model matrix elements of the Reid potential (Force B). This interaction is the sum of three Yakawas with the ranges chosen to reflect various meson exchanges. Central, tensor, and spin-orbit components were included. This force predicted the central and tensor contributions to the angular distributions of unnatural parity states to be similar in magnitude.

It would be of interest to study inelastic scattering

of protons by ^{206}Pb at higher bombarding energies. Based on the apparent simple wave functions of many states in ^{206}Pb, this nucleus provides an ideal target to examine the energy dependence of the central, tensor, and spin-orbit forces. Also of interest would be a study, similar to the present work, on ^{88}Sr. The low-lying states of ^{88}Sr are described by two interacting proton holes in the ^{90}Zr core. Included in these low-lying states are the 1^+ and 3^+ levels described by very simple wave functions. The proton hole wave functions of these states are analogous to the neutron hole wave functions used to describe the low-lying 1^+ and 3^+ states of ^{206}Pb.

APPENDICES

APPENDIX I

ANALYSIS OF THE DATA

The plate data was scanned in vertical strips whose height was dictated by the optical systems of the scanning microscopes. Each band was scanned so that extraneous background was excluded. For each exposure, the separate passes were combined using the program JABBERWOCKY [Ref. 1] written by S. Ewald. This program allowed combination of the separate vertical passes in two ways: straight addition or addition after shifting of the passes so that the centroids of specified peaks were alligned as closely as possible. The latter option permits compensation for skewness in the focal plane images or zeroing errors in scanning. The counter data was taken with the data acquisition program TOOTSIE [Ref. 2].

With the data in counts-versus-channel number form, the program SCOPEFIT was used for the data reduction. In extracting the area of the peaks, the shapes were assumed to be identical for all peaks and the areas were extracted by an iterative procedure. The shape of the strongest isolated peak in each spectrum was assumed to be representative of all peaks. The low energy tail was varied to assure a best fit for all peaks of interest. This method allowed extraction of weakly excited peaks on the shoulder

of strongly excited peaks and permitted the separation of barely resolvable peaks. Peak stripping methods would not be able to extract the areas of peaks in these situations.

With the reduced data, the programs DOALL [Ref. 4] and SKRUNCH [Ref. 5] were used for further analysis. The correspondence between excitation energy and focal plane position was found with the code DOALL which can perform a search on beam energy, scattering angle, and focal plane parameters to determine the best fit to the positions of peaks of known energy. For this data, the searches were limited to the angle and to the focal plane variables because, since particles other than protons were excluded from the emulsions, the beam energy could not be uniquely determined. Instead, the bombarding energy was determined using the bending magnets' nuclear magnetic resonance readings and a correction empirically established using the momentum cross-over technique [Ref. 6]. Beam energies can be calculated better than 1 part in 1000 with the correction.

The focal plane parameters from DOALL were entered into the program SKRUNCH [Ref.5]. This program transforms a counts-versus-channel number spectrum, which is assumed to be quadratic in energy, into a counts-versus-channel number spectrum which is linear in energy. With spectra in this form there is a one-to-one correspondence between channel number and excitation energy at all angles. This

simplifies greatly the extraction of angular distributions for all levels.

To determine cross sections from the reduced data the program SIGPLT [Ref. 7] was used. Using the output of this program plots were contructed of angular distributions, angular distributions compared to collective model calculations, and angular distributions compared to microscopic model calculations, using the computer programs [Ref. 8] PLOTTER, COLL MOD PLOTTER, and DWBA-70 PLOTTER respectively.

APPENDIX II

SAMPLES OF DWUCK AND DWBA-70 INPUT

The DWBA analysis in this paper was performed using the programs DWUCK [Ref. 9] for collective model calculations. In this appendix sample inputs for these two programs are listed including control cards for the Sigma-7 computer. The cases examined are the 3^- state at 2.648 MeV for the collective model example (Table A.II.1), and the 6^- state at 2.385 MeV for the microscopic model example (Table A.II.2). The punched output of DWBA-70 is very cumbersome so an auxilliary program (DWBA70 MASHER [Ref. 8]) is used to output predicted cross sections in a more convenient format.

TABLE A.II.1.

SAMPLE INPUT TO THE PROGRAM DWUCK FOR
THE 3^- STATE AT 2.648 MEV OF EXCITATION

```
!JOB 47303, FINCK 9
!LIMIT (TIME,7)
!ASSIGN M:BI (FILE,DWUCK),(OLD),(ACC,CYCLO)
!ASSIGN M:MAP (FILE,DWUCK:MAP),(OLD),(ACC,CYCLO)
!ABS
:ASSIGN F:2 (FILE,TEMP)
:ASSIGN F:4 (FILE,SCRATCH)
:ASSIGN F:5 (DEVICE,CR)
:ASSIGN F:6 (DEVICE,LP)
:ASSIGN F:106 (DEVICE,NO)
:RUN
100010003000                    206PB(P,P') 3- EX-2.648
 73.0000   .0000  2.5000
 25  1  3  6
   .1000          20.0000   .0000
          1.0078  1.0000206.0000 82.0000  1.1885
2.       53.2470  1.1700   .7500           5.0000  1.3200   .6527
-3.                                      -21.9864  1.3200   .6527
 35.0000  1.0078  1.0000206.0000 82.0000  1.1885                    1.
1.       -53.2470  1.1700   .7500          -5.0000  1.3200   .6527
2.                                        21.9864  1.3200   .6527
-4.      -24.8000  1.0100   .7500
 -2.6480  1.0078  1.0000206.0000 82.0000  1.1885                    1.,1.
 1.      -54.0985  1.1700   .7500          -4.4146  1.3200   .6527
 2.                                        24.6474  1.3200   .6527
 -4.     -24.8000  1.0100   .7500
<END-OF-FILE>
```

TABLE A.II.2

SAMPLE INPUT TO THE PROGRAM DWBA-70 FOR THE 6^- STATE AT .2385 MEV OF EXCITATION

```
!JOB 47303,FINCK 9
!LIMIT (TIME,10)
!ASSIGN M:BI (FILE,EDWBA76),(ACC,47303),(OLD)
!ABS
:ASSIGN F:6 (DEVICE,LP)
:ASSIGN F:106 (FILE,TEMP),(HOLD)
:RUN
    1
   70
0.15
   13     0
SM  OH
    1     5    -1  .405
    2     3     1  .405
    1     6     1  .405
    3     1     1  .405
    2     3    -1  .405
    3     1    -1  .405
    2     4     1  .405
    1     6    01  .405
    1     7     1  .405
    3     2     1  .405
    4     0     1  .405
    2     4    -1  .405
    2     2    -1  .405
    2
    4     1
        0.  12454.     21227.
            5018.                -3733.
```

TABLE A.II.2 CONTINUED

```
        .25         .25         .25         .25         .25
         0.   -3835.     -6622.     -813.     -1259.6
              1810.                -427.3      283.
         .4          .4          .4          .4          .4
         0.                                   -28.41
         0.                                   13.62
         .7          .7          .7          .7          .7
         0.   -10.463   -10.463

       1.4         1.4         1.4         1.4         1.4
    3
   20    73  0.        180.
ECH
    3          3
    4
205.97446 1.007825 82.         35.
1.189     53.247   1.17        0.750       5.00        1.32        0.653       5.497
1.32      0.653    6.20        1.01        0.750       0.00        1.01        0.750
    5
    1
205.97446 1.007825 82.         2.385
1.189     54.247   1.17        0.750       4.422       1.32        0.653       6.153
1.32      0.653    6.20        1.01        0.750       0.00        1.01        0.750
    6
    6   -1     1
NON XX
     1.0        1.0
    3     6  0.9866
    7
206PB(P,P') 6- EX-2.385 FORCE B C+T+L*S
```

TABLE A.II.2 CONTINUED

```
   1

!ASSIGN M:BI (FILE,DWBA70 MASHER),(ACC,47303),(OLD)
!ABS
:ASSIGN F:105 (FILE,TEMP),(HOLD)
:REW F:105
:ASSIGN F:5 (DEVICE,CP)
:RUN
<END-OF-FILE>
```

APPENDIX III

^{206}PB ANGULAR DISTRIBUTIONS

Tabulated on the following pages are the angular distributions of ^{206}Pb measured in this experiment (Table A.III.1). All cross sections are given in microbarns per steradian.

EX=0.000 MEV

THETA	SIGMA	ERROR
10.1	.192E+06	.137E+03
12.1	.596E+05	.672E+02
16.1	.170E+05	.194E+03
20.1	.597E+04	.548E+01
24.1	.191E+04	.472E+01
28.1	.790E+03	.751E+00
32.2	.340E+03	.469E+00
34.2	.225E+03	.304E+00
38.2	.149E+03	.249E+00
40.2	.140E+03	.256E+00
44.2	.122E+03	.161E+00
48.2	.789E+02	.133E+00
52.2	.317E+02	.813E-01
56.2	.104E+02	.475E-01
60.3	.138E+02	.430E-01
64.3	.211E+02	.435E-01
68.3	.180E+02	.242E-01
72.3	.992E+01	.382E-01
76.3	.312E+01	.173E-01
80.3	.206E+01	.137E-01
84.3	.388E+01	.182E-01
88.3	.466E+01	.170E-01
92.3	.366E+01	.148E-01
96.3	.186E+01	.115E-01
100.3	.744E+00	.667E-02
104.3	.642E+00	.102E-01
108.3	.994E+00	.118E-01

EX=0.803 MEV

THETA	SIGMA	ERROR
16.1	.263E+01	.211E+00
20.1	.341E+01	.131E+00
24.1	.235E+01	.760E+00
28.1	.749E+00	.235E+00
34.2	.370E+00	.126E+00
38.2	.556E+00	.159E+00
40.2	.519E+00	.156E+00
44.2	.431E+00	.151E+00
48.2	.257E+00	.761E+00
52.2	.230E+00	.694E+00
56.2	.210E+00	.817E+00
60.3	.187E+00	.646E+00
64.3	.132E+00	.344E+00
68.3	.953E+00	.102E+02
72.3	.991E+00	.104E+02
76.3	.961E+00	.103E+02
80.3	.775E+00	.103E+02
84.3	.542E+00	.102E+02
88.3	.438E+00	.102E+02
92.3	.414E+00	.102E+02
96.3	.420E+00	.102E+02
100.3	.427E+00	.102E+02
104.3	.317E+00	.102E+02
108.3	.272E+00	.102E+02

EX=1.170 MEV

THETA	SIGMA	ERROR
20.1	.261E+00	.103E+02
24.1	.267E+00	.103E+02
25.1	.319E+00	.105E+02
28.1	.135E+00	.103E+02
32.2	.104E+00	.102E+02
35.2	.887E+00	.202E+02
50.2	.893E+00	.201E+02
52.2	.824E+00	.201E+02
57.3	.347E+00	.208E+02
65.3	.420E+00	.210E+02

EX=1.344 MEV

THETA	SIGMA	ERROR
20.1	.276E+00	.103E+02
24.1	.234E+00	.102E+02
25.1	.253E+00	.104E+02
28.1	.188E+00	.103E+02
32.2	.223E+00	.102E+02
32.7	.349E+00	.110E+02
34.2	.305E+00	.104E+02
35.2	.287E+00	.102E+02
38.2	.200E+00	.102E+02
50.2	.193E+00	.102E+02
52.2	.211E+00	.102E+02
57.3	.161E+00	.101E+02
61.3	.141E+00	.102E+02
65.3	.137E+00	.101E+02
68.3	.122E+00	.109E+02
70.3	.113E+00	.101E+02
75.3	.104E+00	.101E+02
85.3	.617E+00	.207E+02

EX=1.469 MEV

THETA	SIGMA	ERROR
16.1	.179E+00	.107E+00
20.1	.131E+00	.128E+00
22.1	.120E+00	.947E+00
24.1	.859E+00	.108E+02
26.1	.646E+00	.106E+02
30.1	.488E+00	.104E+02
32.2	.352E+00	.105E+02
34.2	.276E+00	.103E+02
48.2	.262E+00	.103E+02
54.2	.261E+00	.102E+02
56.3	.342E+00	.103E+02
58.3	.315E+00	.102E+02
60.3	.368E+00	.103E+02
64.3	.390E+00	.102E+02
66.3	.217E+00	.109E+02
68.3	.225E+00	.101E+02
69.3	.181E+00	.110E+02
70.3	.187E+00	.101E+02
72.3	.203E+00	.102E+02
74.3	.126E+00	.101E+02
78.3	.689E+00	.208E+02

EX=1.686 MEV

THETA	SIGMA	ERROR
12.1	.392E+00	.432E+00
16.1	.211E+00	.173E+00
20.1	.150E+00	.138E+00
22.1	.178E+00	.100E+00
24.1	.183E+00	.109E+00
26.1	.199E+00	.795E+00
30.1	.236E+00	.716E+00
34.2	.223E+00	.861E+00
38.2	.178E+00	.486E+00
40.2	.157E+00	.708E+00
42.2	.119E+00	.425E+00
50.2	.538E+00	.104E+02
58.3	.703E+00	.103E+02
62.3	.546E+00	.102E+02
66.3	.435E+00	.102E+02
70.3	.348E+00	.102E+02
74.3	.233E+00	.102E+02
78.3	.181E+00	.101E+02
82.3	.138E+00	.101E+02
86.3	.146E+00	.110E+02
90.3	.182E+00	.102E+02
94.3	.152E+00	.108E+02
98.3	.137E+00	.107E+02

EX=1.708 MEV

THETA	SIGMA	ERROR
20.1	.344E+00	.103E+02
25.1	.223E+00	.104E+02
32.2	.167E+00	.102E+02
38.2	.173E+00	.102E+02
50.2	.155E+00	.101E+02
52.2	.109E+00	.101E+02
57.3	.117E+00	.101E+02
61.3	.838E+00	.201E+02
65.3	.266E+00	.209E+02
70.3	.206E+00	.207E+02
80.3	.322E+00	.206E+02

EX=1.787 MEV

THETA	SIGMA	ERROR
20.1	.185E+00	.102E+02
24.1	.836E+00	.202E+02
25.1	.823E+00	.203E+02
28.1	.985E+00	.202E+02
32.2	.122E+00	.102E+02
35.2	.184E+00	.102E+02
38.2	.138E+00	.102E+02
52.2	.878E+00	.201E+02
61.3	.502E+00	.201E+02
70.3	.318E+00	.208E+02

EX=1.998 MEV

THETA	SIGMA	ERROR
16.1	.119E+00	.187E+00
20.1	.808E+00	.181E+02
22.1	.718E+00	.108E+02
24.1	.741E+00	.108E+02
26.1	.816E+00	.106E+02
30.1	.761E+00	.105E+02
38.2	.452E+00	.102E+02
40.2	.267E+00	.103E+02
42.2	.191E+00	.102E+02
46.2	.202E+00	.102E+02
58.3	.336E+00	.102E+02
62.3	.287E+00	.102E+02
66.3	.213E+00	.109E+02
69.3	.168E+00	.109E+02
70.3	.139E+00	.101E+02
74.3	.106E+00	.101E+02
78.3	.615E+00	.208E+02
82.3	.406E+00	.206E+02
86.3	.638E+00	.206E+02
94.3	.208E+00	.203E+02
98.3	.199E+00	.203E+02

EX=2.151 MEV

THETA	SIGMA	ERROR
20.1	.341E+00	.102E+02
24.1	.212E+00	.102E+02
25.1	.157E+00	.103E+02
28.1	.127E+00	.102E+02
32.7	.159E+00	.105E+02
35.2	.168E+00	.102E+02
38.2	.145E+00	.101E+02
44.2	.166E+00	.102E+02
50.2	.882E+00	.201E+02
57.3	.338E+00	.208E+02
65.3	.266E+00	.207E+02
70.3	.345E+00	.207E+02
75.3	.322E+00	.207E+02
80.3	.329E+00	.206E+02

EX=2.200 MEV

THETA	SIGMA	ERROR
16.1	.183E+00	.201E+00
20.1	.134E+00	.139E+00
22.1	.119E+00	.934E+00
24.1	.102E+00	.870E+00
26.1	.108E+00	.660E+00
30.1	.950E+00	.105E+02
34.2	.877E+00	.105E+02
38.2	.627E+00	.103E+02
40.2	.588E+00	.104E+02
42.2	.517E+00	.103E+02
46.2	.546E+00	.103E+02
50.2	.597E+00	.102E+02
58.3	.411E+00	.103E+02
66.3	.182E+00	.108E+02
69.3	.164E+00	.109E+02
70.3	.178E+00	.101E+02
74.3	.123E+00	.101E+02
78.3	.132E+00	.101E+02
82.3	.141E+00	.101E+02
86.3	.146E+00	.110E+02
90.3	.124E+00	.108E+02
98.3	.103E+00	.106E+02

EX=2.385 MEV

THETA	SIGMA	ERROR
20.1	.261E+00	.102E+02
24.1	.240E+00	.102E+02
25.1	.236E+00	.103E+02
30.1	.232E+00	.103E+02
32.7	.240E+00	.104E+02
35.2	.214E+00	.102E+02
38.2	.168E+00	.101E+02
40.2	.212E+00	.104E+02
44.2	.179E+00	.102E+02
50.2	.187E+00	.102E+02
52.2	.185E+00	.101E+02
61.3	.113E+00	.101E+02
70.3	.603E+00	.209E+02
75.3	.732E+00	.208E+02
80.3	.475E+00	.207E+02
85.3	.375E+00	.206E+02
90.3	.247E+00	.204E+02
94.3	.216E+00	.203E+02

EX=2.422 MEV

THETA	SIGMA	ERROR
20.1	.193E+00	.102E+02
25.1	.181E+00	.103E+02
28.1	.140E+00	.108E+02
32.2	.561E+00	.201E+02
38.2	.330E+00	.209E+02
40.2	.576E+00	.203E+02
52.2	.913E+00	.201E+02
61.3	.713E+00	.201E+02
75.3	.330E+00	.206E+02
80.3	.175E+00	.205E+02

EX=2.648 MEV

THETA	SIGMA	ERROR
12.1	.672E+00	.494E+00
16.1	.116E+01	.306E+00
20.1	.258E+01	.310E+00
22.1	.367E+01	.301E+00
24.1	.447E+01	.349E+00
26.1	.494E+01	.285E+00
30.1	.432E+01	.245E+00
34.2	.272E+01	.256E+00
38.2	.149E+01	.140E+00
40.2	.119E+01	.198E+00
42.2	.119E+01	.134E+00
46.2	.146E+01	.155E+00
50.2	.160E+01	.102E+00
54.2	.131E+01	.140E+00
58.3	.109E+01	.130E+00
62.3	.706E+00	.760E+00
66.3	.524E+00	.424E+00
69.3	.514E+00	.516E+00
74.3	.462E+00	.678E+00
78.3	.407E+00	.627E+00
82.3	.362E+00	.540E+00
86.3	.275E+00	.420E+00
90.3	.226E+00	.348E+00
94.3	.184E+00	.276E+00
98.3	.159E+00	.250E+00

EX=2.782 MEV

THETA	SIGMA	ERROR
16.1	.169E+00	.215E+00
20.1	.139E+00	.143E+00
22.1	.116E+00	.888E+00
24.1	.121E+00	.899E+00
26.1	.134E+00	.713E+00
30.1	.143E+00	.580E+00
34.2	.152E+00	.605E+00
38.2	.150E+00	.445E+00
40.2	.139E+00	.665E+00
42.2	.121E+00	.428E+00
46.2	.942E+00	.104E+02
50.2	.553E+00	.102E+02
54.2	.375E+00	.102E+02
58.3	.335E+00	.102E+02
66.3	.395E+00	.101E+02
69.3	.342E+00	.101E+02
70.3	.325E+00	.102E+02
78.3	.201E+00	.101E+02
82.3	.123E+00	.110E+02
86.3	.106E+00	.108E+02
90.3	.114E+00	.108E+02
94.3	.124E+00	.107E+02
98.3	.879E+00	.206E+02

EX=2.861 MEV

THETA	SIGMA	ERROR
25.1	.134E+00	.102E+02
26.1	.142E+00	.104E+02
32.7	.999E+00	.203E+02
40.2	.120E+00	.103E+02
52.2	.110E+00	.101E+02
69.3	.414E+00	.205E+02

EX=2.920 MEV

THETA	SIGMA	ERROR
12.1	.297E+00	.418E+00
16.1	.265E+00	.238E+00
20.1	.160E+00	.149E+00
22.1	.182E+00	.982E+00
24.1	.182E+00	.102E+00
26.1	.215E+00	.826E+00
30.1	.231E+00	.701E+00
34.2	.237E+00	.756E+00
38.2	.177E+00	.484E+00
40.2	.118E+00	.669E+00
42.2	.103E+00	.396E+00
46.2	.803E+00	.104E+02
50.2	.545E+00	.102E+02
54.2	.440E+00	.103E+02
58.3	.586E+00	.103E+02
66.3	.585E+00	.102E+02
69.3	.444E+00	.102E+02
70.3	.439E+00	.102E+02
78.3	.213E+00	.101E+02
82.3	.190E+00	.101E+02
86.3	.177E+00	.101E+02
90.3	.153E+00	.109E+02
94.3	.138E+00	.108E+02
98.3	.105E+00	.106E+02

EX=2.960 MEV

THETA	SIGMA	ERROR
32.7	.146E+00	.104E+02
40.2	.746E+00	.202E+02
44.2	.240E+00	.207E+02
50.2	.480E+00	.207E+02
57.3	.301E+00	.206E+02
65.3	.698E+00	.208E+02

EX=2.988 MEV

THETA	SIGMA	ERROR
25.1	.176E+00	.102E+02
32.7	.550E+00	.203E+02
44.2	.642E+00	.209E+02
50.2	.430E+00	.207E+02
57.3	.180E+00	.205E+02

EX=3.014 MEV

THETA	SIGMA	ERROR
22.1	.530E+00	.106E+02
24.1	.510E+00	.107E+02
26.1	.463E+00	.105E+02
30.1	.437E+00	.105E+02
34.2	.580E+00	.104E+02
38.2	.556E+00	.103E+02
42.2	.428E+00	.103E+02
46.2	.299E+00	.102E+02
50.2	.205E+00	.101E+02
54.3	.131E+00	.101E+02
58.3	.141E+00	.101E+02
70.3	.153E+00	.101E+02
74.3	.789E+00	.209E+02
82.3	.354E+00	.205E+02
90.3	.405E+00	.205E+02
94.3	.396E+00	.204E+02
98.3	.424E+00	.204E+02

EX=3.121 MEV

THETA	SIGMA	ERROR
22.1	.530E+00	.107E+02
26.1	.218E+00	.104E+02
30.1	.219E+00	.103E+02
34.2	.264E+00	.103E+02
38.2	.184E+00	.102E+02
40.2	.135E+00	.103E+02
42.2	.115E+00	.101E+02
46.2	.134E+00	.101E+02
50.2	.102E+00	.108E+02
54.3	.474E+00	.208E+02
58.3	.393E+00	.208E+02
62.3	.480E+00	.206E+02
70.3	.506E+00	.207E+02
82.3	.149E+00	.203E+02
86.3	.174E+00	.203E+02
90.3	.146E+00	.203E+02
98.3	.213E+00	.203E+02

EX=3.193 MEV

THETA	SIGMA	ERROR
22.1	.452E+00	.107E+02
26.1	.306E+00	.104E+02
30.1	.336E+00	.104E+02
34.2	.266E+00	.103E+02
38.2	.269E+00	.103E+02
40.2	.211E+00	.104E+02
42.2	.219E+00	.102E+02
46.2	.153E+00	.102E+02
50.2	.106E+00	.101E+02
54.3	.118E+00	.101E+02
58.3	.649E+00	.201E+02
62.3	.720E+00	.208E+02
69.3	.102E+00	.107E+02
74.3	.558E+00	.207E+02
82.3	.500E+00	.206E+02
86.3	.376E+00	.205E+02
94.3	.291E+00	.203E+02

EX=3.257 MEV

THETA	SIGMA	ERROR
12.1	.117E+00	.178E+00
16.1	.659E+00	.101E+02
20.1	.650E+00	.106E+02
22.1	.451E+00	.107E+02
24.1	.366E+00	.106E+02
25.1	.441E+00	.105E+02
26.1	.327E+00	.104E+02
30.1	.321E+00	.103E+02
35.2	.339E+00	.103E+02
38.2	.341E+00	.103E+02
40.2	.453E+00	.103E+02
42.2	.425E+00	.102E+02
45.2	.462E+00	.103E+02
46.2	.475E+00	.103E+02
48.2	.439E+00	.102E+02
50.2	.235E+00	.102E+02
55.3	.313E+00	.102E+02
58.3	.283E+00	.102E+02
62.3	.165E+00	.101E+02
63.3	.201E+00	.101E+02
69.3	.242E+00	.101E+02
74.3	.198E+00	.101E+02
85.3	.635E+00	.206E+02
90.3	.513E+00	.205E+02
95.3	.472E+00	.205E+02

EX=3.277 MEV

THETA	SIGMA	ERROR
12.1	.109E+00	.177E+00
16.1	.864E+00	.101E+02
20.1	.593E+00	.106E+02
22.1	.372E+00	.107E+02
24.1	.433E+00	.107E+02
25.1	.442E+00	.105E+02
26.1	.441E+00	.105E+02
30.1	.405E+00	.103E+02
35.2	.485E+00	.103E+02
40.2	.486E+00	.103E+02
42.2	.455E+00	.102E+02
45.2	.357E+00	.103E+02
46.2	.352E+00	.102E+02
48.2	.255E+00	.102E+02
55.3	.137E+00	.101E+02
58.3	.186E+00	.102E+02
62.3	.193E+00	.101E+02
70.3	.174E+00	.101E+02
85.3	.519E+00	.205E+02
90.3	.508E+00	.205E+02
95.3	.536E+00	.205E+02

EX=3.399 MEV

THETA	SIGMA	ERROR
12.1	.762E+00	.102E+02
16.1	.101E+00	.107E+00
20.1	.896E+00	.107E+02
22.1	.718E+00	.108E+02
24.1	.755E+00	.108E+02
25.1	.731E+00	.106E+02
26.1	.797E+00	.106E+02
30.1	.842E+00	.103E+02
34.2	.101E+00	.613E+00
35.2	.897E+00	.105E+02
38.2	.927E+00	.105E+02
40.2	.863E+00	.104E+02
42.2	.854E+00	.103E+02
45.2	.603E+00	.104E+02
46.2	.642E+00	.103E+02
48.2	.477E+00	.103E+02
50.2	.470E+00	.102E+02
54.3	.277E+00	.102E+02
55.3	.292E+00	.102E+02
58.3	.310E+00	.102E+02
63.3	.255E+00	.101E+02
66.3	.282E+00	.101E+02
74.3	.153E+00	.102E+02
85.3	.106E+00	.107E+02
90.3	.105E+00	.108E+02
95.3	.976E+00	.207E+02

EX=3.450 MEV

THETA	SIGMA	ERROR
16.1	.710E+00	.101E+02
20.1	.777E+00	.107E+02
22.1	.991E+00	.109E+02
24.1	.120E+00	.804E+00
25.1	.112E+00	.665E+00
26.1	.119E+00	.726E+00
30.1	.115E+00	.383E+00
34.2	.100E+00	.720E+00
35.2	.807E+00	.104E+02
38.2	.585E+00	.104E+02
40.2	.407E+00	.103E+02
42.2	.347E+00	.102E+02
45.2	.283E+00	.103E+02
46.2	.365E+00	.102E+02
48.2	.302E+00	.102E+02
50.2	.395E+00	.102E+02
54.3	.436E+00	.103E+02
55.3	.378E+00	.102E+02
58.3	.328E+00	.102E+02
63.3	.203E+00	.101E+02
85.3	.116E+00	.107E+02
90.3	.667E+00	.207E+02
95.3	.429E+00	.205E+02

EX=3.478 MEV

THETA	SIGMA	ERROR
25.1	.137E+00	.102E+02
32.7	.993E+00	.203E+02
40.2	.107E+00	.102E+02
44.2	.630E+00	.209E+02
52.2	.100E+00	.206E+02
57.3	.150E+00	.205E+02

EX=3.515 MEV

THETA	SIGMA	ERROR
12.1	.131E+00	.191E+00
16.1	.597E+00	.110E+02
20.1	.474E+00	.105E+02
25.1	.357E+00	.105E+02
30.1	.333E+00	.103E+02
35.2	.297E+00	.103E+02
40.2	.287E+00	.103E+02
42.2	.272E+00	.104E+02
45.2	.181E+00	.103E+02
48.2	.145E+00	.102E+02
55.3	.109E+00	.109E+02
63.3	.137E+00	.101E+02
90.3	.611E+00	.206E+02
95.3	.436E+00	.205E+02

EX=3.558 MEV

THETA	SIGMA	ERROR
16.1	.101E+00	.109E+00
20.1	.918E+00	.107E+02
25.1	.849E+00	.106E+02
30.1	.991E+00	.105E+02
35.2	.110E+00	.509E+00
40.2	.892E+00	.104E+02
42.2	.824E+00	.104E+02
45.2	.590E+00	.104E+02
48.2	.389E+00	.102E+02
55.3	.242E+00	.101E+02
63.3	.264E+00	.101E+02
90.3	.103E+00	.108E+02
95.3	.718E+00	.206E+02

EX=3.603 MEV

THETA	SIGMA	ERROR
25.1	.403E+00	.103E+02
32.7	.155E+00	.103E+02
44.2	.114E+00	.101E+02
52.2	.840E+00	.209E+02
65.3	.765E+00	.208E+02
75.3	.458E+00	.208E+02

EX=3.718 MEV

THETA	SIGMA	ERROR
16.1	.143E+00	.122E+00
20.1	.103E+00	.917E+00
25.1	.228E+00	.375E+00
30.1	.195E+00	.412E+00
35.2	.105E+00	.513E+00
40.2	.524E+00	.104E+02
42.2	.629E+00	.103E+02
45.2	.563E+00	.104E+02
48.2	.603E+00	.103E+02
55.3	.375E+00	.102E+02
63.3	.227E+00	.101E+02
70.3	.275E+00	.101E+02
85.3	.106E+00	.107E+02
90.3	.911E+00	.208E+02
95.3	.529E+00	.205E+02

EX=3.737 MEV

THETA	SIGMA	ERROR
25.1	.220E+00	.102E+02
32.7	.152E+00	.103E+02
40.2	.361E+00	.202E+02
44.2	.370E+00	.207E+02

EX=3.772 MEV

THETA	SIGMA	ERROR
12.1	.295E+00	.225E+00
16.1	.279E+00	.142E+00
20.1	.283E+00	.106E+00
25.1	.302E+00	.467E+00
30.1	.386E+00	.565E+00
35.2	.396E+00	.883E+00
40.2	.387E+00	.839E+00
42.2	.378E+00	.818E+00
45.2	.386E+00	.782E+00
48.2	.226E+00	.547E+00
55.3	.125E+00	.308E+00
63.3	.101E+00	.276E+00
70.3	.690E+00	.102E+02
85.3	.356E+00	.101E+02
90.3	.385E+00	.102E+02
95.3	.276E+00	.101E+02

EX=3.827 MEV

THETA	SIGMA	ERROR
25.1	.690E+00	.202E+02
32.7	.641E+00	.202E+02
44.2	.602E+00	.210E+02
52.2	.699E+00	.208E+02
70.3	.297E+00	.206E+02

EX=3.847 MEV

THETA	SIGMA	ERROR
25.1	.161E+00	.102E+02
32.7	.459E+00	.202E+02
44.2	.320E+00	.208E+02
50.2	.275E+00	.205E+02
52.2	.223E+00	.205E+02

EX=3.963 MEV

THETA	SIGMA	ERROR
32.7	.168E+00	.103E+02
40.2	.123E+00	.103E+02
44.2	.101E+00	.101E+02
52.2	.123E+00	.110E+02
65.3	.102E+00	.101E+02
70.3	.473E+00	.208E+02

EX=3.988 MEV

THETA	SIGMA	ERROR
25.1	.294E+00	.103E+02
32.7	.397E+00	.104E+02
40.2	.206E+00	.103E+02
44.2	.243E+00	.101E+02
52.2	.362E+00	.102E+02
57.3	.147E+00	.101E+02
65.3	.201E+00	.101E+02
70.3	.971E+00	.210E+02

EX=3.997 MEV

THETA	SIGMA	ERROR
25.1	.382E+00	.103E+02
40.2	.502E+00	.104E+02
44.2	.466E+00	.102E+02
52.2	.608E+00	.102E+02
57.3	.381E+00	.102E+02
65.3	.419E+00	.102E+02
70.3	.226E+00	.101E+02

EX=4.006 MEV

THETA	SIGMA	ERROR
25.1	.808E+00	.104E+02
32.7	.124E+00	.647E+00
40.2	.574E+00	.105E+02

EX=4.044 MEV

THETA	SIGMA	ERROR
25.1	.399E+00	.103E+02
32.7	.327E+00	.104E+02
40.2	.235E+00	.103E+02
44.2	.297E+00	.102E+02
52.2	.305E+00	.101E+02
57.3	.136E+00	.101E+02
70.3	.845E+00	.210E+02

EX=4.059 MEV

THETA	SIGMA	ERROR
25.1	.350E+00	.103E+02
32.7	.384E+00	.104E+02
40.2	.312E+00	.104E+02
44.2	.234E+00	.102E+02
52.2	.158E+00	.101E+02
65.3	.119E+00	.101E+02
70.3	.454E+00	.208E+02

EX=4.107 MEV

THETA	SIGMA	ERROR
12.1	.354E+00	.253E+00
16.1	.839E+00	.817E+00
20.1	.150E+01	.273E+00
25.1	.924E+00	.700E+00
30.1	.365E+00	.554E+00
35.2	.259E+00	.750E+00
40.2	.445E+00	.910E+00
42.2	.486E+00	.229E+00
45.2	.384E+00	.871E+00
48.2	.288E+00	.654E+00
55.3	.185E+00	.620E+00
63.3	.127E+00	.364E+00
70.3	.131E+00	.366E+00
74.3	.119E+00	.666E+00
85.3	.472E+00	.102E+02
90.3	.495E+00	.102E+02
95.3	.498E+00	.102E+02

EX=4.123 MEV

THETA	SIGMA	ERROR
25.1	.118E+00	.467E+00
32.7	.533E+00	.105E+02
40.2	.594E+00	.105E+02
50.2	.648E+00	.102E+02
52.2	.521E+00	.102E+02
57.3	.278E+00	.101E+02
65.3	.347E+00	.102E+02

EX=4.168 MEV

THETA	SIGMA	ERROR
25.1	.325E+00	.103E+02
32.7	.163E+00	.103E+02
40.2	.166E+00	.103E+02
44.2	.113E+00	.101E+02
50.2	.750E+00	.210E+02
52.2	.811E+00	.209E+02
57.3	.521E+00	.208E+02
65.3	.665E+00	.209E+02
70.3	.491E+00	.209E+02
75.3	.360E+00	.208E+02

EX=4.219 MEV

THETA	SIGMA	ERROR
12.1	.146E+00	.233E+00
16.1	.121E+00	.129E+00
20.1	.122E+00	.167E+00
25.1	.897E+00	.104E+02
30.1	.835E+00	.103E+02
35.2	.535E+00	.104E+02
40.2	.427E+00	.104E+02
42.2	.381E+00	.104E+02
45.2	.394E+00	.104E+02
48.2	.238E+00	.103E+02
55.3	.206E+00	.102E+02
63.3	.157E+00	.102E+02
70.3	.128E+00	.102E+02
85.3	.616E+00	.205E+02
90.3	.625E+00	.208E+02

EX=4.242 MEV

THETA	SIGMA	ERROR
12.1	.203E+00	.242E+00
16.1	.189E+00	.141E+00
20.1	.128E+00	.168E+00
25.1	.764E+00	.104E+02
30.1	.748E+00	.103E+02
35.2	.504E+00	.104E+02
40.2	.471E+00	.104E+02
42.2	.423E+00	.104E+02
45.2	.432E+00	.104E+02
48.2	.378E+00	.103E+02
55.3	.421E+00	.102E+02
63.3	.301E+00	.102E+02
70.3	.229E+00	.102E+02
74.3	.208E+00	.103E+02
85.3	.102E+00	.107E+02
90.3	.666E+00	.208E+02

EX=4.292 MEV

THETA	SIGMA	ERROR
20.1	.885E+00	.102E+02
25.1	.706E+00	.103E+02
30.1	.612E+00	.104E+02
35.2	.374E+00	.104E+02
40.2	.267E+00	.103E+02
42.2	.267E+00	.104E+02
45.2	.311E+00	.104E+02
48.2	.303E+00	.103E+02
55.3	.322E+00	.102E+02
63.3	.151E+00	.102E+02
70.3	.983E+00	.201E+02
74.3	.790E+00	.202E+02
85.3	.120E+00	.108E+02
90.3	.996E+00	.209E+02
95.3	.566E+00	.206E+02

EX=4.333 MEV

THETA	SIGMA	ERROR
12.1	.566E+00	.283E+00
16.1	.536E+00	.182E+00
20.1	.526E+00	.217E+00
25.1	.608E+00	.613E+00
30.1	.812E+00	.809E+00
35.2	.702E+00	.118E+00
40.2	.484E+00	.970E+00
42.2	.401E+00	.989E+00
45.2	.282E+00	.823E+00
48.2	.209E+00	.602E+00
55.3	.256E+00	.518E+00
63.3	.268E+00	.523E+00
70.3	.163E+00	.410E+00
74.3	.128E+00	.692E+00
85.3	.915E+00	.102E+02
90.3	.946E+00	.103E+02
95.3	.788E+00	.102E+02

EX=4.357 MEV

THETA	SIGMA	ERROR
12.1	.410E+00	.271E+00
16.1	.420E+00	.172E+00
20.1	.349E+00	.200E+00
25.1	.275E+00	.456E+00
30.1	.311E+00	.517E+00
35.2	.343E+00	.883E+00
40.2	.384E+00	.883E+00
42.2	.413E+00	.101E+00
45.2	.442E+00	.996E+00
48.2	.381E+00	.772E+00
55.3	.241E+00	.508E+00
63.3	.135E+00	.395E+00
70.3	.126E+00	.360E+00
74.3	.126E+00	.686E+00
85.3	.876E+00	.102E+02
90.3	.666E+00	.102E+02
95.3	.486E+00	.102E+02

EX=4.391 MEV

THETA	SIGMA	ERROR
25.1	.265E+00	.103E+02
32.7	.257E+00	.104E+02
40.2	.388E+00	.104E+02
50.2	.104E+00	.101E+02
57.3	.640E+00	.209E+02

EX=4.420 MEV

THETA	SIGMA	ERROR
25.1	.361E+00	.103E+02
32.7	.844E+00	.105E+02
40.2	.213E+00	.103E+02
44.2	.257E+00	.102E+02
50.2	.630E+00	.201E+02
52.2	.674E+00	.209E+02
57.3	.380E+00	.208E+02
70.3	.790E+00	.201E+02

EX=4.456 MEV

THETA	SIGMA	ERROR
25.1	.157E+00	.526E+00
32.7	.874E+00	.105E+02
40.2	.801E+00	.105E+02
44.2	.716E+00	.103E+02
50.2	.444E+00	.102E+02
52.2	.322E+00	.102E+02
57.3	.132E+00	.101E+02
65.3	.291E+00	.102E+02
70.3	.227E+00	.102E+02

EX=4.474 MEV

THETA	SIGMA	ERROR
25.1	.900E+00	.104E+02
32.7	.450E+00	.104E+02
40.2	.576E+00	.105E+02
44.2	.457E+00	.102E+02
50.2	.247E+00	.102E+02
52.2	.160E+00	.101E+02
57.3	.114E+00	.101E+02

EX=4.496 MEV

THETA	SIGMA	ERROR
25.1	.616E+00	.104E+02
32.7	.166E+00	.103E+02
40.2	.233E+00	.103E+02
44.2	.226E+00	.102E+02
50.2	.132E+00	.101E+02
52.2	.119E+00	.101E+02
57.3	.447E+00	.208E+02
75.3	.801E+00	.201E+02

EX=4.534 MEV

THETA	SIGMA	ERROR
25.1	.477E+00	.103E+02
32.7	.577E+00	.105E+02
40.2	.443E+00	.104E+02
44.2	.326E+00	.102E+02
50.2	.240E+00	.102E+02
52.2	.301E+00	.102E+02
57.3	.770E+00	.202E+02
65.3	.158E+00	.101E+02
70.3	.619E+00	.201E+02
75.3	.103E+00	.101E+02

EX=4.580 MEV

THETA	SIGMA	ERROR
16.1	.222E+00	.154E+00
20.1	.178E+00	.176E+00
25.1	.117E+00	.338E+00
30.1	.142E+00	.370E+00
35.2	.115E+00	.629E+00
40.2	.106E+00	.566E+00
42.2	.108E+00	.698E+00
45.2	.117E+00	.698E+00
48.2	.979E+00	.105E+02
55.3	.940E+00	.104E+02
63.3	.853E+00	.103E+02
70.3	.680E+00	.103E+02
74.3	.452E+00	.104E+02
85.3	.367E+00	.101E+02
90.3	.241E+00	.102E+02
95.3	.192E+00	.101E+02

EX=4.595 MEV

THETA	SIGMA	ERROR
25.1	.429E+00	.103E+02
32.7	.114E+00	.606E+00
40.2	.232E+00	.103E+02
44.2	.187E+00	.102E+02
50.2	.258E+00	.102E+02

EX=4.614 MEV

THETA	SIGMA	ERROR
25.1	.665E+00	.202E+02
32.7	.283E+00	.104E+02
40.2	.794E+00	.202E+02
44.2	.807E+00	.202E+02
52.2	.905E+00	.201E+02
70.3	.246E+00	.207E+02
75.3	.529E+00	.209E+02

EX=4.647 MEV

THETA	SIGMA	ERROR
25.1	.125E+00	.102E+02
32.7	.150E+00	.103E+02
44.2	.492E+00	.202E+02
50.2	.805E+00	.201E+02
52.2	.127E+00	.101E+02
57.3	.240E+00	.200E+02
65.3	.545E+00	.201E+02
70.3	.160E+00	.200E+02
75.3	.239E+00	.207E+02

EX=4.664 MEV

THETA	SIGMA	ERROR
25.1	.261E+00	.103E+02
32.7	.297E+00	.104E+02
40.2	.217E+00	.103E+02
44.2	.204E+00	.102E+02
50.2	.798E+00	.201E+02
57.3	.567E+00	.209E+02
65.3	.544E+00	.201E+02
70.3	.585E+00	.201E+02
75.3	.542E+00	.209E+02

EX=4.710 MEV

THETA	SIGMA	ERROR
25.1	.515E+00	.103E+02
32.7	.564E+00	.105E+02
40.2	.480E+00	.104E+02
44.2	.225E+00	.102E+02
50.2	.216E+00	.102E+02
52.2	.204E+00	.102E+02
57.3	.808E+00	.201E+02
65.3	.102E+00	.101E+02
70.3	.116E+00	.101E+02
75.3	.120E+00	.101E+02

EX=4.729 MEV

THETA	SIGMA	ERROR
32.7	.376E+00	.104E+02
40.2	.455E+00	.104E+02
44.2	.163E+00	.102E+02
50.2	.260E+00	.102E+02
52.3	.265E+00	.102E+02
57.3	.814E+00	.201E+02
65.3	.108E+00	.101E+02
70.3	.638E+00	.201E+02

EX=4.742 MEV

THETA	SIGMA	ERROR
25.1	.154E+00	.102E+02
32.7	.184E+00	.103E+02
44.2	.630E+00	.202E+02
50.2	.142E+00	.102E+02
52.3	.108E+00	.101E+02
57.3	.574E+00	.210E+02
75.3	.105E+00	.101E+02

EX=4.770 MEV

THETA	SIGMA	ERROR
25.1	.553E+00	.104E+02
32.7	.703E+00	.105E+02
40.2	.297E+00	.104E+02
44.2	.418E+00	.103E+02
50.2	.356E+00	.102E+02
52.3	.394E+00	.102E+02
57.3	.179E+00	.101E+02
65.3	.140E+00	.102E+02
70.3	.103E+00	.101E+02
75.3	.136E+00	.101E+02

EX=4.793 MEV

THETA	SIGMA	ERROR
25.1	.684E+00	.104E+02
32.7	.985E+00	.106E+02
40.2	.832E+00	.106E+02
44.2	.659E+00	.103E+02
50.2	.515E+00	.103E+02
52.3	.410E+00	.102E+02
57.3	.174E+00	.101E+02
65.3	.249E+00	.102E+02
70.3	.123E+00	.101E+02
75.3	.168E+00	.101E+02

EX=4.809 MEV

THETA	SIGMA	ERROR
25.1	.266E+00	.103E+02
32.7	.322E+00	.104E+02
40.2	.302E+00	.104E+02
44.2	.262E+00	.103E+02
52.3	.196E+00	.102E+02
57.3	.113E+00	.101E+02

EX=4.828 MEV

THETA	SIGMA	ERROR
25.1	.765E+00	.104E+02
32.7	.891E+00	.106E+02
40.2	.645E+00	.105E+02
44.2	.611E+00	.103E+02
50.2	.639E+00	.103E+02
52.3	.570E+00	.103E+02
57.3	.277E+00	.102E+02
65.3	.399E+00	.102E+02
70.3	.273E+00	.102E+02
75.3	.342E+00	.102E+02

EX=4.860 MEV

THETA	SIGMA	ERROR
25.1	.218E+00	.103E+02
32.7	.127E+00	.103E+02
40.2	.122E+00	.103E+02
44.2	.159E+00	.102E+02
50.2	.118E+00	.102E+02
52.3	.122E+00	.102E+02
70.3	.504E+00	.201E+02
75.3	.647E+00	.201E+02

EX=4.889 MEV

THETA	SIGMA	ERROR
32.7	.708E+00	.105E+02
40.2	.195E+00	.103E+02
44.2	.121E+00	.102E+02
50.2	.334E+00	.102E+02
52.3	.319E+00	.102E+02
57.3	.156E+00	.102E+02
65.3	.188E+00	.102E+02
70.3	.117E+00	.101E+02
75.3	.950E+00	.201E+02

EX=4.916 MEV

THETA	SIGMA	ERROR
32.7	.510E+00	.105E+02
40.2	.149E+00	.103E+02
44.2	.216E+00	.103E+02
50.2	.301E+00	.102E+02
52.3	.233E+00	.102E+02
57.3	.116E+00	.101E+02
70.3	.844E+00	.201E+02
75.3	.834E+00	.201E+02

EX=4.939 MEV

THETA	SIGMA	ERROR
32.7	.685E+00	.106E+02
40.2	.507E+00	.105E+02
44.2	.535E+00	.103E+02
50.2	.520E+00	.103E+02
52.3	.445E+00	.103E+02
57.3	.165E+00	.102E+02
65.3	.213E+00	.102E+02
70.3	.159E+00	.102E+02
75.3	.198E+00	.102E+02

EX=4.960 MEV

THETA	SIGMA	ERROR
32.7	.494E+00	.105E+02
40.2	.281E+00	.104E+02
44.2	.366E+00	.103E+02
50.2	.377E+00	.102E+02
52.3	.400E+00	.102E+02
57.3	.179E+00	.102E+02
70.3	.184E+00	.102E+02
75.3	.187E+00	.101E+02

EX=4.986 MEV

THETA	SIGMA	ERROR
25.1	.139E+00	.561E+00
32.7	.620E+00	.105E+02
40.2	.232E+00	.104E+02
44.2	.320E+00	.103E+02
50.2	.270E+00	.102E+02
52.3	.225E+00	.102E+02
57.3	.140E+00	.102E+02

EX=5.007 MEV

THETA	SIGMA	ERROR
25.1	.115E+00	.520E+00
32.7	.134E+00	.695E+00
40.2	.498E+00	.105E+02
44.2	.433E+00	.103E+02
50.2	.521E+00	.103E+02
52.3	.590E+00	.103E+02
57.3	.375E+00	.102E+02
65.3	.474E+00	.103E+02
70.3	.285E+00	.102E+02
75.3	.163E+00	.102E+02

EX=5.025 MEV

THETA	SIGMA	ERROR
25.1	.493E+00	.104E+02
32.7	.620E+00	.106E+02
40.2	.171E+00	.103E+02
44.2	.104E+00	.103E+02
50.2	.307E+00	.102E+02
52.3	.300E+00	.102E+02
57.3	.170E+00	.102E+02
65.3	.226E+00	.102E+02
70.3	.204E+00	.102E+02

EX=5.045 MEV

THETA	SIGMA	ERROR
25.1	.317E+00	.103E+02
32.7	.296E+00	.105E+02
40.2	.774E+00	.202E+02
44.2	.945E+00	.202E+02
50.2	.104E+00	.102E+02
52.3	.990E+00	.202E+02

EX=5.069 MEV

THETA	SIGMA	ERROR
25.1	.415E+00	.104E+02
32.7	.153E+00	.104E+02
40.2	.160E+00	.103E+02
44.2	.870E+00	.202E+02
50.2	.131E+00	.102E+02
57.3	.112E+00	.101E+02
65.3	.107E+00	.102E+02
70.3	.603E+00	.201E+02
75.3	.913E+00	.201E+02

EX=5.092 MEV

THETA	SIGMA	ERROR
25.1	.458E+00	.104E+02
32.7	.372E+00	.105E+02
40.2	.157E+00	.103E+02
44.2	.174E+00	.103E+02
50.2	.147E+00	.102E+02
52.3	.150E+00	.102E+02
57.3	.910E+00	.201E+02

EX=5.111 MEV

THETA	SIGMA	ERROR
25.1	.551E+00	.104E+02
32.7	.691E+00	.106E+02
40.2	.195E+00	.104E+02
44.2	.149E+00	.102E+02
50.2	.150E+00	.102E+02
52.3	.136E+00	.102E+02
65.3	.137E+00	.102E+02
75.3	.710E+00	.201E+02

EX=5.126 MEV

THETA	SIGMA	ERROR
25.1	.443E+00	.104E+02
32.7	.420E+00	.105E+02
40.2	.252E+00	.104E+02
44.2	.217E+00	.103E+02
50.2	.146E+00	.102E+02
52.3	.187E+00	.102E+02
57.3	.719E+00	.201E+02
65.3	.926E+00	.202E+02
70.3	.904E+00	.201E+02
75.3	.100E+00	.102E+02

EX=5.138 MEV

THETA	SIGMA	ERROR
25.1	.443E+00	.104E+02
32.7	.339E+00	.105E+02
40.2	.187E+00	.104E+02
50.2	.742E+00	.202E+02
52.3	.374E+00	.202E+02

EX=5.169 MEV

THETA	SIGMA	ERROR
25.1	.761E+00	.105E+02
32.7	.798E+00	.106E+02
40.2	.275E+00	.104E+02
44.2	.301E+00	.103E+02
50.2	.186E+00	.102E+02
52.3	.223E+00	.102E+02
57.3	.986E+00	.201E+02
65.3	.838E+00	.202E+02
70.3	.534E+00	.201E+02
75.3	.594E+00	.201E+02

EX=5.190 MEV

THETA	SIGMA	ERROR
25.1	.544E+00	.104E+02
32.7	.492E+00	.106E+02
40.2	.107E+00	.103E+02
44.2	.119E+00	.102E+02
50.2	.820E+00	.202E+02
52.3	.915E+00	.202E+02
57.3	.374E+00	.201E+02
65.3	.782E+00	.201E+02
70.3	.443E+00	.201E+02
75.3	.366E+00	.201E+02

EX=5.209 MEV

THETA	SIGMA	ERROR
25.1	.191E+00	.103E+02
40.2	.696E+00	.203E+02
44.2	.128E+00	.102E+02
50.2	.705E+00	.202E+02
52.3	.107E+00	.102E+02
57.3	.258E+00	.201E+02
75.3	.347E+00	.201E+02

EX=5.245 MEV

THETA	SIGMA	ERROR
25.1	.158E+00	.639E+00
40.2	.530E+00	.106E+02
44.2	.573E+00	.103E+02
50.2	.590E+00	.103E+02
52.3	.637E+00	.103E+02
57.3	.385E+00	.102E+02
65.3	.477E+00	.103E+02
70.3	.246E+00	.102E+02
75.3	.193E+00	.102E+02

EX=5.279 MEV

THETA	SIGMA	ERROR
25.1	.712E+00	.105E+02
40.2	.151E+00	.104E+02
44.2	.289E+00	.103E+02
50.2	.225E+00	.102E+02
52.3	.354E+00	.102E+02
57.3	.113E+00	.102E+02
70.3	.101E+00	.102E+02
75.3	.108E+00	.102E+02

EX=5.296 MEV

THETA	SIGMA	ERROR
25.1	.387E+00	.104E+02
40.2	.148E+00	.104E+02
44.2	.177E+00	.103E+02
50.2	.230E+00	.102E+02
52.3	.293E+00	.102E+02
57.3	.108E+00	.101E+02
65.3	.126E+00	.102E+02

EX=5.309 MEV

THETA	SIGMA	ERROR
25.1	.399E+00	.104E+02
40.2	.145E+00	.104E+02
44.2	.102E+00	.103E+02
50.2	.170E+00	.102E+02
52.3	.173E+00	.102E+02
57.3	.137E+00	.102E+02
65.3	.115E+00	.102E+02
70.3	.948E+00	.202E+02
75.3	.126E+00	.102E+02

EX=5.332 MEV

THETA	SIGMA	ERROR
25.1	.483E+00	.104E+02
40.2	.120E+00	.103E+02
44.2	.136E+00	.102E+02
50.2	.160E+00	.102E+02
52.3	.165E+00	.102E+02
57.3	.102E+00	.102E+02
65.3	.940E+00	.202E+02
70.3	.101E+00	.102E+02
75.3	.747E+00	.202E+02

EX=5.365 MEV

THETA	SIGMA	ERROR
25.1	.400E+00	.104E+02
32.7	.364E+00	.105E+02
40.2	.125E+00	.103E+02
44.2	.225E+00	.103E+02
50.2	.195E+00	.102E+02
57.3	.127E+00	.102E+02
65.3	.145E+00	.102E+02
70.3	.123E+00	.102E+02
75.3	.835E+00	.202E+02

EX=5.403 MEV

THETA	SIGMA	ERROR
32.7	.414E+00	.106E+02
40.2	.197E+00	.104E+02
44.2	.818E+00	.202E+02
52.3	.522E+00	.202E+02
75.3	.258E+00	.210E+02

EX=5.422 MEV

THETA	SIGMA	ERROR
25.1	.578E+00	.104E+02
32.7	.101E+00	.731E+00
40.2	.315E+00	.105E+02
44.2	.241E+00	.103E+02
50.2	.250E+00	.102E+02
52.3	.159E+00	.102E+02
57.3	.138E+00	.102E+02
65.3	.168E+00	.102E+02
70.3	.137E+00	.102E+02
75.3	.122E+00	.102E+02

EX=5.435 MEV

THETA	SIGMA	ERROR
25.1	.578E+00	.105E+02
40.2	.202E+00	.104E+02
44.2	.218E+00	.103E+02
52.3	.306E+00	.102E+02
65.3	.172E+00	.102E+02

EX=5.452 MEV

THETA	SIGMA	ERROR
25.1	.541E+00	.104E+02
32.7	.658E+00	.107E+02
40.2	.193E+00	.104E+02
44.2	.213E+00	.103E+02
50.2	.223E+00	.102E+02
52.3	.183E+00	.102E+02
57.3	.155E+00	.102E+02
65.3	.158E+00	.102E+02

EX=5.463 MEV

THETA	SIGMA	ERROR
25.1	.452E+00	.105E+02
44.2	.182E+00	.103E+02
50.2	.281E+00	.102E+02
52.3	.211E+00	.102E+02
57.3	.160E+00	.102E+02
65.3	.106E+00	.102E+02
70.3	.898E+00	.202E+02
75.3	.598E+00	.202E+02

EX=5.485 MEV

THETA	SIGMA	ERROR
25.1	.614E+00	.105E+02
32.7	.734E+00	.107E+02
44.2	.248E+00	.103E+02
50.2	.230E+00	.102E+02
52.3	.256E+00	.102E+02
57.3	.136E+00	.102E+02
65.3	.134E+00	.102E+02
70.3	.120E+00	.102E+02
75.3	.129E+00	.102E+02

EX=5.507 MEV

THETA	SIGMA	ERROR
25.1	.310E+00	.104E+02
32.7	.543E+00	.106E+02
40.2	.106E+00	.103E+02
44.2	.190E+00	.102E+02
50.2	.197E+00	.102E+02
52.3	.223E+00	.102E+02
57.3	.114E+00	.102E+02
65.3	.120E+00	.102E+02
70.3	.424E+00	.201E+02
75.3	.715E+00	.202E+02

EX=5.533 MEV

THETA	SIGMA	ERROR
25.1	.408E+00	.104E+02
32.7	.754E+00	.107E+02
40.2	.316E+00	.105E+02
50.2	.245E+00	.102E+02
52.3	.261E+00	.102E+02
65.3	.215E+00	.102E+02
70.3	.117E+00	.102E+02
75.3	.127E+00	.102E+02

EX=5.561 MEV

THETA	SIGMA	ERROR
25.1	.599E+00	.105E+02
32.7	.120E+00	.789E+00
40.2	.630E+00	.106E+02
44.2	.336E+00	.103E+02
50.2	.329E+00	.103E+02
52.3	.361E+00	.103E+02
65.3	.312E+00	.102E+02
70.3	.105E+00	.102E+02
75.3	.109E+00	.102E+02

EX=5.588 MEV

THETA	SIGMA	ERROR
25.1	.759E+00	.105E+02
32.7	.685E+00	.107E+02
40.2	.826E+00	.107E+02
44.2	.648E+00	.103E+02
50.2	.422E+00	.103E+02
52.3	.332E+00	.103E+02
57.3	.204E+00	.102E+02
65.3	.398E+00	.103E+02
70.3	.326E+00	.102E+02
75.3	.373E+00	.102E+02

EX=5.619 MEV

THETA	SIGMA	ERROR
25.1	.428E+00	.104E+02
32.7	.653E+00	.107E+02
44.2	.251E+00	.102E+02
50.2	.155E+00	.102E+02
52.3	.247E+00	.102E+02
70.3	.135E+00	.102E+02
75.3	.130E+00	.102E+02

EX=5.640 MEV

THETA	SIGMA	ERROR
25.1	.477E+00	.105E+02
32.7	.324E+00	.106E+02
44.2	.135E+00	.102E+02
50.2	.211E+00	.102E+02
52.3	.174E+00	.102E+02
65.3	.132E+00	.102E+02
70.3	.506E+00	.201E+02

EX=5.653 MEV

THETA	SIGMA	ERROR
25.1	.248E+00	.104E+02
44.2	.167E+00	.103E+02
50.2	.172E+00	.102E+02
57.3	.513E+00	.201E+02

EX=5.676 MEV

THETA	SIGMA	ERROR
25.1	.456E+00	.104E+02
32.7	.392E+00	.106E+02
44.2	.191E+00	.103E+02
50.2	.261E+00	.103E+02
52.3	.248E+00	.102E+02
57.3	.199E+00	.102E+02
65.3	.217E+00	.102E+02
70.3	.134E+00	.102E+02
75.3	.869E+00	.202E+02

EX=5.703 MEV

THETA	SIGMA	ERROR
25.1	.255E+00	.104E+02
32.7	.520E+00	.106E+02
44.2	.280E+00	.103E+02
50.2	.188E+00	.102E+02
52.3	.635E+00	.202E+02
57.3	.104E+00	.102E+02

EX=5.715 MEV

THETA	SIGMA	ERROR
25.1	.398E+00	.104E+02
32.7	.538E+00	.106E+02
44.2	.144E+00	.102E+02
52.3	.197E+00	.102E+02
57.3	.114E+00	.102E+02
65.3	.232E+00	.102E+02
70.3	.234E+00	.102E+02
75.3	.154E+00	.102E+02

EX=5.722 MEV

THETA	SIGMA	ERROR
25.1	.300E+00	.104E+02
32.7	.236E+00	.105E+02
50.2	.122E+00	.102E+02
52.3	.803E+00	.202E+02

EX=5.747 MEV

THETA	SIGMA	ERROR
25.1	.271E+00	.104E+02
32.7	.343E+00	.106E+02
44.2	.181E+00	.102E+02
52.3	.511E+00	.202E+02

EX=5.763 MEV

THETA	SIGMA	ERROR
32.7	.346E+00	.106E+02
44.2	.231E+00	.103E+02
50.2	.109E+00	.102E+02
57.3	.823E+00	.201E+02
65.3	.209E+00	.102E+02
70.3	.117E+00	.102E+02
75.3	.141E+00	.102E+02

EX=5.779 MEV

THETA	SIGMA	ERROR
25.1	.381E+00	.104E+02
32.7	.407E+00	.106E+02
40.2	.352E+00	.105E+02
44.2	.273E+00	.103E+02
50.2	.153E+00	.102E+02
52.3	.163E+00	.102E+02
57.3	.883E+00	.201E+02
70.3	.461E+00	.201E+02

EX=5.796 MEV

THETA	SIGMA	ERROR
25.1	.308E+00	.104E+02
32.7	.322E+00	.106E+02
40.2	.324E+00	.105E+02
44.2	.142E+00	.102E+02
50.2	.109E+00	.102E+02
57.3	.109E+00	.102E+02
65.3	.133E+00	.102E+02
70.3	.116E+00	.102E+02
75.3	.102E+00	.102E+02

EX=5.823 MEV

THETA	SIGMA	ERROR
25.1	.640E+00	.105E+02
32.7	.552E+00	.106E+02
40.2	.331E+00	.105E+02
50.2	.177E+00	.102E+02
57.3	.130E+00	.102E+02
70.3	.937E+00	.202E+02

EX=5.843 MEV

THETA	SIGMA	ERROR
25.1	.363E+00	.104E+02
32.7	.347E+00	.106E+02
40.2	.250E+00	.104E+02
50.2	.165E+00	.102E+02
57.3	.125E+00	.102E+02
70.3	.107E+00	.102E+02

EX=5.860 MEV

THETA	SIGMA	ERROR
25.1	.677E+00	.105E+02
32.7	.450E+00	.106E+02
50.2	.107E+00	.102E+02
57.3	.104E+00	.102E+02
70.3	.943E+00	.202E+02
75.3	.153E+00	.102E+02

EX=5.885 MEV

THETA	SIGMA	ERROR
25.1	.605E+00	.105E+02
32.7	.336E+00	.106E+02
40.2	.209E+00	.105E+02
50.2	.208E+00	.102E+02
57.3	.153E+00	.102E+02
70.3	.116E+00	.102E+02
75.3	.101E+00	.102E+02

EX=5.911 MEV

THETA	SIGMA	ERROR
25.1	.110E+00	.594E+00
32.7	.126E+00	.709E+00
40.2	.953E+00	.107E+02
50.2	.199E+00	.102E+02
52.3	.239E+00	.102E+02
57.3	.302E+00	.102E+02
65.3	.416E+00	.103E+02
70.3	.241E+00	.102E+02

EX=5.949 MEV

THETA	SIGMA	ERROR
32.7	.388E+00	.106E+02
40.2	.309E+00	.105E+02
52.3	.125E+00	.102E+02
57.3	.764E+00	.201E+02
65.3	.144E+00	.102E+02
75.3	.149E+00	.102E+02

EX=5.959 MEV

THETA	SIGMA	ERROR
32.7	.174E+00	.105E+02
40.2	.230E+00	.104E+02
50.2	.165E+00	.102E+02
52.3	.146E+00	.102E+02
57.3	.109E+00	.102E+02

EX=5.974 MEV

THETA	SIGMA	ERROR
32.7	.145E+00	.105E+02
40.2	.142E+00	.104E+02
50.2	.804E+00	.202E+02
52.3	.809E+00	.202E+02

EX=5.990 MEV

THETA	SIGMA	ERROR
32.7	.160E+00	.105E+02
40.2	.127E+00	.104E+02
57.3	.152E+00	.209E+02
70.3	.434E+00	.201E+02
75.3	.706E+00	.201E+02

EX=6.065 MEV

THETA	SIGMA	ERROR
32.7	.526E+00	.106E+02
40.2	.140E+00	.104E+02
44.2	.206E+00	.102E+02
50.2	.114E+00	.102E+02
52.3	.748E+00	.202E+02
57.3	.555E+00	.201E+02
65.3	.115E+00	.102E+02

EX=6.083 MEV

THETA	SIGMA	ERROR
44.2	.162E+00	.102E+02
50.2	.116E+00	.102E+02
52.3	.641E+00	.202E+02
57.3	.255E+00	.201E+02
75.3	.490E+00	.201E+02

EX=6.117 MEV

THETA	SIGMA	ERROR
32.7	.497E+00	.106E+02
40.2	.143E+00	.104E+02
44.2	.164E+00	.102E+02
50.2	.113E+00	.102E+02
52.3	.201E+00	.102E+02
57.3	.113E+00	.101E+02
65.3	.184E+00	.102E+02
70.3	.984E+00	.202E+02
75.3	.125E+00	.102E+02

EX=6.146 MEV

THETA	SIGMA	ERROR
32.7	.239E+00	.105E+02
40.2	.169E+00	.104E+02
44.2	.200E+00	.102E+02
50.2	.166E+00	.102E+02
52.3	.723E+00	.202E+02
57.3	.130E+00	.102E+02
65.3	.209E+00	.102E+02
70.3	.157E+00	.102E+02
75.3	.181E+00	.102E+02

EX=6.167 MEV

THETA	SIGMA	ERROR
32.7	.259E+00	.106E+02
40.2	.231E+00	.104E+02
44.2	.215E+00	.102E+02
50.2	.154E+00	.102E+02
52.3	.665E+00	.202E+02
57.3	.822E+00	.201E+02
65.3	.160E+00	.102E+02
70.3	.128E+00	.102E+02
75.3	.137E+00	.102E+02

EX=6.181 MEV

THETA	SIGMA	ERROR
40.2	.124E+00	.104E+02
44.2	.159E+00	.102E+02
50.2	.199E+00	.102E+02
52.3	.514E+00	.202E+02
57.3	.680E+00	.201E+02

EX=6.198 MEV

THETA	SIGMA	ERROR
32.7	.140E+00	.105E+02
40.2	.217E+00	.104E+02
44.2	.173E+00	.102E+02
52.3	.163E+00	.102E+02
57.3	.578E+00	.201E+02
65.3	.766E+00	.202E+02
70.3	.508E+00	.201E+02
75.3	.876E+00	.202E+02

EX=6.229 MEV

THETA	SIGMA	ERROR
32.7	.206E+00	.105E+02
40.2	.771E+00	.203E+02
44.2	.135E+00	.102E+02
50.2	.641E+00	.201E+02
52.3	.969E+00	.202E+02
57.3	.319E+00	.201E+02
65.3	.455E+00	.201E+02
70.3	.680E+00	.201E+02
75.3	.112E+00	.102E+02

EX=6.264 MEV

THETA	SIGMA	ERROR
32.7	.187E+00	.105E+02
44.2	.249E+00	.102E+02
50.2	.184E+00	.102E+02
52.3	.840E+00	.202E+02
65.3	.965E+00	.202E+02
70.3	.687E+00	.202E+02
75.3	.422E+00	.201E+02

EX=6.284 MEV

THETA	SIGMA	ERROR
32.7	.538E+00	.106E+02
40.2	.162E+00	.104E+02
44.2	.221E+00	.102E+02
52.3	.614E+00	.202E+02
57.3	.520E+00	.201E+02
65.3	.148E+00	.102E+02
70.3	.684E+00	.202E+02
75.3	.823E+00	.202E+02

EX=6.302 MEV

THETA	SIGMA	ERROR
32.7	.468E+00	.106E+02
40.2	.165E+00	.104E+02
44.2	.220E+00	.102E+02
52.3	.196E+00	.102E+02
57.3	.522E+00	.201E+02
65.3	.145E+00	.102E+02
70.3	.862E+00	.202E+02
75.3	.150E+00	.102E+02

EX=6.332 MEV

THETA	SIGMA	ERROR
32.7	.277E+00	.106E+02
44.2	.178E+00	.102E+02
50.2	.774E+00	.202E+02
57.3	.198E+00	.201E+02
65.3	.796E+00	.202E+02
70.3	.409E+00	.201E+02
75.3	.513E+00	.201E+02

EX=6.346 MEV

THETA	SIGMA	ERROR
32.7	.200E+00	.105E+02
44.2	.218E+00	.102E+02
50.2	.871E+00	.202E+02
57.3	.627E+00	.201E+02
70.3	.282E+00	.201E+02

EX=6.382 MEV

THETA	SIGMA	ERROR
32.7	.723E+00	.107E+02
40.2	.160E+00	.104E+02
44.2	.167E+00	.102E+02
57.3	.135E+00	.102E+02
65.3	.271E+00	.102E+02
70.3	.126E+00	.102E+02
75.3	.146E+00	.102E+02

EX=6.408 MEV

THETA	SIGMA	ERROR
32.7	.342E+00	.106E+02
40.2	.752E+00	.204E+02
44.2	.136E+00	.102E+02
57.3	.817E+00	.201E+02
65.3	.118E+00	.102E+02
70.3	.629E+00	.202E+02

EX=6.433 MEV

THETA	SIGMA	ERROR
32.7	.442E+00	.106E+02
44.2	.184E+00	.102E+02
57.3	.440E+00	.201E+02
65.3	.146E+00	.102E+02
70.3	.779E+00	.202E+02
75.3	.683E+00	.202E+02

EX=6.444 MEV

THETA	SIGMA	ERROR
32.7	.435E+00	.106E+02
40.2	.226E+00	.105E+02
44.2	.178E+00	.102E+02
57.3	.490E+00	.201E+02
75.3	.775E+00	.202E+02

EX=6.459 MEV

THETA	SIGMA	ERROR
32.7	.173E+00	.105E+02
44.2	.184E+00	.102E+02
57.3	.517E+00	.201E+02
65.3	.134E+00	.102E+02
75.3	.658E+00	.202E+02

EX=6.480 MEV

THETA	SIGMA	ERROR
32.7	.357E+00	.106E+02
44.2	.219E+00	.102E+02
65.3	.125E+00	.102E+02
70.3	.474E+00	.201E+02
75.3	.851E+00	.202E+02

EX=6.524 MEV

THETA	SIGMA	ERROR
32.7	.277E+00	.105E+02
40.2	.121E+00	.104E+02
44.2	.243E+00	.102E+02
70.3	.714E+00	.202E+02
75.3	.718E+00	.201E+02

EX=6.545 MEV

THETA	SIGMA	ERROR
32.7	.458E+00	.106E+02
40.2	.183E+00	.105E+02
44.2	.231E+00	.102E+02
57.3	.339E+00	.201E+02
70.3	.981E+00	.202E+02
75.3	.808E+00	.202E+02

EX=6.574 MEV

THETA	SIGMA	ERROR
32.7	.448E+00	.106E+02
40.2	.238E+00	.105E+02
44.2	.116E+00	.102E+02
57.3	.386E+00	.201E+02
70.3	.728E+00	.202E+02
75.3	.689E+00	.202E+02

EX=6.593 MEV

THETA	SIGMA	ERROR
32.7	.368E+00	.106E+02
40.2	.203E+00	.105E+02
44.2	.106E+00	.102E+02
57.3	.548E+00	.201E+02
70.3	.853E+00	.202E+02

EX=6.617 MEV

THETA	SIGMA	ERROR
32.7	.375E+00	.106E+02
40.2	.193E+00	.105E+02
44.2	.111E+00	.102E+02
57.3	.686E+00	.201E+02
75.3	.482E+00	.201E+02

EX=6.634 MEV

THETA	SIGMA	ERROR
32.7	.287E-01	.562E-02
40.2	.212E-01	.475E-02
44.2	.142E-01	.188E-02
75.3	.578E-02	.158E-02
80.3	.767E-02	.183E-02

APPENDIX IV

ABSTRACTS OF PUBLICATIONS

On the following pages are titles and abstracts of published papers which I have co-authored while a graduate and undergraduate student at Michigan State University. My contributions to these publications are indicated by a letter key following the title. The key is as follows:

A. Data taking.

B. Analysis of data.

C. Performing theoretical calculations.

D. Assisting in the preparation of the paper.

E. Principal writer of the paper.

F. Presented the paper at a meeting or conference.

A. "A SURVEY OF THE (^{3}He, ^{7}Be) REACTIONS AT 70 MeV" [A, B, C, D]

W. F. Steele, P. A. Smith, J. E. Finck, and G. M. Crawley, Nucl. Phys. A266 (1976) 424.

ABSTRACT

A study of the (^{3}He, ^{7}Be) reaction has been undertaken using a 70 MeV ^{3}He beam. By surveying a wide range of target nuclides, namely $^{12, 13}$C, ^{16}O, $^{24, 26}$Mg, $^{40, 42, 44}$Ca, $^{58, 60, 62, 64}$Ni, ^{90}Zr, $^{120, 124}$Sn, ^{144}Sm and ^{206}Pb, systematics of the α-clustering phenomenon were investigated. In addition, masses and energy levels of ^{60}Fe and ^{120}Cd were measured. The ^{7}Be particles were detected in a single wire proportional counter backed by a plastic scintillator in the focal plane of an Enge spectrometer to ensure adequate particle identification. Total energy resolution as small as 140 keV full width at half maximum was obtained, although in most cases the target thickness limited the energy resolution to larger values. Differential cross sections as low as 20 nb/sr were measured. The finite range programs LOLA and LOLITA were used to calculate differential cross sections for comparison to data, assuming the reaction to proceed by a direct α-transfer. The spectroscopic factors which were extracted show a marked decrease with increasing atomic mass number, implying a decrease in surface α-clustering for heavier nuclei.

B. "THE ^{54}Fe(p, d)^{53}Fe REACTION AT 40 MeV AND THE DWBA ANALYSIS" [A, B, D]

T. Suehiro, J. E. Finck, and J. A. Nolen, Jr., Proceedings of Int. Conf. on Nuclear Structure, Tokyo, 1977. J. Phys. Soc. Japan 44 (1978) Suppl. 534.

ABSTRACT

Angular distributions of deuterons from the ^{54}Fe (p, d)^{53}Fe reaction were measured with 40.16 MeV protons using a split-pole spectrograph and position sensitive proportional counter. The measurement was done with 15 keV resolution. Peaks previously unresolved in the (p, d) reaction were clearly observed. Calculations performed with zero-range local DWBA and the adiabatic model are shown to give poor results. Fits are improved with Finite-range and non-local corrections for $7/2^-$ states. By use of the effective binding procedure fits were much improved for the $1/2^-$, $3/2^-$, and $5/2^-$ states.

C. "EXTRACTION OF DEFORMATION PARAMETERS FROM INELASTIC PROTON SCATTERING" [A, B, C, D]

C. H. King, G. M. Crawley, J. A. Nolen, Jr., and J. E. Finck, Proc. Int. Conf. Nucl. Structure, Tokyo, 1977. J. Phys. Soc. Japan 44 (1978) Suppl. 564.

ABSTRACT

This experiment reports the measurement of the inelastic scattering of 35 MeV protons from the nuclei ^{154}Sm, ^{176}Yb, ^{232}Th and ^{238}U. Angular distributions were extracted for the ground state rotational band. The data were compared with coupled channel calculations using a deformed optical potential and values of the deformation parameters β_2 and β_4 were extracted. These values, together with the multipole potential moments are compared to the results of Coulomb excitation, electron scattering, and inelastic α-sscattering measurements. In general, the potential moments extracted from the present (p, p') measurements agree better with those from the Coulomb excitation and electron scattering measurements than with the moments from (α, α'). However, the deformation parameters from (p, p'), corrected for the projectile size, agree much better with values obtained from high energy α-scattering than with deformation parameters extracted from Coulomb excitation and electron scattering experiments.

D. "INELASTIC PROTON SCATTEIRNG FROM LANTHANIDE AND ACTINIDE NUCLEI" [A, B, C, D]

G. M. Crawley, C. H. King, J. A. Nolen, Jr., and J. E. Finck, Int. Symp. on Nuclear Physics at Cyclotron Energies, Calcutta, India, September 14-16, (1977) 239.

ABSTRACT

The inelastic scattering of 35 MeV protons is reported from the nuclei ^{154}Sm, ^{176}Yb, ^{232}Th and ^{238}U. Angular distributions were extracted for the ground state rotational band. The data were compared with coupled channel calculations using a deformed optical potential and values of the deformation parameters β_2 and β_4 were extracted. These values, together with the multipole potential moments are compared to the results of Coulomb excitation, electron scattering, and inelastic α-scattering measurements. The deformation parameters generally do not show good agreement for the different methods although the values obtained from the proton measurements are reasonably consistent with the values from high energy α-scattering. However, the potential moments from the present (p, p') measurements agree better with those from the Coulomb excitation and electron scattering measurements than with the moments from (α, α').

E. "A STUDY OF THE ^{54}Fe(p, d)^{53}Fe REACTION AT 40 MeV" [A, B, D]

T. Suehiro, J. E. Finck, and J. A. Nolen, Jr., Nucl. Phys. A313 (1979), 141.

ABSTRACT

The ^{54}Fe(p, d)^{53}Fe reaction was studied using 40 MeV protons with a split-pole magnetic spectrograph. A total of 53 states were observed up to an excitation energy of 7.364 MeV in ^{53}Fe. At least 29 of these states have not been previously reported. Angular distributions were measured from 6° to 90° for transitions to 35 of these states, and were analyzed with distorted-wave Born approximation calculations. Excitation energies, transferred L-values, spectroscopic factors and the implied J^{π} values are given. Difficulties encountered in obtaining a reliable set of spectroscopic factors are discussed in relation to various prescriptions in the DWBA calculations, and to the one-nucleon transfer sum rule.

F. "OCTUPOLE STATES IN ^{63}Cu AND THE WEAK-COUPLING PICTURE" [A, B, D]

Y. Iawasaki, G. M. Crawley, R. G. Markham, J. E. Finck, and J. H. Kim, Phys. Rev. C 20 (1979), 861.

ABSTRACT

A high-resolution experiment of proton inelastic scattering by ^{63}Cu at E_p = 40 MeV has resolved three octupole states at E_x = 3.81, 3.84, and 3.89 MeV for the first time, thus showing the existence of seven strong octuopole states in ^{63}Cu. This finding is direct evidence that the traditional simple weak-coupling model in terms of one quartet $2p_{3/2} \otimes 3^-_1$ is adequate for the octuopole core-excited states in ^{63}Cu. This is not evidence, however, that the weak-coupling picture in general is incorrect for the octupole states in ^{63}Cu. It is shown that to be consistent with the present experimental data, the weak-coupling picture for the octupole states requires a ground-state wave function substantially different from the ground-state wave function of the conventional particle-core-coupling model.

G. "MULTIPOLE MOMENTS OF ^{154}Sm, ^{176}Yb, ^{232}Th, AND ^{238}U FROM PROTON INELASTIC SCATTERING" A, B, C, D

C. H. King, J. E. Finck, G. M. Crawley, J. A. Nolen, Jr., and R. M. Ronningen, Phys. Rev. C 20 (1979), 2048.

ABSTRACT

We have measured the inelastic scattering of 35 MeV protons from the nuclei ^{154}Sm, ^{176}Yb, ^{232}Th, and ^{238}U. Angular distributions were extracted for $J^{\pi} = 0^{+}-8^{+}$ members of ground state rotational bands. These data were analzyed using coupled channels calculations for scattering from a deformed optical potential. Searches were made on some of the parameters of this potential, including the deformation parameters β_2 and β_4. The multipole moments of the potential distribution were calculated from the parameter values and are compared to the results of Coulomb excitation, electron scattering, and inelastic, alpha-particle scattering studies. In general, these moments deduced in our investigation agree better with those from Coulomb excitation and electron scattering than with moments deduced from α-particle scattering. But we also find the moments from our study to be systematically smaller than those from Coulomb excitation.

H. "CORE EXCITATIONS IN ^{63}Cu BY THE ^{63}Cu(p, p') AND ^{65}Cu(p, t)^{63}Cu REACTIONS" A, B, D

Y. Iawasaki, G. M. Crawley, J. E. Finck, Phys. Rev. C 23 (1981), 1960.

ABSTRACT

Core excitations up to E_x = 4 MeV in ^{63}Cu(p, p')^{63}Cu and ^{65}Cu(p, t)^{63}Cu at 40 MeV proton energy. The tranferred angular momentum L has been determined for each transition on the basis of the angular distribution shape. A quartet-plus-doublet pattern is consistently observed for the groups of states corresponding to the 2^+_1, 3^-_1, and 4^+_1 states of the core nucleus ^{62}Ni. This implies the existence of doublets arising from the coupling of collective states of the core with $2p_{1/2}$ proton orbital, in addition to the quartets from the coupling with the $2p_{3/2}$ proton orbital considered in the conventional weak-coupling excited-core model. It is pointed out that the existence of a weak-coupling situation cannot be proved only on the basis of transfer-reaction data, and in this regard the importance of a comparative study of the inelastic-scattering and transfer-reaction data is emphasized.

I. "MULTIPOLE MOMENTS OF ^{232}Th and $^{234, 236, 238}$U FROM PROTON INELASTIC SCATTERING" A, B, C, D

R. C. Melin, R. M. Ronningen, J. A. Nolen, Jr., G. M. Crawley, C. H. King, J. E. Finck, and C. E. Bemis, Jr., Proceedings of Int. Conf. on Band Structure and Nuclear Dynamics, Vol. 1 (1980), 69.

ABSTRACT

We have measured the inelastic scattering of 35 MeV protons from ^{232}Th and $^{234, 236, 238}$U. Angular distributions were extracted for $J^{\pi} = 0^{+}$-8^{+} members of the ground state rotational bands. These data are being analyzed using coupled channels calculations for scattering from a deformed optical potential. Our preliminary values for the quadrupole and hexadecapole moments of the potential distribution are compared to moments from Coulomb excitation, electron scattering, and alpha particle scattering, as well as theory. Preliminary values of β_6 for ^{232}Th and ^{238}U are given.

J. "SYSTEMATICS OF COLLECTIVE STATES IN LEAD NUCLEI FROM INELASTIC PROTON SCATTERING" A, B, C, E

J. E. Finck, G. M. Crawley, J. A. Nolen, Jr., and R. Kouzes, Phys. Lett. 107B (1981), 182.

ABSTRACT

From the scattering of 35 MeV protons from ^{206}Pb accurate excitation energies and angular distributions have been determined for the strongly excited collective states. These states are compared to corresponding states in $^{207, 208}Pb$. A possible explanation of the anomaly in the 5^- strength is given in terms of the core wave functions.

K. "A STUDY OF ^{206}Pb BY INELASTIC SCATTERING OF 35 MeV PROTONS" A, B, C, E

J. E. Finck, G. M. Crawley, J. A. Nolen, Jr., and R. T. Kouzes, submitted for publication.

ABSTRACT

Using high resolution techniques the inelastic scattering of 35 MeV protons by ^{206}Pb is measured. Approximately 180 levels with excitation energies up to 6.8 MeV are identified and angular distributions of most of these states are measured. L-transfers and deformation parameters are determined by comparison of the angular distributions to collective model calculations. Microscopic calculations of natural parity states are presented and allow a test of RPA and TDA wave functions. Unnatural parity states are also studied microscopically and permit an examination of the central and noncentral forces in the effective interaction.

L. "INELASTIC PROTON SCATTERING FROM ^{176}Yb AND ^{154}Sm" A, B, C, E

J. E. Finck, G. M. Crawley, and J. A. Nolen, Jr., BAPS 21 (1976), 662.

ABSTRACT

Because of the complementary nature of (e, e') and (p, p') in proving proton and neutron transition densities and because there are existing (e, e') data on ^{154}Sm and ^{176}Yb, measurements of the (p, p') reaction on these nuclei was carried out with 35 and 40 MeV proton beams from the MSU Cyclotron. The protons were detected both with a delay line counter and with nuclear emulsions in the focal plane of the Enge spectrometer. States up to 8^+ in the ground state band of both nuclei were observed and many levels in other bands were also seen. Angular distributions have been measured from 20° to 80°. Calculations of the angular distributions will be presented.

M. "DEFORMATION PARAMETERS VIA THE (p, p') REACTION" [A, B, C, E]

J. E. Finck, G. M. Crawley, C. H. King, and J. A. Nolen, Jr., BAPS 21 (1976), 985.

ABSTRACT

The (p, p') reaction is being studied on targets of ^{154}Sm, ^{176}Yb, ^{232}Th, and ^{238}U at a beam energy of 35 MeV. Data have been obtained via a magnetic spectrograph with a position-sensitive proportional counter (8-10 keV FWHM) and with nuclear emulsions (5 keV FWHM). Qualitatively the angular distributions of the 0^+, 2^+, 4^+, and 6^+ members of the ground state rotational bands are much more structured than either those from (p, p') reactions on spherical nuclei or on deformed nuclei at lower bombarding energies. Coupled channel calculations including interference between direct and multiple step excitations, using the nuclear deformation parameters, β_2, β_4, and β_6, from (α, α') work at 50 MeV, and using Becchetti-Greenlees global optical model parameters, produce good fits to the ^{154}Sm and ^{238}U data, but do not do well for the ^{176}Yb. The present results will also be compared to those from previous studies of Coulomb excitation, Coulomb-nuclear interference, and inelastic electron scattering experiments.

N. "PROTON SCATTERING AT 35 MeV TO GROUND BAND STATES IN $^{152, 154}Sm$, ^{176}Yb, ^{186}W, ^{232}Th, and ^{238}U" A, B, C, E

R. M. Ronningen, G. M. Crawley, J. E. Finck, C. H. King, R. C. Melin, J. A. Nolen, Jr., P. T. Deason, and F. M. Bernthal, BAPS 24 (1979),

ABSTRACT

Angular distributions of elastically and inelastically scattered protons were measured over angular ranges of 20° to typically 120° but to 140° for ^{154}Sm and ^{176}Yb, in step sizes of 2.5° and 5°. Angular distributions for states in the ground band, with $I^{\pi}=0^{+}$ through 8^{+}, are being analyzed within a coupled channels framework. Quadrupole, hexadecapole, and in some cases higher order mass moments, are being deduced. Particular attention is being paid to correlations and uncertainties in the optical model parameters and these moments. The results will be compared to moments from (e, e'), (α, α'), and Coulomb excitation studies. A comparison will also be made between moments deduced with and without the employment of a spin-orbit interaction.

O. "PROTON SCATTERING AT 35 MeV TO GROUND BAND STATES IN ^{232}Th, and $^{234, 236, 238}$U" A, B, C, D

R. C. Melin, R. M. Ronningen, J. A. Nolen, Jr., G. M. Crawley, J. E. Finck, and C. E. Bemis, Jr., BAPS 24 (1979), 837.

ABSTRACT

Angular distributions of elastically and inelastically scattered protons have been measured in the angular range of 20° to 144.5° in steps of 2.5° and 5°. A 35.3 MeV dispersion-matched proton beam from the M.S.U. cyclotron was used. The scattered protons were detected in the focal plane of an Enge split-pole spectrograph with the 25 cm inclined cathode, delay-line detector. The angular distributions for states in the ground band with $J^{\pi}=0^{+}$ through 6^{+} are being analyzed within a coupled channels framework. Quadrupole, hexadecapole, and possibly higher order mass moments will be presented. The results will be compared to moments from (e, e'), (α, α'), and Coulomb excitation studies.

P. "MULTIPOLE MOMENTS FROM PROTON SCATTERING AT 35 MeV TO GROUND STATE BAND STATES IN ^{232}Th AND $^{234, 236, 238}$U" A, B, C, D

R. M. Ronningen, R. C. Melin, J. A. Nolen, Jr., G. M. Crawley, J. E. Finck, and C. E. Bemis, Jr., BAPS 25 (1980), 740.

ABSTRACT

Angular distributions of elastically and inelastically scattered protons have been measured in the angular range of 20° to 144.5° in steps of 2.5° and 5°. The scattered protons were detected in the focal plane of an Enge split-pole spectrograph with a delay-line detector. The angular distributions for states in the ground band with $J^{\pi}=0^{+}$ through 8^{+} were analyzed within a coupled channels framework. Quadrupole, hexacapole, and hexakontattetara mass moments were deduced. The sign of the deformation parameter β_6 was determined to be positive for ^{232}Th and $^{234, 236}$U, and negative for ^{238}U. Our results will be compared to those form (e, e'), (α, α'), Coulomb excitation, and (p, p') studies.

REFERENCES FOR APPENDICES

1. S. C. Ewald, Unpublished.
2. R. Kouzes, Unpublished.
3. H. David and R. Fox, Unpublished.
4. G. Hamilton and L. Vance, Unpublished.
5. W. T. Wagner, Unpublished
6. G. F. Trentelman and E. Kashy, Nucl. Inst. Meth. 82 (1970), 304.
7. W. F. Steele, Unpublished.
8. J. E. Finck, Unpublished.
9. J. Kunz, University of Colorado, Unpublished.
10. R. Schaeffer and J. Raynal, Unpublished.